SLAC-R-129

INELASTIC ELECTRON SCATTERING AT LARGE ANGLES

GUTHRIE MILLER
STANFORD LINEAR ACCELERATOR CENTER
STANFORD UNIVERSITY
Stanford, California 94305

PREPARED FOR THE U.S. ATOMIC ENERGY
COMMISSION UNDER CONTRACT NO. AT(04-3)-515

January 1971

ABSTRACT

Electron-proton scattering cross sections have been measured at electron scattering angles of 18°, 26°, and 34° for incident electron energies up to 18 GeV. This data extends in four momentum transfer squared (q^2) from 1 GeV^2 to 20 GeV^2 and in missing mass squared (W^2) up to 25 GeV^2. Using previously reported data at 6° and 10°, a separation of the two inelastic form factors has been made in the deep inelastic region ($W^2 > 4$ GeV^2) for q^2 from 1.5 to 8 GeV^2. The transverse form factor is found to dominate in agreement with the expectations of various "parton" theories (for spin 1/2 partons). Determination of the inelastic form factor W_2 allowed an investigation of the question of "scaling" i.e. that $\nu W = F(\nu/q^2)$ in the deep inelastic large q^2 region.

ACKNOWLEDGMENTS

Credit for the success of this experiment goes to the physicists of the SLAC-MIT collaboration, consisting of Elliott Bloom, David Coward, Herbert DeStaebler, Jurgen Drees, Charles Jordan, Luke Mo and Richard Taylor from SLAC Group A and Jerome Friedman, George Hartmann and Henry Kendall from MIT. Martin Breidenbach and Leslie Cottrell made many useful contributions of their expertise. I would like to thank Professor W. K. H. Panofsky for serving as my thesis adviser and sponsor in Group A and enabling me to participate in this endeavor. Of course the SLAC electron scattering experiments really began with the planning and construction of the accelerator and the spectrometer facility itself. The existence of SLAC is due to the efforts of a great many people, but especially to Professor Panofsky. Despite his role as laboratory director, to me Pief remains first an exemplary experimental physicist. I've benefited greatly as a physicist from close association with various members of the group, in particular Elliott Bloom, during the initial stages of the experiment and Charles Jordan during the analysis.

Thanks are due to Richard Early for many well-designed computer programs, especially for his numerical solution of the diffusion equation (at the instigation of Hobey DeStaebler) which injected a healthy dose of fact into an increasingly philosophical debate over radiative corrections which was raging at the time. Thanks also to Sunny Sund for

ACKNOWLEDGMENTS

help with programming. Finally, I would like to thank Anna Laura Berg for her typing of the manuscript.

TABLE OF CONTENTS

CHAPTER 1 --- INTRODUCTION

Scattering experiments involving a weakly interacting probe particle are extremely fruitful because of the ease with which the experimental results can be interpreted. When the bombarding particle scatters because of a single interaction process the experiment directly measures the probability of transferring a quantum of energy and momentum to the target material. Constituent particles in the target are revealed in the data by causing the energy transfer to be a function of the magnitude of the momentum transfer.

In the scattering of high energy electrons from target nuclei with charge Z, the interaction strength is of the order $Z\alpha$, with $\alpha =$ "1/137". The electron in addition is interacting with the omnipresent photon field and produces radiated photons with a probability on the order of $2\alpha/\pi \log(q^2/m^2)$, where q^2 is the four momentum transfer squared and m is the electron mass. For high energy electron scattering from hydrogen the measured cross section can be corrected for the effects of its coupling to the radiation field and otherwise the parameter α appears to be sufficiently small so that the dominant process is the exchange of a single photon.

The process of elastic electron - proton scattering is studied by examining the "elastic peak" in the electron scattering cross section that occurs for the energy transfer ν equal to $q^2/(2M)$, where M is the proton mass. Elastic scattering can be parameterized by two form factors which

CHAPTER 1 --- INTRODUCTION

are functions of the momentum transfer q^2. Measurements of elastic electron - proton scattering for high energies begun by Hofstadter and collaborators at Stanford[1] and continued up to momentum transfers of 25 GeV^2 at SLAC[11] have shown that the form factors of the proton's charge and electromagnetic currents are rapidly and smoothly falling with increasing momentum transfer. If we interpret the form factor as the fourier transform of a spacial density of charge or current, this means the proton's charge is not concentrated at a point but rather evenly extended over a small region (radius of the order of 10^{-13} cm).

This picture of the proton as an extended structure is in keeping with basic notions of its composite nature -- for example of it being composed of a cloud of interacting "bare" protons and pions. However it may be advantageous to think of the proton as being composed of other constituents (quarks perhaps) in the same way that low temperature He^4 is best thought of as a system of weakly interacting phonons and rotons, rather than as a system of rather strongly interacting Helium atoms. However in the case of liquid Helium the phonons and rotons are plainly evident when slow neutrons are scattered from the liquid. The neutron - Helium atom interaction is effectively weak so the excitation spectrum can be directly measured. An example of the actual experimental data[2] is shown in Figure 1. The excitation of phonons is characterized by the linear

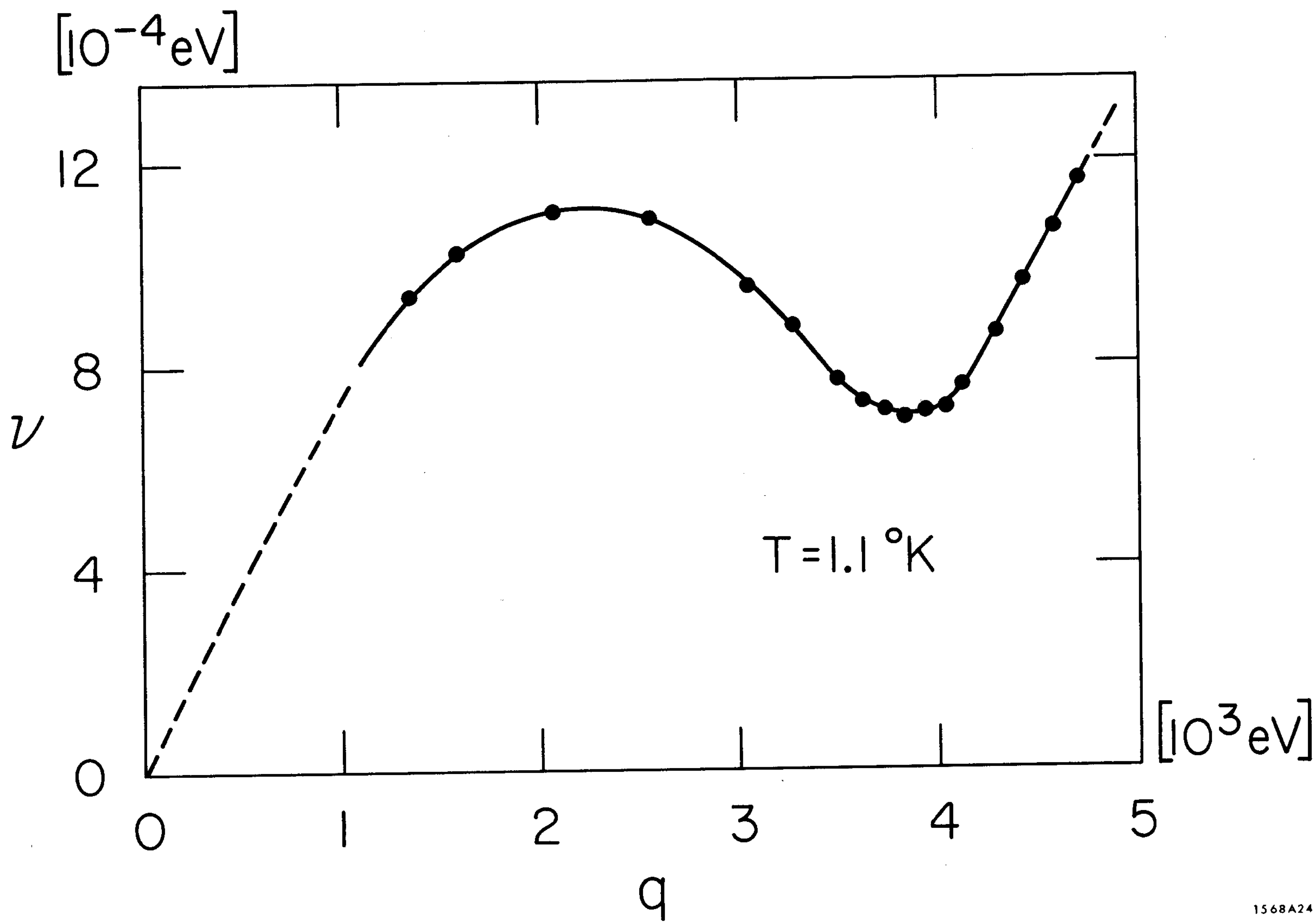

Fig. 1

dependence of ν on q, $\nu = qc$ where c is the velocity of sound (240 m/sec). For higher q, rotons are excited with $\nu = \Delta + (q-q_0)^2/(2\mu)$.

From the data presented here on inelastic electron proton scattering no such clear cut evidence for quark - like constituents of the proton is present. That is, there is no definite quasi - elastic peak (or line) in the inelastic cross section data as a function of q and ν. Howerever certain aspects of the data are very suggestive of some sort of interpretation in terms of constituents which seem to be pointlike. This is called "scaling" and refers to the fact that for large q^2 and ν, the inelastic form factors νW_2 and $2MW_1$ are a function only of the ratio of q^2 to ν. Scaling comes about naturally if the proton were composed of pointlike constituents with mass m, since the cross section would be concentrated along a line with $q^2/\nu = 2m$, being spread out somewhat by internal motion within the proton.

The possibility exists that diffraction processes are masking a quasi - elastic peak. The question can really only be resolved experimentally either by measurements of electron - neutron inelastic scattering or by direct measurement of the diffractive channels in electron - proton inelastic scattering.

This is a report of inelastic electron scattering measurements conducted at SLAC in November 1968 using the

SLAC 8 GeV spectrometer at angles of 18, 26, and 34 degrees. Previously, measurements were made at 6° and 10° [3,4] where scaling was first observed. Measurements also have been previously reported from 1.5° [15]. In all cases the data covers a range of energies with the initial energy limited by the maximum accelerator energy and the secondary energy down to about 20% of its maximum (elastic peak) value.

The discovery of scaling has prompted a large number of interesting theoretical works too numerous to attempt to list here. One may optimistically hope that someone may gain some insight from this to a soluble theory of strong interactions.

CHAPTER 2 --- DESCRIPTION OF THE EXPERIMENT

The experiment consisted of the scattering of electrons of energy E from target protons into the small solid angle and momentum range accepted by the spectrometer, which is set at an angle θ and energy E'. The measured cross section, which will be denoted by $d\sigma_{RAD}/d\Omega dE'$ to distinguish it from the radiatively corrected cross section is defined by the following formula.

$$\frac{d\sigma_{RAD}}{d\Omega dE'}(E, E', \theta) = \frac{N}{N_{in}\, n(\Delta\Omega\, \Delta E')} \qquad (1)$$

where N is the number of scattered electrons for N_{in} incident electrons, n is the number of target protons per cm² and $(\Delta\Omega\Delta E')$ is the spectrometer acceptance.

The radiatively corrected cross section is by definition the cross section for the scattering process calculated to lowest order in α. This quantity is proportional to the electromagnetic current tensor of the proton $W_{\mu\nu}$ (see appendix B), where $W_{\mu\nu}$ summarizes the electromagnetic structure of the proton. The tensor $W_{\mu\nu}$ can be reduced to two scalar quantities (form factors) W_1 and W_2, which are functions of two variables usually taken to be $q^2 = q_\mu q_\mu$ and $\nu = -P_\mu q_\mu / M$, where q_μ is the four momentum transfer, P_μ is the four momentum of the target proton, and M is the proton mass, .9383 GeV. Other important kinematic parameters are the missing mass² $W^2 = -(P_\mu + q_\mu)^2$ which is slightly more convenient than ν, and the quantities x and ω.

These are expressed in terms of E, E', and θ as follows:

$$q^2 = 4EE' \sin^2 \theta/2$$

$$\nu = E - E'$$

$$W^2 = M^2 + 2M\nu - q^2$$

$$x = q^2/(2M\nu)$$

$$\omega = 1/x \tag{2}$$

The experiment was designed to allow the separate determination of the two form factors over a large kinematic range. This is accomplished by measuring the cross section at two or more angles at the same values of q^2 and W^2. The position of a measured point can be conveniently plotted on the W^2, q^2 plane as shown in Fig. 2. All the measurements at one angle span a triangular region in q^2, W^2 space. Each measured line with E and θ constant would be a straight line on such a plot. The intercepts of this line with the $q^2 = 0$ axis and the line W = M are given by

$$W^2_{max} = M^2 + 2ME$$

$$q^2_{max} = \frac{4E^2 \sin^2 \theta/2}{1 + \frac{2E}{M} \sin^2 \theta/2} \tag{3}$$

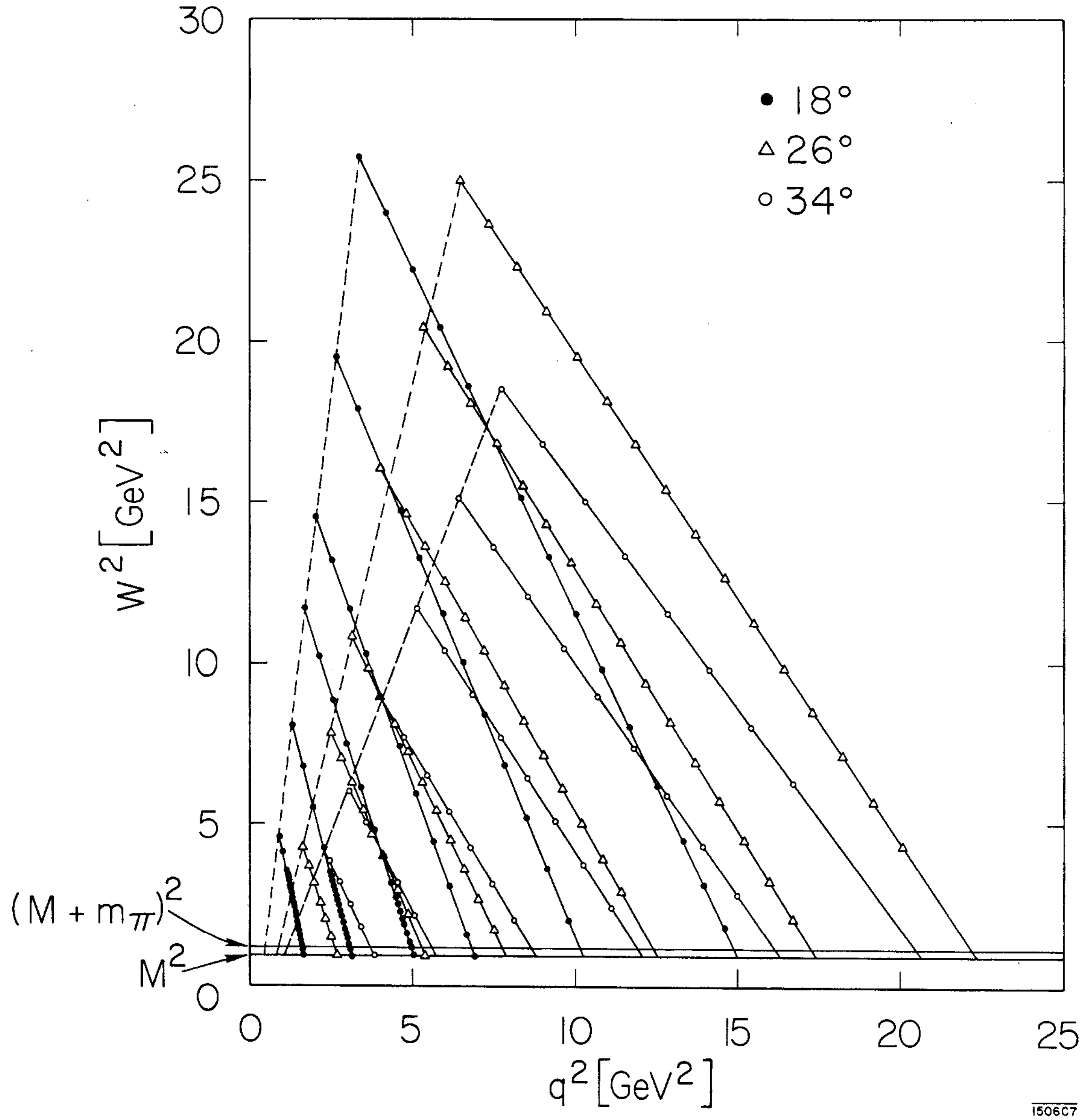

30
25
20
15
10
5
0
0
5
10
15
20
25
• 18°
△ 26°
○ 34°
W^2 [GeV^2]
q^2 [GeV^2]
(M + m$_\pi$)^2
M^2
1506C7

Fig. 2

The curve x = constant would be a straight line passing through the point $q^2 = 0$, $W^2 = M^2$.

For the three lowest energy 18-degree lines the data points are closely spaced. In the kinematic region $W < 2$ GeV, the cross section shows resonant structure as a function of missing mass, so for these lines the spectrometer settings were overlapped and events within the spectrometer acceptance were binned in missing mass in order to obtain a continuous missing mass spectrum of the cross section. Outside of the resonance region the variation of the cross section over the spectrometer acceptance is not significant and the entire acceptance was used, yielding a single cross section for each setting.

The cross section was measured for the three angles -- 18, 26, and 34 degrees -- for E and E' values throughout the range shown in Fig. 3. This is due to the necessity for making radiative corrections, which require knowledge of the entire behavior of the measured cross section as a function of E and E' for a given angle. The radiative correction procedure yields the corrected cross section for all the measured E, E' points at that angle.

The measured cross section, in addition to being a function of E, E', and θ, depends somewhat on the nature and amount of material before and after the point of scattering. Efforts were made to minimize the total radiation lengths of material in the path of the incident and scattered

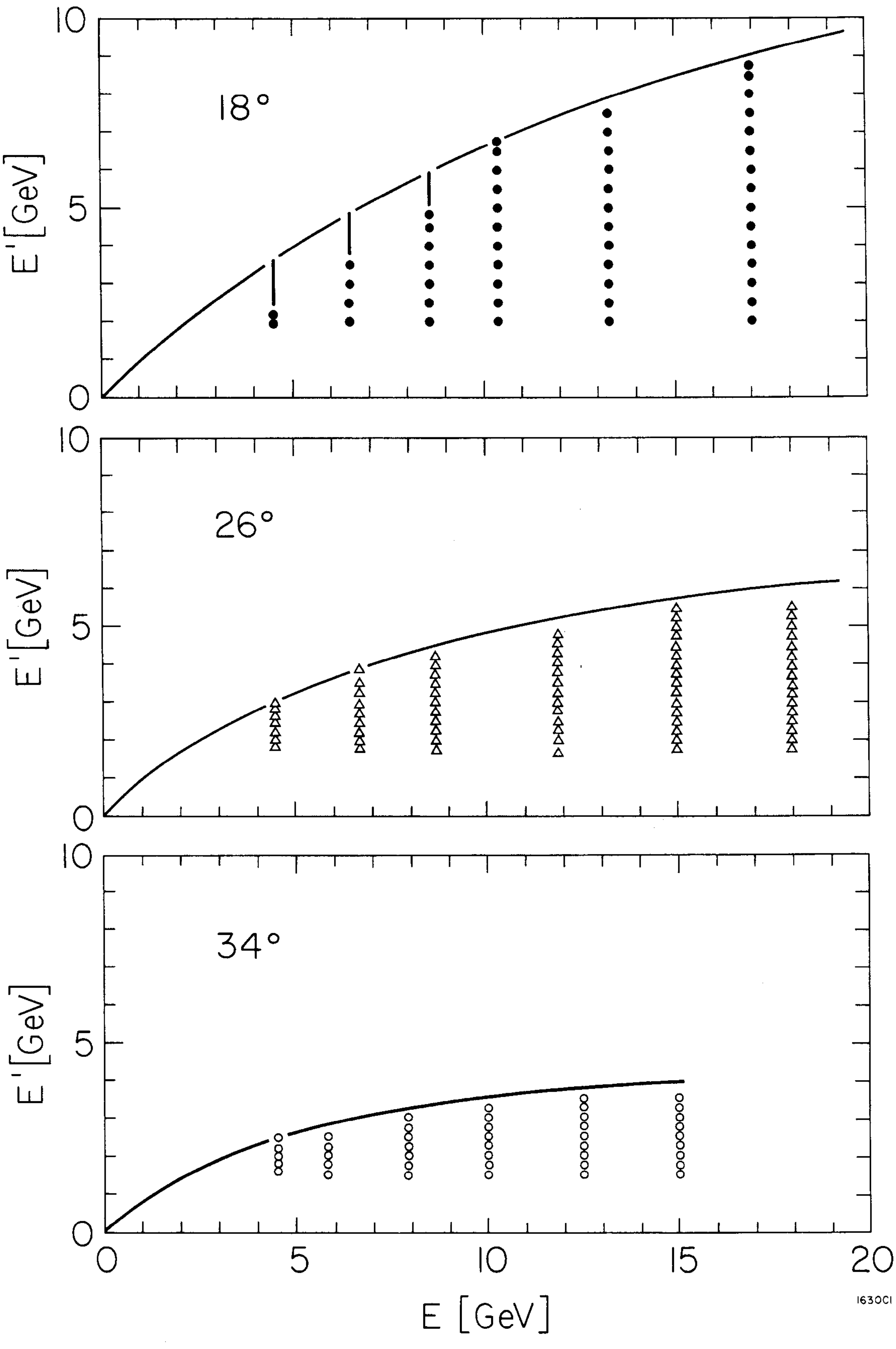

Fig. 3

electrons; in fact, most of the material consisted of the small amount of target hydrogen itself. Because of the electron's small mass it can radiate a considerable fraction of its total energy during collisions with the atoms in a material.

Background electrons were detected that were not the result of scattering from the liquid hydrogen. These were due to scattering in the walls of the target cell or in the window on the scattering chamber (the only material besides the target hydrogen within view of the spectrometer), and also due to processes creating electron-positron pairs. The former is taken into account by measuring the cross section for scattering from an empty target cell (dummy target measurement) and subtracting it. Pair creation processes, mainly $\pi_0 \longrightarrow \gamma e^+ e^-$, were taken into account by measuring the cross section for detecting positrons in the spectrometer, subtracting the dummy target background from this, and subtracting the result which was assumed equal to the electron background originating from such charge-symmetric processes. The positron background was only significant for E' small compared to E. However, dummy target runs were usually made for each spectrometer setting. were usually made for each spectrometer setting.

CHAPTER 3 --- APPARATUS

3.1 Beam

The Stanford Linear Accelerator is a 2-mile-long assembly of disk-loaded copper waveguides.[5] Disk loading destroys the symmetry of the waveguide structure to translation along its axis and allows transmission of waves with axial electric field having a phase velocity near the velocity of light. Electrons are injected at one end in short bunches, occupying 5° of phase interval relative to the traveling rf wave and are accelerated by microwave power (2856 MHz) supplied by 245 klystron amplifier tubes positioned along the accelerator at 40-foot intervals. The klystrons are operated in two modes, "accelerate" and "standby", to achieve energy control, with each klystron capable of contributing roughly 90 MeV to the electron beam energy. In this experiment the accelerator beam energies ranged from 4.5 GeV to 18 GeV.

A high-power modulator supplies each klystron with 2.5-microsecond long 250-kV pulses with a maximum current of 260 A. The repetition is 360 pulses/sec. Electrons are accelerated for only 1.6 microseconds during each pulse. A phenomenon known as beam breakup[6] limited the peak beam current in the accelerator to 55 mA.

The beam pulses from the accelerator structure are channeled into the various experimental areas in the beam switchyard. The beam into the spectrometer area is first deflected a small amount (0.5°) by pulsed magnets, then bent

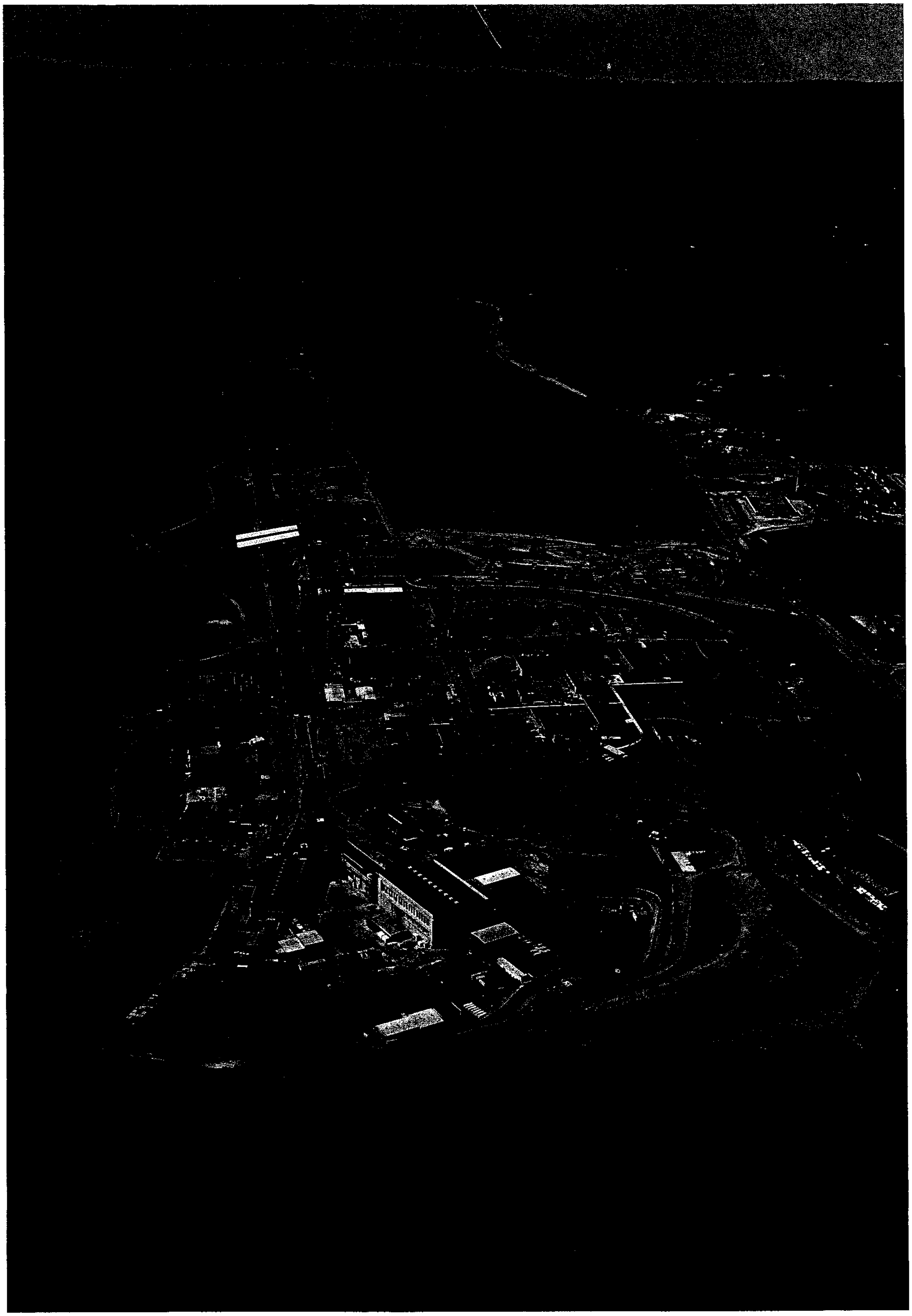

Fig. 4

12° in a series of bending magnets and passed through a set of high-power momentum-defining slits. The slits were typically set to pass a 1% range in momentum. The mean momentum of the beam is defined by the beam switchyard to an accuracy of ±0.2%. The switchyard beam-transport system is made achromatic by a second 12° bend with a quadrupole placed midway between. The quadrupole focuses the dispersed momenta which are then recombined in the second set of bending magnets.

Quadrupoles and steering magnets allowed focusing and aligning the beam on the target. This was done with the aid of 3 fluorescent ZnS screens, two mounted at distances of 53 feet and 10 feet in front of the target, and the third a distance of 5 feet behind the target. The screens in front of the target were retractably mounted inside the beam vacuum system and were normally out of the beam path except for alignment checks. The third screen behind the target was permanently mounted in the air. Typically the beam was focused to have the shape of an ellipse with height 0.3 cm and width 0.6 cm. The last quadrupole had an aperture of 3 in. and was located a distance of 332 ft before the target. This limited the angular divergence of the beam to less than ±0.4 mr. The direction of the beam was known to ±0.3 mr by reading the position of the beam spot on the fluorescent screen.

CHAPTER 3 --- APPARATUS

The maximum current through the switchyard energy slits was about 30 mA, or roughly 3×10^{11} electrons per pulse. This maximum-intensity beam was required only for runs at high secondary energy and large q^2, where the cross section was very small. Otherwise, the beam current had to be decreased to limit the counting rates in the fastest counting electronics circuits.

A lucite block mounted on the end of a photomultiplier tube was placed in the vicinity of the target. This served as a Cerenkov detector responding to the instantaneous flux of beam-produced particles and was used to monitor the relative constancy of the beam current. The accelerator was "tuned" to provide a flat top current pulse as much as possible, in order to minimize the instantaneous particle rates.

The primary incident beam-charge monitors were a pair of toroidal transformers (toroids) with the electron beam forming the primary winding.[7] These devices were internally calibrated by a single turn of wire carrying a precisely determined charge to simulate the beam. Previous experiments have involved extensive checking of one of the toroids used with a Faraday cup, which has shown no disagreement at the 1% level. Several comparisons of the toroids with the Faraday cup were made during the experiment as checks. The incident beam charge measured by the two toroids always agreed to within 0.5%.

3.2 Target

The electrons were scattered from liquid hydrogen contained in a 7.026-cm diameter circular-cylindrical cell with 0.003-inch aluminum walls. The cylinder axis was vertical and the beam passed through the cell along a diameter. An identical empty target cell was mounted below the full target and used to measure the scattering coming from the target walls (dummy target measurement).

The beam deposited roughly 2 MeV per incident electron in the target hydrogen. At maximum current and repetition rate this is an average power of 36 watts. In earlier electron-scattering experiments at SLAC this had caused a reduction of the target density, either due to boiling of the hydrogen around the beam path or to formation of a cylindrical shock wave along the beam path during the 1.6 μsec duration of the pulse. To prevent the former, the hydrogen in the target was forced to circulate around a ring by a small motor-driven fan. The target hydrogen, maintained at about 1 atm overpressure, was driven through the scattering cell and up through a heat exchanger. A large reservoir of liquid hydrogen absorbed the heat from the heat exchange and gave the system thermal stability.

Before the data taking began the circulating target was tested to see if the target density was reduced at high beam

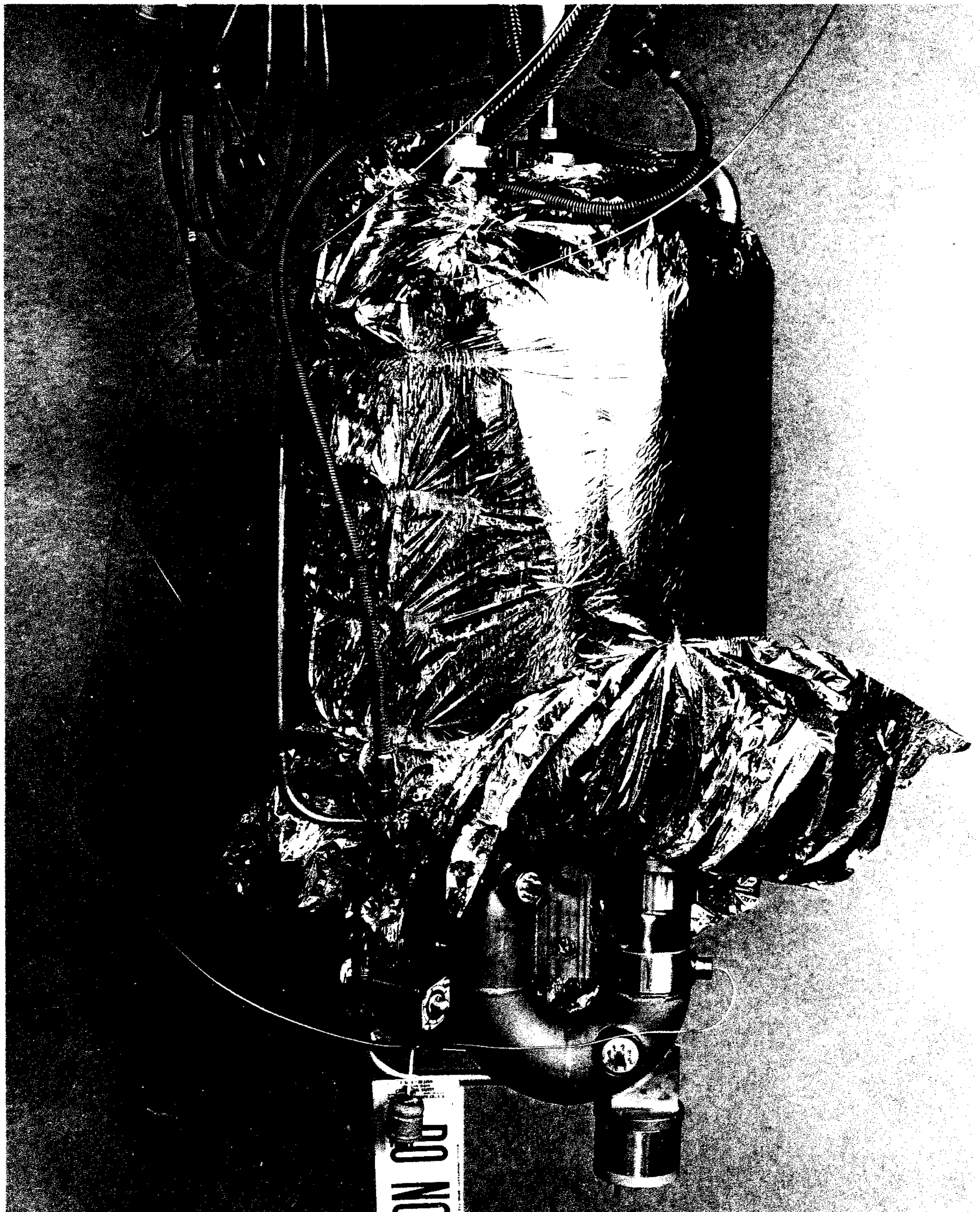

1568A5

Fig. 5

intensities. It was checked that the calculated cross section was independent of beam current, spot size, and beam pulse length. As an additional check on the target density the SLAC 1.6-GeV spectrometer was used to measure the cross section for detecting protons from elastic scattering at fixed proton momentum and angle. The only variation expected in this cross section after correction for counting rate effects is due to a reduction in the target density caused by beam heating. The cross section was measured at low current for every initial energy to provide normalization. No significant target density reduction was observed with the 1.6 GeV spectrometer used in this way and no target density correction was made.

The hydrogen was in a two-phase system, liquid in equilibrium with vapor so the hydrogen density is determined by temperature. The temperature was measured by measuring the hydrogen vapor pressure in a small bulb placed in good thermal contact with the target hydrogen. The average temperature was 20.6°K. However, deposition of energy by the beam and refilling of the hydrogen reservoir caused short-term temperature variations on the order of 1°K. This causes a 1.7% uncertainty in the liquid hydrogen density.

3.3 Material in the Beam Path

CHAPTER 3 --- APPARATUS

Because of the electron's small mass, the acceleration caused by collisions with the atoms of a material can cause the electron to radiate a large fraction of its total energy. The probability of an energy loss occurring by this process (bremsstrahlung) depends on the amount of material measured in radiation lengths. The radiation length is defined by Equ. A.III.7. Energy degeneration can also be caused by radiation occurring during the large-angle scattering. The details of the radiation problem are discussed in the appendix. However, in an approximate sense, a scattering with momentum transfer q^2 from the electron is equivalent as far as radiation is concerned to passage of the electron through t/2 radiation length of material before the scattering, which takes place with no radiation, and passage through a further t/2 radiation length. t is called the equivalent radiator and is given by formula A.I.16. This equivalence is exact only for the limiting case of soft photons.

For $q^2 = 1$ GeV^2, the equivalent radiator is 0.066. The total radiation length of material in the beam path was small compared with this number. Assuming the scattering takes place at the center of the target in an average sense, that is, including half the target hydrogen before and half after, the total radiator before was 0.0052 r.l. and the radiator after was 0.0126 r.l. For the target hydrogen the radiation length was taken to be 847 cm.

The biggest contributors to the total radiator were first 0.0102 r.l. from the target hydrogen and aluminum target cell windows, 0.0078 r.l. from the aluminum spectrometer spectrometer entrance window, and 0.0018 r.l. from 21 inches of air along the path of the scattered electron.

3.4 Spectrometer

The SLAC 8-GeV spectrometer as shown schematically in Fig. 7 consists of two bending magnets and three quadrupole magnets. The spectrometer was designed to allow determination of the momentum of particles coming from the target from a knowledge of the vertical position at a plane of the particle's trajectory after passage through the spectrometer's magnetic elements. An array of narrow, horizontally oriented scintillation detectors (hodoscope) covered the momentum measuring plane. Similarly, the spectrometer allowed determination of the horizontal scattering angle of a particle from the target with the use of a single array of vertically oriented hodoscope counters at the horizontal angle-measuring plane. The momentum hodoscope was 11.938 cm across in the vertical direction divided into 40 bins by the counters. The momentum hodoscope plane was tilted at an angle of 14.7° with respect to the spectrometer horizontal plane. Variations in the

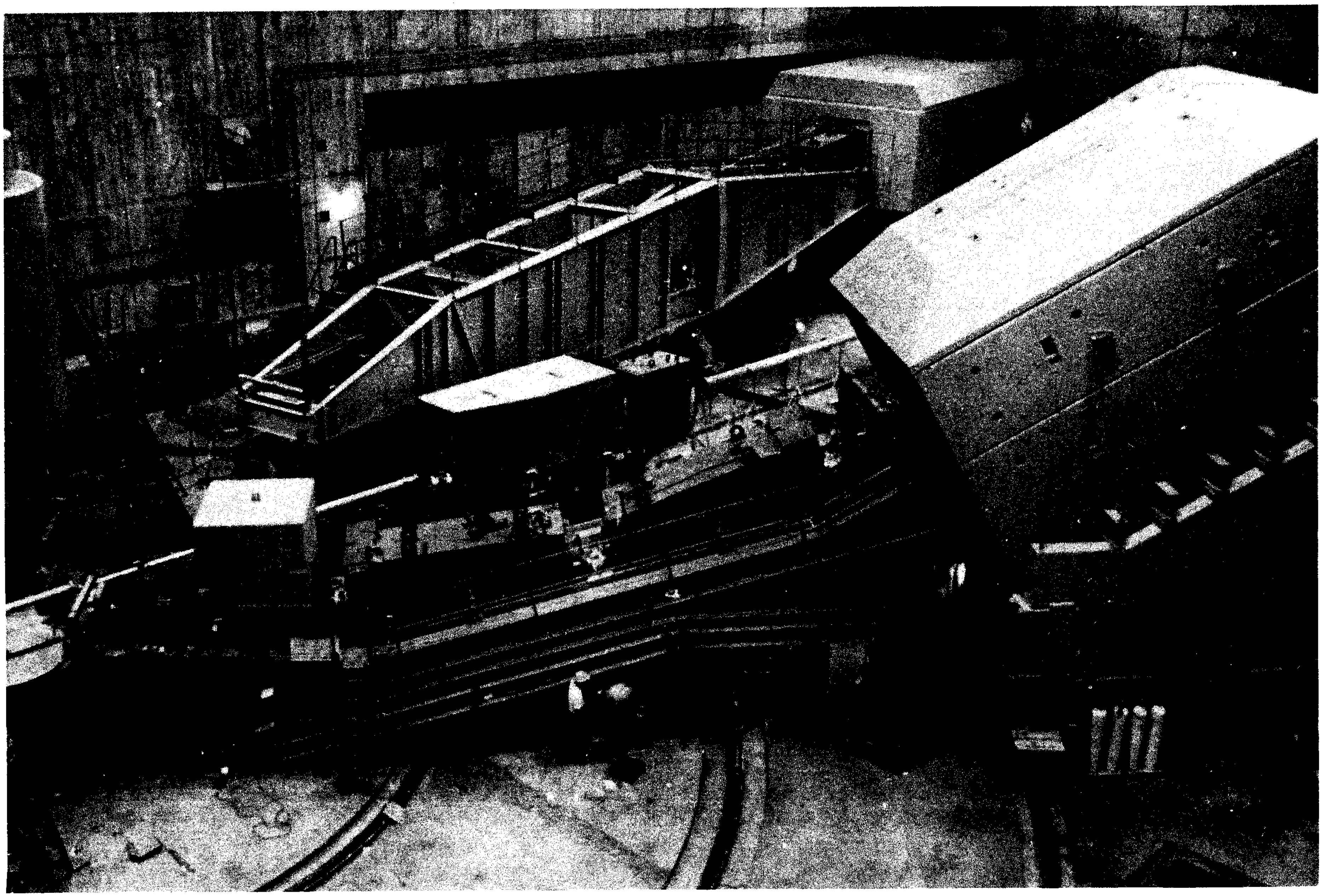

Fig. 6

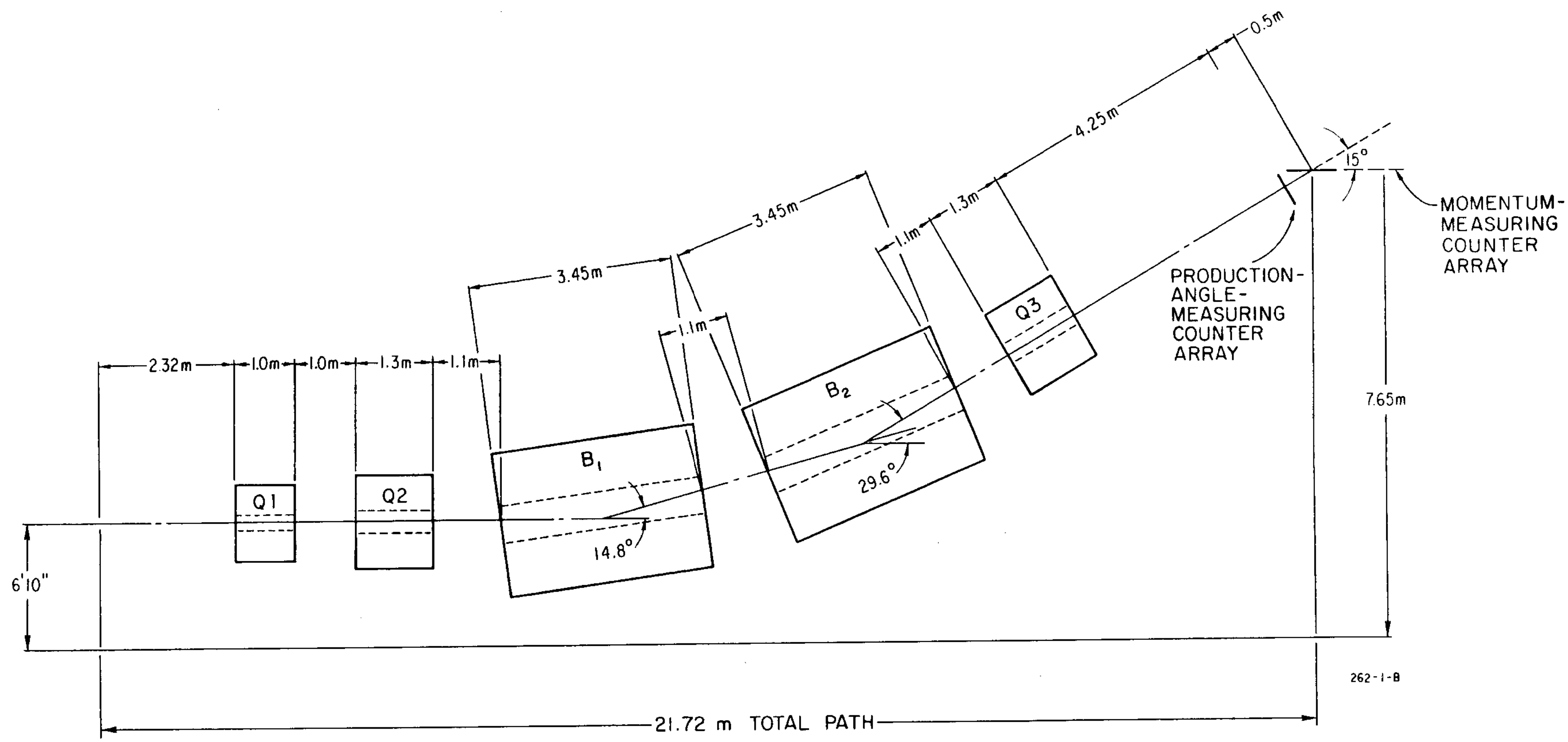

MAGNET ARRANGEMENT, 8-BeV/c SPECTROMETER.

Fig. 7

vertical angle at the target had no effect on the particle's vertical position at the momentum hodoscope (ϕ_0 focus). The theta hodoscope was 68.5 cm wide in the horizontal direction and was divided into 54 bins. Variations in a particle's horizontal coordinate at the target were focused out at the theta hodoscope.

Both bending magnets bent vertically (each 15°). The entire spectrometer, including the shielding around the particle detector area, some 750 tons total weight, was mounted on rails and pivoted around the position of the target. There was a system of taut wire position sensors that allowed monitoring the position of each of the magnetic elements. An online computer program converted the measured wire displacements to relative movements of the magnets, and compared with tolerances established for the 8-GeV spectrometer.[8] This check was done after every movement of the spectrometer to a different angle and the displacements of the magnets observed were always within tolerance.

The current versus field curve of each magnet had been measured using NMR, varying the currents in a standard degaussing cycle. Only the bending magnets showed appreciable saturation. The central momentum of the spectrometer was set by setting the currents in the magnets using the standard degaussing cycle. The magnet currents were monitored by reading the voltage across precision shunt resistors in series with the magnets. The actual task of adjusting the power supplies was handled by an online computer program that continuously monitored the shunt voltages and changed the power supply output currents until the desired shunt voltages were obtained.

The spectrometer was designed assuming ideal magnetic elements and calculating the transformation of particle rays by the spectrometer to second order in the deviation from the central ray. In the standard central- ray coordinate system notation [9] $x_0, y_0, \theta_0, \phi_0, \delta_0$ are the coordinates of the ray at the target and $x, y, \theta, \phi, \delta$ are the coordinates at a definite z position following the last magnetic element, for instance, at the momentum hodoscope position. The transformation of the initial ray at the target to the final ray was calculated to second order in the small quantities $x_0, y_0, \theta_0, \phi_0, \delta_0$.

The actual performance of the spectrometer was measured in a series of optics tests conducted in November, 1967. This resulted in very small correction factors to be applied to the magnet current settings to achieve the desired central ray and the desired quadrupole focusing. The transport coefficients were determined from these measurements, and it was found necessary to change the effective field strengths of the three ideal quadrupoles in the first- and second-order model in order to reproduce exactly the measured results for the coefficients $(x|x_0)$, $(x|\theta_0)$, and $(y|\delta_0)$.[10] Also, these coefficients were found to be slightly energy dependent. The measured theta dispersion $(x|\theta_0)$ changed by 1.2% from 3 GeV to 8 GeV. The measured momentum dispersion $(y|\delta_0)$ changed by -1.8% from 3 GeV to 8 GeV.

For the calculation of the acceptance, a first- and second-order model was assumed that reproduced identically the measured values of $(x|x_0)$, $(x|\theta_0)$, and $(y|\delta_0)$ at 8 GeV. The parameters of the model are given in Table 1, and the resulting transport coefficients in Table 2.

The 8-GeV spectrometer was used in the elastic electron-proton scattering experiment of Kirk et al.[11] However, the spectrometer was modified afterwards by the installation of lead apertures to more sharply define the acceptance and to simplify the acceptance calculations. Thus, as far as the acceptance is concerned, the earlier elastic measurements were independent. Elastic cross sections were measured to compare with previous measurements as a check against a normalization error.

The acceptance was calculated in two different ways to check the program mechanics using the same model of the spectrometer as a starting point in each case. In one method rays were randomly generated with a uniform distribution in $x_0, \theta_0, \phi_0, \delta_0$ space and transported through the spectrometer. A check was made at each of the limiting apertures to see that the ray could successfully pass. Successful events were placed in hodoscope counter bins,

TABLE 1

Model of 8 GeV Spectrometer, P = 8.008 GeV

- drift from target 1m
- spectrometer entrance window
- drift 1.2995 m
- quadrupole Q81 (1.026 m, a = 13.97 cm, 7.551 kg, vertically defocusing)
- drift .352 m
- aperture 1 $\left(\text{circular, } \sqrt{x^2 + (y + .24)^2} < 13.02\right)$
- drift .6165 m
- quadrupole Q82 (1.336 m, a = 19.3675 cm, -10.823 kg, vertically focusing)
- drift .9610 m
- 1/2 bending magnet B81 (1.8135 m, 7.5°, 19.267 kg, vertical bend)
- aperture (-19.21 cm < y < 34.47 cm)
- 1/2 bending magnet B81
- drift .3863 m
- aperture 2 $\left(\text{octogon, } |y| < 16.5 \text{ cm, } |x| < 14.5 \text{ cm, } |y| < 24.6 \text{ cm} \left(1 - \frac{|x|}{18.2 \text{ cm}}\right)\right)$
- drift .5387 m
- bending magnet B82 (3.627 m, 7.5°, 19.267 kg, vertical bend)
- drift 1.003 m
- quadrupole Q83 (1.336 m, a = 19.3675 cm, -7.319 kg, vertically focusing)
- drift 4.197 m
- theta hodoscope (-34.29 cm x < 34.29 cm, 54 bins)
- drift .555 m
- p hodoscope (-5.969 cm < y < 5.969 cm, 40 bins, tilted 14.7°)

TABLE 2

8 GeV Spectrometer Transport Coefficients

x at theta hodoscope

y, ϕ at momentum hodoscope

x_0, θ_0, ϕ_0, δ_0 at target

$y_0 = 0$

	x_0	θ_0	ϕ_0	δ_0	x_0^2	$x_0\theta_0$	$x_0\phi_0$	$x_0\delta_0$	θ_0^2	$\theta_0\phi_0$	$\theta_0\delta_0$	ϕ_0^2	$\phi_0\delta_0$	δ_0^2
x	.0383	4.3060					.0001	.0393		-.0009	-.0163	.0001	-.0016	.0039
y			- .0139	-2.9070		-.0002		-.0003	.0003	.0001	.0009		.0127	.0020
ϕ			-1.090	.2034			.0002	-.0004	-.0001	-.0008	.0012		-.0026	-.0506

which resulted in a distribution of events proportional to the acceptance of each bin. The total acceptance of the spectrometer was limited by lead masks bounding the hodoscopes.

The second method of calculating the acceptance worked with individual p, θ hodoscope bins, where such a bin is a small region in the 5-dimensional ray space with the x coordinate at the theta hodoscope in the range Δx, and the y coordinate at the momentum hodoscope in the range Δy. y_0 was taken as zero and x_0 was given a fixed value which was averaged over in the final step. Thus, rays in a particular p, θ hodoscope bin have essentially one degree of freedom which can be taken as ϕ_0. The situation is illustrated in Fig. 8. The limiting values of ϕ_0 for the bin were found by a trial-and-error procedure, where ϕ_0 was varied while checking the ray at all the limiting apertures. The acceptance of the bin was calculated using the formula

$$\Delta x \Delta y \int_{\phi_{0\,\min}}^{\phi_{0\,\max}} \frac{\partial(\delta_0, \theta_0)}{\partial(y, x)} \, d\phi_0$$

The Jacobian is a known function of x, y, x_0, y_0, ϕ_0, given by

$$\frac{1}{\dfrac{\partial y}{\partial \delta_0}\dfrac{\partial x}{\partial \theta_0} - \dfrac{\partial y}{\partial \theta_0}\dfrac{\partial x}{\partial \delta_0}}$$

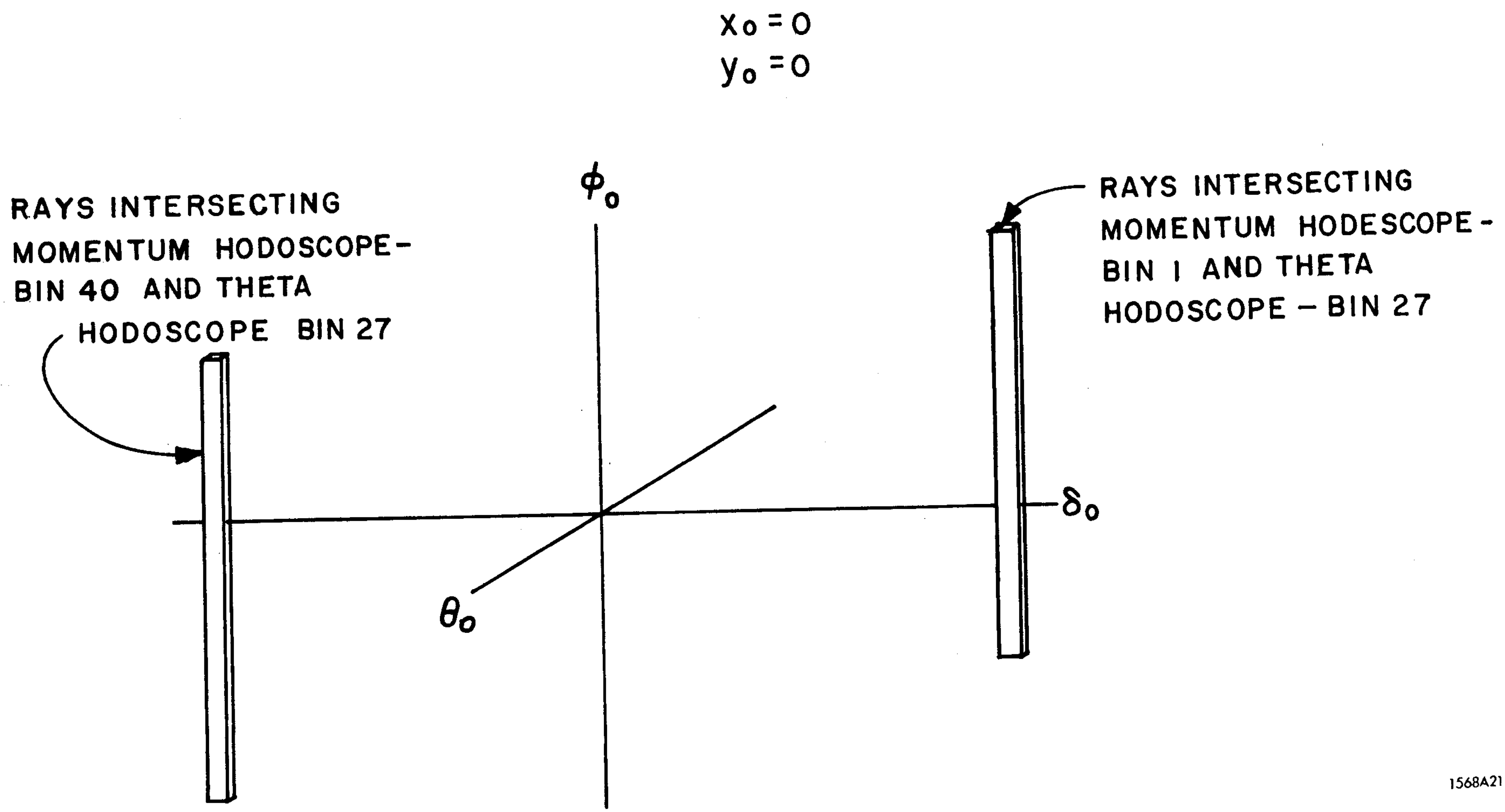

$x_o = 0$
$y_o = 0$
ϕ_o
RAYS INTERSECTING MOMENTUM HODOSCOPE-BIN 40 AND THETA HODOSCOPE BIN 27
RAYS INTERSECTING MOMENTUM HODESCOPE-BIN 1 AND THETA HODOSCOPE – BIN 27
δ_o
θ_o
1568A21

Fig. 8

where the derivatives are calculated using first- and second-order transport coefficients.

The second method of calculating acceptances had the advantage over the Monte Carlo method for accurate calculation of the very small acceptance of a hodoscope bin, since to achieve the necessary large number of Monte Carlo successes in each bin was very time consuming. The two methods agreed to 0.6% for the total acceptance with no bin-by-bin deviation discernible within the Monte Carlo statistical error of 3%. The result for the total acceptance of the spectrometer was $(\Delta p/p)\Delta\Omega = 25.40\times10^{-6}$ sr, and for the acceptance of the restricted hodoscope, p bins 5 through 36 and bins 4 through 51, the result was $(\Delta p/p)\Delta\Omega = 21.64 \times 10^{-6}$ sr. The momentum range accepted by the restricted hodoscope was roughly $\Delta p/p = \pm1.57\%$ and the theta range was roughly $\Delta\theta_0 = \pm6.88$ mr. The momentum resolution of the hodoscope was $\Delta p/p = \pm.05\%$ and the theta resolution was $\Delta\theta = \pm.15$ mr.

3.5 Particle Detectors

The primary task of the particle detection system was to detect electrons with high efficiency and to discriminate with a large rejection factor the non-electron background, consisting mostly of pions. This was accomplished using a total absorption shower counter (TA counter), a threshold

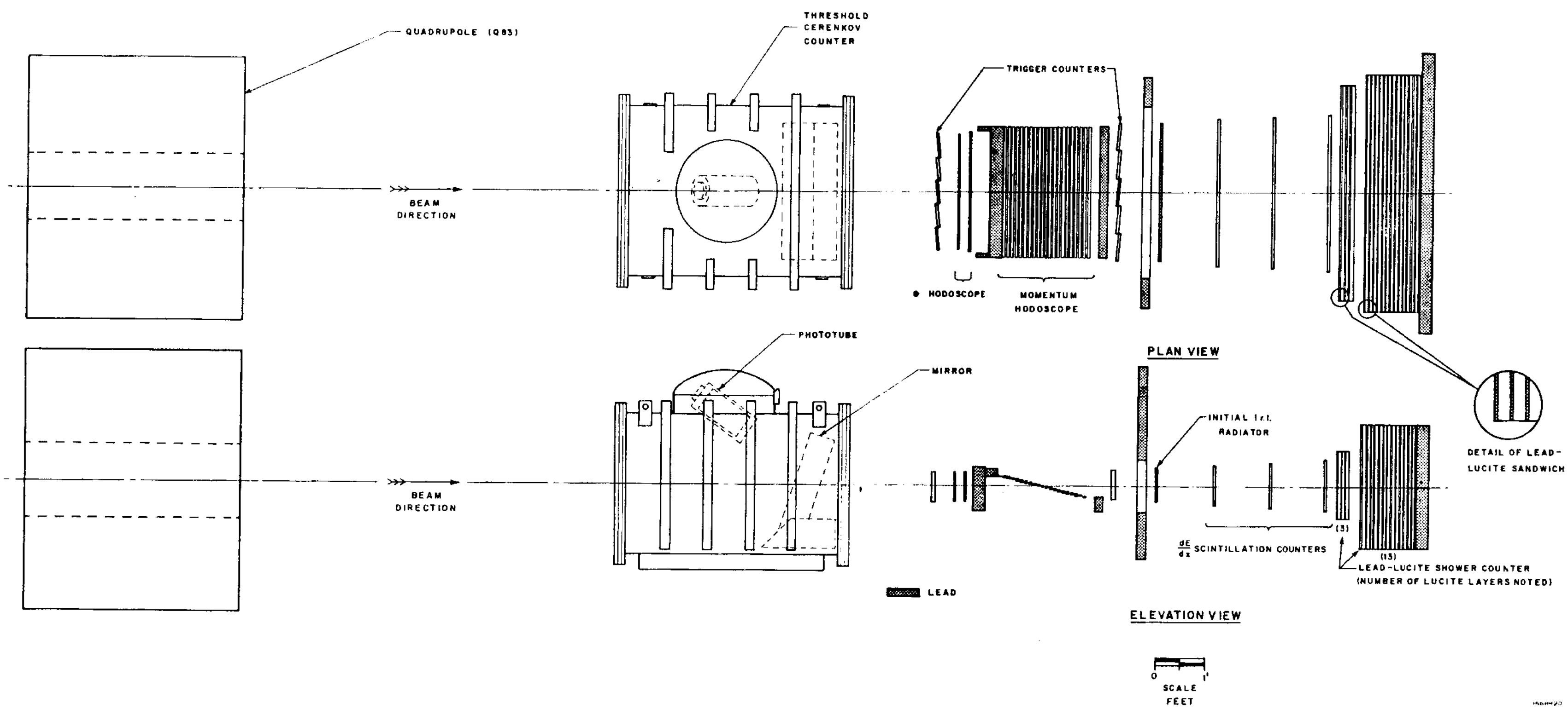
QUADRUPOLE (Q83)
THRESHOLD
CERENKOV
COUNTER
TRIGGER COUNTERS
BEAM
DIRECTION
HODOSCOPE
MOMENTUM
HODOSCOPE
PLAN VIEW
PHOTOTUBE
MIRROR
INITIAL 1 r.l.
RADIATOR
DETAIL OF LEAD-
LUCITE SANDWICH
BEAM
DIRECTION
dE/dx SCINTILLATION COUNTERS
(3)
(13)
LEAD-LUCITE SHOWER COUNTER
(NUMBER OF LUCITE LAYERS NOTED)
LEAD
ELEVATION VIEW
0
1'
SCALE
FEET

Fig. 9

gas Cerenkov counter, and a system of three scintillation counters used to count the number of particles produced in a 1-r.l. lead sheet (the dE/dx counter).

Two large multi-segmented scintillation counters covering the entire acceptance (front and rear trigger counters) were used for timing purposes. The trigger counter signals, when in coincidence with the Cerenkov signal in the fast logic circuitry, was one definition of a likely electron event.

The two arrays of hodoscope scintillation counters (55 theta and 41 momentum counters) provided momentum and angular resolution. For most of the experiment this resolution was not used except to define the spectrometer acceptance. Normally, all events with p bin in the range 5 to 36 and θ bin in the range 4 to 51 were added together to yield a single number for the cross section. The hodoscope counters and the trigger counters were the same as used in the elastic electron scattering experiment of Kirk et al.[11]

The TA counter consisted of 16 one-r.l. sheets of lead interleaved with 16 1-inch thick slabs of Plexiglas in a sandwich arrangement. An incident high-energy electron produced a cascade electromagnetic shower in the lead containing many fast electrons and positrons which make Cerenkov light in the Plexiglas. Each sheet of Plexiglas was viewed by four RCA 6346A photomultiplier tubes, which had their high voltages set for equal output from each tube for a standard light source placed in good optical contact with the center of the Plexiglas sheet.

The anode signals from all the photomultiplier tubes were linearly added. This combined TA output produced an approximately Gaussian pulse-height distribution for electrons. The most probable TA pulse height was proportional to the energy of the incident electron. At 2 Gev, the most probable pulse height for an electron was 85 channels above pedestal (zero) and the Gaussian sigma was approximately 10 channels. Pions produced a peak about 16 channels above pedestal corresponding to the pion making light along a single fast particle track in each sheet of Plexiglas. An exponential tail extended to higher channel numbers and corresponds to the pion interacting in the material of the counter, producing additional fast particles. At a momentum of 2 GeV about 3% of all pions produced TA pulse-heights greater than 55 channels above pedestal.

The Cerenkov counter contained Freon gas (CCl_2F_2) at an absolute pressure of 456 mm Hg. High-energy electrons produce Cerenkov light in a narrow cone about their direction of motion. This light was collected and focused onto the face of a photomultiplier tube by a large low-mass parabolic mirror (made of aluminum-coated polyethylene) covering the rear aperture of the counter. The photomultiplier tube(RCA C70133) had a high photocathode quantum efficiency of approximately 30%.

The number of Cerenkov light photons produced is a function of the velocity of the particle,

$$N = N_{max} \frac{n^2 v^2 - 1}{(n^2 - 1) v^2}$$

where N_{max} is the number of photons produced when $v \longrightarrow 1$ and n is the index of refraction of the medium. Assuming 100% light collection, and a 45-inch path length, a high-energy electron was calculated to produce an average of 100 photons at the photomultiplier tube face and an average of 30 photoelectrons. There is a threshold for production of Cerenkov light at $v = 1/n$. For pions this was calculated to be a momentum of 3.7 GeV. The Cerenkov threshold for pions was measured to be 3.3 GeV.

At a spectrometer momentum of 2 GeV, the Cerenkov counter efficiency for detecting pions was found to be roughly 1%, while its electron detection efficiency was close to 100%. It appears that the mechanism responsible for pion detection below Cerenkov threshold is the production of a fast secondary electron which then accompanies the pion through the Cerenkov counter. This occurs in material somewhere in front of the counter, probably in the lead aperture-defining masks.

The dE/dx counter system discriminated against pions by requiring initiation of an electron shower in a one-r.l.

thick lead sheet. Particles produced at small angles in the initial radiator accompanied the incident particle through three scintillators making light pulses proportional to ionization energy loss (dE/dx). A high-energy particle that did not interact in the initial radiator made a light pulse distribution in each scintillator corresponding to the Landau distribution[12] of dE/dx losses for a single minimum ionizing fast particle. An electron with rather high probability (0.7 to 0.9) produced additional particles in the initial radiator and caused larger-than-minimum ionizing pulse heights in each of the three scintillators. An electron event was required to have a large pulse height in all three scintillators. Inasmuch as the Landau tails of the pulse height distributions produced by a pion in the three scintillators were completely independent, having three scintillators instead of one would cube the pion rejection of the system.

The dE/dx system was placed in front of the TA counter. There was some correlation between signals in the two counters for pions, since if a pion interacted in the initial radiator it had a greater probability of producing a large TA pulse height. For example, a sample of 11300 pions at 2 GeV momentum were detected in the TA with probability $p_1 \cong 0.03$ and in the dE/dx system with probability $p_2 \cong 0.03$. Twenty pions, or 0.2% had both the TA and dE/dx requirements, which implies a correlation C = 5%, where C is defined by the equation,

$$p_{12} = p_1 p_2 (1 - C) + p_1 C$$

The electron detection efficiency of the dE/dx was not correlated with that of the TA, since whether or not the electron interacted in the initial radiator its total energy ended up in the shower counter and hence it produced the same TA pulse height.

3.6 Electronics

The primary fast detector signals were phototube anode pulses coming from the TA counter, the Cerenkov counter, and the front and rear trigger counters. The TA counter contained 64 photomultiplier tubes, the Cerenkov counter a single tube, and the trigger counters each contained 5 tubes. The anode pulses were carried separately on low-loss coaxial cables from the spectrometer to the experimenters' control room (counting house) which contained all the counting electronics and the online computer.

The 64 TA counter photomultiplier tube signal pulses were linearly added to produce a single signal pulse, fed into discriminator D14, as shown in Fig. 10. The pulses from the five-segmented trigger counters were separately channeled into discriminators (D1-10) and the output pulses combined in logical OR circuits to produce a single front

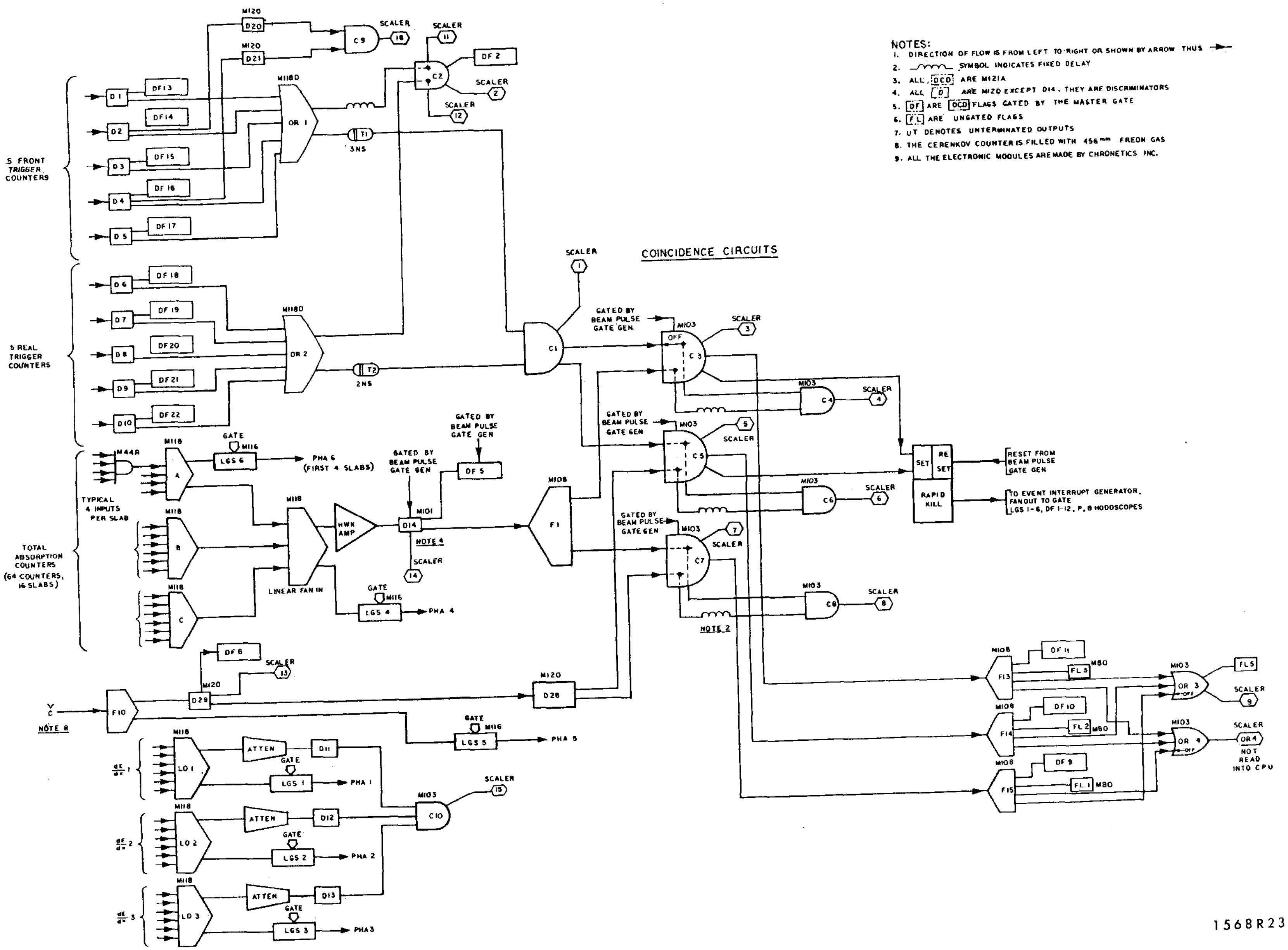
COINCIDENCE CIRCUITS
NOTES:
1. DIRECTION OF FLOW IS FROM LEFT TO RIGHT OR SHOWN BY ARROW THUS
2. SYMBOL INDICATES FIXED DELAY
3. ALL DCD ARE M121A
4. ALL D ARE M120 EXCEPT D14. THEY ARE DISCRIMINATORS
5. DF ARE DCD FLAGS GATED BY THE MASTER GATE
6. FL ARE UNGATED FLAGS
7. UT DENOTES UNTERMINATED OUTPUTS
8. THE CERENKOV COUNTER IS FILLED WITH 456mm FREON GAS
9. ALL THE ELECTRONIC MODULES ARE MADE BY CHRONETICS INC.
5 FRONT TRIGGER COUNTERS
5 REAR TRIGGER COUNTERS
TOTAL ABSORPTION COUNTERS (64 COUNTERS, 16 SLABS)
TYPICAL 4 INPUTS PER SLAB
LINEAR FAN IN
GATED BY BEAM PULSE GATE GEN
RESET FROM BEAM PULSE GATE GEN
TO EVENT INTERRUPT GENERATOR, FANOUT TO GATE LGS 1-6, DF 1-12, P, θ HODOSCOPES
RAPID KILL
NOT READ INTO CPU
PHA 6 (FIRST 4 SLABS)
NOTE 4
NOTE 2
NOTE 8
1568R23

Fig. 10

trigger pulse (CR1) and a single rear trigger pulse (OR2). The discriminators D14, D28 (Cerenkov counter), and D1-10 had 12-nsec output pulse lengths.

A likely electron event (event) was defined on the basis of fast logic performed on the output from the discriminators D14, D28, OR1 and OR2. An event gate pulse resulted if there occurred either a D14 pulse or a coincidence between D28 and (OR1 and OR2) -- (C5). This event gate pulse was fanned out to discriminator coincidence-discriminator (DCD) units receiving input from the hodoscope counters. The event gate pulse acted as a strobe to interrogate the state of the hodoscope counter discriminators and various discriminators in the fast electronics (electronics flags). Other important information about the event was the digitized pulse height of the signals from the TA counter, the Cerenkov counter, and the three dE/dx scintillation counters. A 50-nsec pulse was generated by an event and served as a coincidence gate for the signal pulses coming from these counters in linear gate and stretcher units (LGS) that preceded the analog-to-digital converters.

A latch-type flip-flop (rapid kill flip-flop) was set by the event pulse and reset immediately before the next beam pulse was due to arrive. The event pulse also set an interrupt flag in the computer which caused the computer to read-in the event information waiting in the buffers. The total event information was stored in 12 24-bit words, and it included the following: 55 theta-hodoscope counter bits, 41 momentum counter hodoscope bits, pulse-height channel numbers for the TA, Cerenkov, and three dE/dx counters, and various electronics flag bits. The total number of events was recorded on a scaler. However, not all of these events triggered a readout if more than one event occurred per beam pulse.

The fastest counting rate was in the front trigger counter discriminator and was normally kept below about 2 MHz by limiting the incident beam current. High counting rates, corresponding to large cross sections were obtained at low E'. Here, typically, the Cerenkov counter (D28) rate was a factor of 10 less than the front trigger and the shower counter (D14) rate was less than the Cerenkov rate.

The event rate was kept below about 0.3 per pulse by limiting the beam current. At this average rate, roughly 85% of the events trigger a computer readout of all event information.

The pulse height from the TA counter for an incident electron is proportional to the energy of the electron. The D14 discriminator threshold was set high enough to avoid triggers from very small TA pulses which were probably pions. At E' = 1 GeV, some electrons produced pulses less than this threshold. However, these would cause a C5 coincidence and not be lost. The event logic was chosen to avoid a large number of event triggers caused by the pion background at low E'.

3.7 Data Recording

All the information necessary to analyze the data was written on magnetic tape. This included the status of individual counters and pulse height information for each event trigger, the energy, spectrometer momentum and angle for the run, the target type, the scaler and beam monitor readings before and after the run, the spectrometer magnet shunt voltages, and typed-in comments about the run. Essentially all the information content of the experiment was recorded on the data tape and the experiment was "played back" many times in the course of the offline analysis.

An online SDS-9300 computer performed the data-logging function as its highest-priority task. An event trigger set a high-priority interrupt flag in the computer causing the program to branch to a subroutine that read the buffered event information into the computer core. The event information was placed in 12 24-bit words which were combined into blocks of 360 words to be written on magnetic tape. The event-logging operation was done rapidly enough to be completed in the time available between machine pulses (3 msec). For the remainder of the time the computer program was in a loop, servicing lower-priority interrupts as time allowed.

The event trigger also set an interrupt to branch to an analysis program. This program was quite sophisticated but the sampling fraction was only 25% for the highest event rates. Cross sections were calculated for various definitions of a good electron event and histograms were built up, showing distributions of the TA, Cerenkov and dE/dx counter pulse heights for various samples of events, and particle distribution across the hodoscope counters. A scope unit and line printer allowed display of selected program information during the run and at the end of the run a large amount of information about the run was dumped out in a fixed format on the line printer.

Most of the control of the experiment was channeled through the computer, for example, starting and stopping of runs and setting the spectrometer magnets. The scope display system allowed the experimenter to immediately inform himself of the status of any of the computer-controlled functions.

CHAPTER 4 --- ANALYSIS OF DATA

The data tapes were read and analyzed on an IBM-360-91 computer. The analyses consisted of two stages; in the first, the cross section for scattering from hydrogen defined by formula 2.1 (radiated cross section) was computed from the information on the tapes. This cross section includes effects of higher-order electromagnetic processes, e. g., photon radiation. The second stage is the radiative correction which is done, angle by angle, using all the measured cross sections at a particular angle.

A run is defined as an accumulation of event data caused by passage of N_{in} incident beam electrons through the target, for a particular initial beam energy E, spectrometer central angle , spectrometer energy E', and target type. The yield of electrons for a run was obtained from the number of events satisfying certain requirements (good electrons) based on the electron-discriminating properties of the counters. Three definitions of a good electron event were used with successively greater rejection of non-electron particles but also with successively decreasing electron detection efficiency.

Definition a: The TA counter pulse height, that is, the ADC channel number, was required to be greater than a certain value (TA cut). For a pure sample of electrons, the TA pulse-height distribution was Gaussian with mean and variance (σ^2) proportional to the electron energy. The TA cut was placed 2.8σ below the position of the mean (peak) of the electron distribution, so approximately 99% of the electrons produced a pulse in the TA larger than the cut. The number of pions contaminating the yield was estimated from the number of events having TA pulse height in a small window 1σ wide immediately below the position of the TA cut. Approximately 1% of the total number of electrons were expected to have pulse heights in this range, and the rest were assumed to be pions. The number of pions with pulse height greater than the TA cut was calculated from the number of pions observed in the 1σ window by assuming the pion pulse height had a falling exponential form.

Calculation of the pion contamination in this way mainly served as a quantitative check that the pion contamination was small. The correction was generally less than 1%, and the largest full target correction was 4%.

A correction was made for the inefficiency introduced by the TA cut which was nominally 1%. This was done for all runs with good statistics (greater than 100 good electron events) by fitting the observed electron peak in the TA pulse-height distribution with a Gaussian and using this analytic form to calculate the number of electrons falling below the TA cut. It was found possible to make fits to a Gaussian that were satisfactory in a chi-squared sense. Also, it was checked that the calculated yield was quite independent of the TA cut, even for inefficiency corrections as large as 30%.

Definition b: In addition to the TA cut, events were required to have Cerenkov counter pulses larger than a minimum level (Cerenkov cut). The cut was such that 97% of a pure electron sample produced pulse heights greater than the cut. The yield was corrected for the 3% inefficiency introduced.

Definition c: In addition to the requirements of b, the minimum pulse height from the dE/dx scintillation counters had to be larger than a certain value (dE/dx cut). The distribution of minimum dE/dx pulse height for an electron sample showed a prominent peak corresponding to a single fast electron passing through the three scintillators, and less distinct secondary peaks at approximately 2,3,4 times the pulse height of the first peak, evidently corresponding to the creation in the initial radiator of additional particles. The dE/dx cut was placed in the first valley of the minimum dE/dx pulse height distribution. The efficiency of the dE/dx system used in this way, for a pure electron sample was 0.606, 0.741 and 0.799 at secondary electron energies of 1, 2, and 3 GeV. It was found possible to fit the dE/dx efficiency as a function of E' by a polynomial of order 2 in 1/E'. The three parameters of the fit can be taken as the values of the efficiency at 1, 2, and 3 GeV as given.

The dE/dx efficiency was considered uncertain by 1.5%, so yields calculated on the basis of Definition c have this additional error added linearly.

All good electron events were required to have the front-rear trigger counter coincidence circuit (C1) flag set. Also the event was required to show a hodoscope bit pattern corresponding to the particle passing unambiguously through the range of momentum counters 5-36 and the range of theta counters 4-51. Corrections were made for C1 inefficiency (typically 1 to 2%), and for ambiguous or undecipherable hodoscope patterns (typically 7%).

The total spectrometer acceptance defined by the hodoscope was $(\Delta p/p)\Delta\Omega = 21.64 \times 10^{-6}$ sr. The cross section was also calculated for each run, ignoring the hodoscope information and using the calculated total acceptance of the trigger counters, 25.40×10^{-6} sr. The yield for this cross section did not require an ambiguous code correction and for kinematic regions where the cross section was slowly varying over the spectrometer acceptance, which was the usual case, these two cross sections were found to agree typically to 1%.

The yield was corrected for computer deadtime, that is, events not logged on tape, by multiplying by the ratio of the number of events recorded on a scaler to the number of events actually found on the data tape. This correction was less than 20% and is considered well known since it just represents an unbaised sampling fraction.

For each line the definition of a good electron a, b, or c was chosen on the basis of agreement between the three yields. The least restrictive requirement was preferred in order to maximize the number of good events and hence the statistical accuracy. However, the point on a line where two yields began to disagree because of pion contamination was the point where the more restrictive requirement began to be used.

For each run a cross section was calculated using the formula,

$$\frac{d\cdot}{d\Omega dE'} = \frac{N}{N_{in}\, n(\Delta p\Delta\Omega)}$$

where N is the corrected electron yield, $\Delta p\Delta\Omega$ is the acceptance, n is the number of protons/cm^2 in the target hydrogen, and N_{in} is the number of incident electrons for the run.

For the three lowest energy 18^o lines only, the data were taken with spectrometer settings overlapped to produce a continuous cross section spectrum in the resonance region. In this case the spectrometer acceptance was divided into missing mass bins using the p and θ hodoscopes, and the cross section was calculated for each bin. The bins were set up with an E' width at the central angle of 0.002 times the secondary elastic scattering energy at that angle. This bin width is larger than the resolution of the spectrometer and was selected in order to decrease the statistical errors while still adequately resolving the resonance missing mass structure. The missing energy bins were constructed to be symmetrical in θ about the spectrometer central angle.

For some of the runs an acceptance correction was necessary because 2 aluminum NMR probes in the spectrometer bending magnets were accidentally left projecting into the active aperture of the spectrometer. The effect of these probes was measured and found to be small but energy dependent. This energy dependence was fit by a form $a + b/E'^2$. The $1/E'^2$ term is attributed to multiple scattering of electrons outside the angular acceptance in the aluminum of the probes. This correction was 4.5% at $E' = 2$ GeV and 3.3% at $E' = 4$ GeV. For cross sections with a probe correction the error is increased by 1.5% added linearly.

The final measured cross section for scattering from hydrogen was calculated from the full target cross section, subtracting the dummy target cross section and the reversed spectrometer polarity cross section (positron cross section), and adding the positron dummy cross section. Generally, the dummy cross section was measured at every setting, but the positron and positron dummy cross sections were insignificant except at the lowest E' points. The largest positron background occurred for the highest energy 18° line. For this line (E = 18 GeV) at E' = 2 GeV, the reversed polarity cross section was 27% of the full target cross section, at E' = 2.5 GeV this percentage was 11% and at E' = 3 GeV it was 6%.

The ratio of dummy to full target cross section was usually in the range 10 to 20%. This roughly agrees with what we would expect if the high q^2 virtual photons were absorbed independently by the nucleons in the aluminum and Mylar that constituted the dummy target and if the neutron cross section were some fraction of the proton cross section. The ratio of protons/cm² along the beam path of the dummy target to that for the full target was 0.09 while the ratio of nucleons/cm² was 0.17. Thus we would expect a dummy to full ratio in the range 0.09 to 0.17.

The final measured cross section is the cross section for scattering from a proton allowing radiation of photons, and it depends somewhat on the radiation length of the target and other material before and after the point of scattering. The second stage of the data analysis required all the measured cross sections at a single angle as input and yielded radiatively corrected cross sections, which are the (theoretical) cross sections for the electron scattering process calculated to first order in α, that is, corrected for the known effect of higher order in α processes. These include radiative processes occurring before and after the scattering as well as radiation during the scattering and electrodynamic corrections to the electron-photon vertex and the photon propagator.

The radiative correction formulas are discussed in detail in the Appendix. The relation of the radiatively corrected cross section to the measured cross section is given by formula A.V.5 of the Appendix. The integrals in this formula require knowledge of the corrected cross section along a line of constant E and a line of constant E' in the E,E' plane (for fixed θ) so values for the integration must be supplied by interpolating and extrapolating the already corrected cross section from the E,E' points where the cross section is actually measured. The corrected cross section values when interpolated and extrapolated throughout the triangle according to the particular scheme chosen, have the property of satisfying Eq. A.V.5 for the E,E' values of every measured point.

There were two main difficulties in making the radiative correction. One is that the cross sections were not determined at a sufficiently dense set of E,E' points particularly in the resonance region, so that different reasonable methods of interpolation or extrapolation of the cross section within the triangle could produce at some points a considerable variation in the result. The sensitivity to the method of interpolation-extrapolation was investigated and only those data points for which the corrected cross section was independent of the method to within one-half of the error bar were included in the final results.

The second difficulty is due to the approximate nature of Eq. A.V.5 in the first place. The radiative tail from inelastic hadronic transitions is only approximated in terms of the two one-dimensional integrals over the corrected cross section. More accurately it is expressed as a two-dimensional integral involving the two form factors $W_1(q^2,W^2)$ and $W_2(q^2,W^2)$ in a different combination from $W_2 + 2\tan^2(\theta/2)W_1$ in which they appear in the cross section. The peaking approximation reduces the two-dimensional integral to two one-dimensional integrals and what can be called the factorization approximation allows the integrand in these integrals to be expressed in terms of the cross section. The validity of the peaking-factorization approximation has been tested for different models of W_1 and W_2, and on this basis the particular form for the equivalent radiators used (formula A.V.7) was selected. The peaking-factorization approximation is only valid to the order of 10%, so Eq. A.V.5 can be used only as long as the error introduced in this way is tolerable.

There are also theoretical uncertainties about the effect of multiple photon radiation. However, these uncertainties are parameterized by the limiting soft-photon energy k_1 appearing in A.V.5 and defined by formula A.V.9.

For photon energy below k_1, multiple photon effects are taken into account, assuming the photons are soft and have no effect on the electron from which they are emitted. For photon energies above k_1 all multiple processes are neglected and only single photon radiation is allowed. By varying k_1 by replacing the 1/3 appearing in formula A.V.9 by other fractions from 0.2 to 0.8 the sensitivity to multiple photon effects was tested. The corrected cross sections generally changed very little and at most by 2 to 3%.

There are also theoretical uncertainties about the effect of radiation from the proton and the final hadronic state. For the case of radiation from elastic scattering, this effect can be estimated and it results in about a 15% increase in the radiative tail at the points with highest momentum transfer to the proton. However, most of the radiative tail comes from hadronic transitions with low momentum transfer so this uncertainty is thought to be smaller than or comparable to that introduced by the peaking-factorization approximation.

The radiative correction increased the error of the measured cross section due to uncertainties in the subtracted radiative tails. Formula A.V.5 can be written as follows:

$$\frac{d\sigma}{d\Omega dE'} = C\left[\frac{d\sigma_{RAD}}{d\Omega dE'} - \text{ELASTIC TAIL-INEALSTIC TAILS}\right] \quad (1)$$

The error was calculated using the formula,

$$\delta\left(\frac{d\sigma}{d\Omega dE'}\right)^2 = C^2\left[\delta\left(\frac{d\sigma_{RAD}}{d\Omega dE'}\right)^2 + \delta(\text{ELASTIC TAIL})^2 + \delta(\text{INELASTIC TAILS})^2\right] \quad (2)$$

The elastic tail was assigned a 3% uncertainty and the inelastic tails given by the two integrals in A.V.5 a 10% uncertainty. The formula 2 for the error neglects the correlation between the first terms in Eq. (1) and the subtracted integrals, so it is correct only for large values of the parameter $\Delta E'$ in A.V.5. For the purposes of error propagation $\Delta E'$ was taken to be the interval between measured points along a line. For 18° this is basically 0.5 Gev, except for the three continuous spectra where it is $0.002 \times E'_{ELASTIC}$. For 26° and 34° it is 0.25 GeV. The actual radiatively corrected cross section was not dependent on the choice of $\Delta E'$ for sufficiently small $\Delta E'$. For example, the last point on the 26°, 18 GeV line changed by 0.2% as $\Delta E'$ was changed by a factor of 4 from 1.1 MeV to 4.5 MeV.

For larger angles the radiative correction became slightly smaller. For 18°, the largest radiative correction occurred for E = 17 GeV, E' = 2 GeV. At this point the elastic tail was 18% of the measured cross section and the total radiative correction factor was 0.54. The error bar was increased by a factor 1.21 by the radiative corrections.

At 26° the largest radiative correction, at E = 18 GeV, E' = 1.75 GeV was 0.70 with the elastic tail 11% of the measured cross section. The error was amplified by a factor 1.23. At 34° the largest correction was 0.78 at E = 15 GeV, E' = 1.5 GeV with the error amplified by a factor 1.15. At that point the elastic tail was 11% of the measured cross section.

CHAPTER 5 --- RESULTS

The inelastic electron-proton cross section data have certain qualitative features that allow the definition of three separate kinematic regimes in the q^2- W^2 plane. These regimes are characterized by three types of behavior that can be thought of as analogous to the behavior of the cross section for electron scattering from an atom. First, there are resonance bumps in the cross section at fixed values of missing mass W which seem to be the result of transitions of the proton to quasi-discrete higher energy excited states. These bumps are evident only for $W \lesssim 2$ GeV. The form factors for these transitions are decreasing rapidly with q^2 like the elastic form factors.[13] Second, for large q^2 and $W \gtrsim 2$ GeV there is a smooth continuum cross section which is analogous to the cross section for the process of knocking out orbital electrons from an atom. If effects caused by the identity of the incident electrons with the atomic electrons are ignored, the continuum cross section from the single ionization process would be given by a sum of contributions from the individual electrons in the atom, each with W_1 and W_2 given by E.17. Since the electron is pointlike, $G_E^2 = G_M^2 = 1$. Going over to the variables $x = q^2/(2M\nu)$ and ν, where M is the mass of the atom, we would have

$$W_1 = Z \frac{1}{2M} \delta(x - m/M)$$

CHAPTER 5 --- RESULTS

$$W_2 = Zx/\nu \quad \delta(x - m/M) \qquad (1)$$

where m is the electron mass and Z is the number of electrons in the atom.

The electron-proton continuum cross section for $q^2 \gtrsim 1$ GeV^2 has this type of behavior in that νW_2 and $q^2/\nu W_1$ appear to be the same function of a single variable q^2/ν, albeit not a delta function. This is the principal result of the SLAC inelastic electron scattering experiments and is referred to as scaling.

The third type of behavior occurs for high energies $\nu \gtrsim 5$ GeV and small $q^2 \lesssim 1$ GeV^2, that is, near the photoproduction region. There diffraction production processes seem to dominate. The term diffraction here is used to describe processes analogous to the pair production processes that dominate photoproduction from an atom at high energies. In the case of electron scattering from an atom for $q^2 \rightarrow 0$, single electron ionization is not possible since the energy transfer to the atomic electron, given by $\nu = q^2/2m$, must be zero. As q^2 increases, the probability of diffraction-type processes rapidly decreases relative to ionization processes, and the atom begins to look like a collection of independent electrons. The diffractive character of the data in the photoproduction region is evidenced by the apparent approach of σ_T to a constant for large ν.

Diffraction behavior of σ_T disagrees with scaling behavior, i.e., if νW_2 is a function of q^2/ν, then σ_T is falling like $1/\nu$ for small q^2, so the two regimes can logically be separated. Similarly, resonance behavior is not a special case of scaling behavior, that is, resonance bumps do not occur at a fixed value of q^2/ν.

The large angle data exist principally in the deep inelastic region, namely, $W > 2$ GeV and $q^2 > 1$ GeV^2, where the scaling behavior first observed at smaller angles[2] would be expected. The structure functions σ_T and σ_S defined by B.10 were separately determined at cross-over points in this region where cross section data existed from 3 or more angles at the same values of q^2 and W^2. The cross section divided by Γ as a function of is fit to $\sigma_T + \epsilon\sigma_S$. Figure 11 shows plots of $d\sigma/d\Omega dE'/\Gamma$ versus ϵ for the 3 cross-over points. The dotted straight lines correspond to 1 standard deviation changes of σ_T and σ_S up and down from the best fit values. The best fit to the data in each case is a straight line centered between the two dotted lines. The solid curve is a global fit to all the large angle data that will be discussed in detail later. It corresponds to a constant ratio of $\sigma_S/\sigma_T = R = 0.15$. The data indicate that R is small in the deep inelastic region and consistent with the value 0.15.

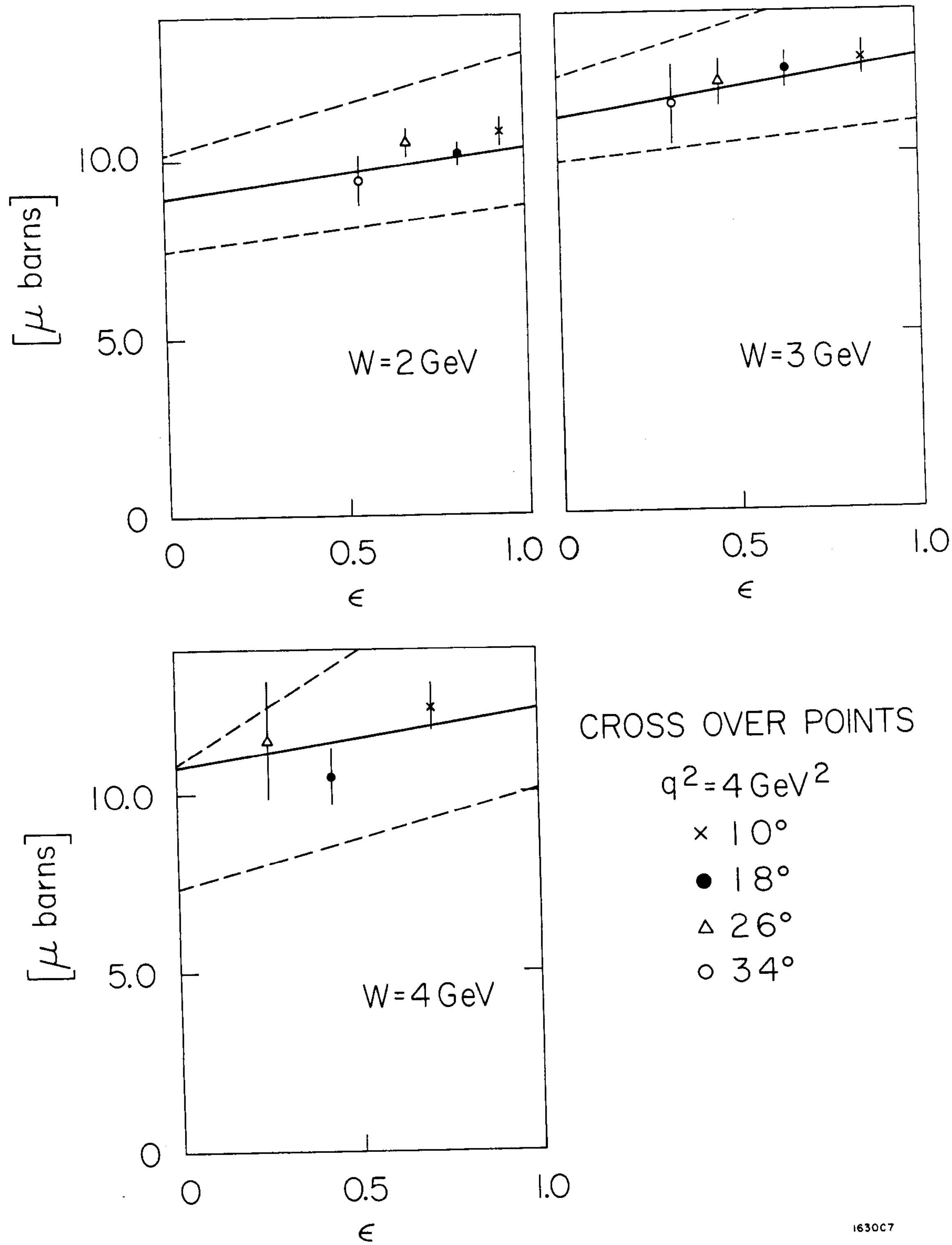
10.0
5.0
0
[μ barns]
W=2 GeV
0
0.5
1.0
ε
W=3 GeV
0
0.5
1.0
ε
W=4 GeV
0
0.5
1.0
ε
CROSS OVER POINTS
q2=4 GeV2
× 10°
● 18°
△ 26°
○ 34°
163OC7

Fig. 11

CHAPTER 5 --- RESULTS

We expect on very general grounds that scaling holds in the limit q^2, $W \longrightarrow \infty$. Assuming a small value of R, the quantity νW_2 extracted from the large-angle data for $W > 1.8$ GeV was found to roughly fall on a universal curve as a function of a single variable $x = q^2/(2M\nu)$. It was found that the universality of νW_2 could be improved, particularly for smaller W values, by another choice of the scaling variable than the quantity x. This new variable is $x' = q^2/(q^2+W^2+a-M^2)$ with $a \cong M^2$. The quantity a was allowed to vary and it was found that $\nu W_2|_{R=.15}$ for the large-angle data with $W > 1.8$ GeV was most universal for $a = 0.96$ GeV^2. Linearizing the dependence of νW_2 on a for small variations in a, the chi-squared error matrix gave the error in a to be $\pm$ 0.08 GeV^2.

Plots of all the large-angle data for $W > 1.8$ GeV versus x' are shown in Fig. 12, The solid curve is a fit to the data for the case $R = 0.15$ and for comparison the same curve is plotted for $R = 0$ and $R = 0.3$ as well. Statistically the νW_2 data for $R = 0.15$ is perfectly consistent with a single universal curve depending on x'. The chi-squared for the fit was 119 for three parameters and 186 data points. Only 7 of the 186 points were more than 2 standard deviations from the fit. Since νW_2 seems to have a simple threshold behavior at $x' = 1$, the fitting function was chosen to be a polynomial in $(1-x')$ with as few terms as possible. The fit shown was obtained with three terms, a

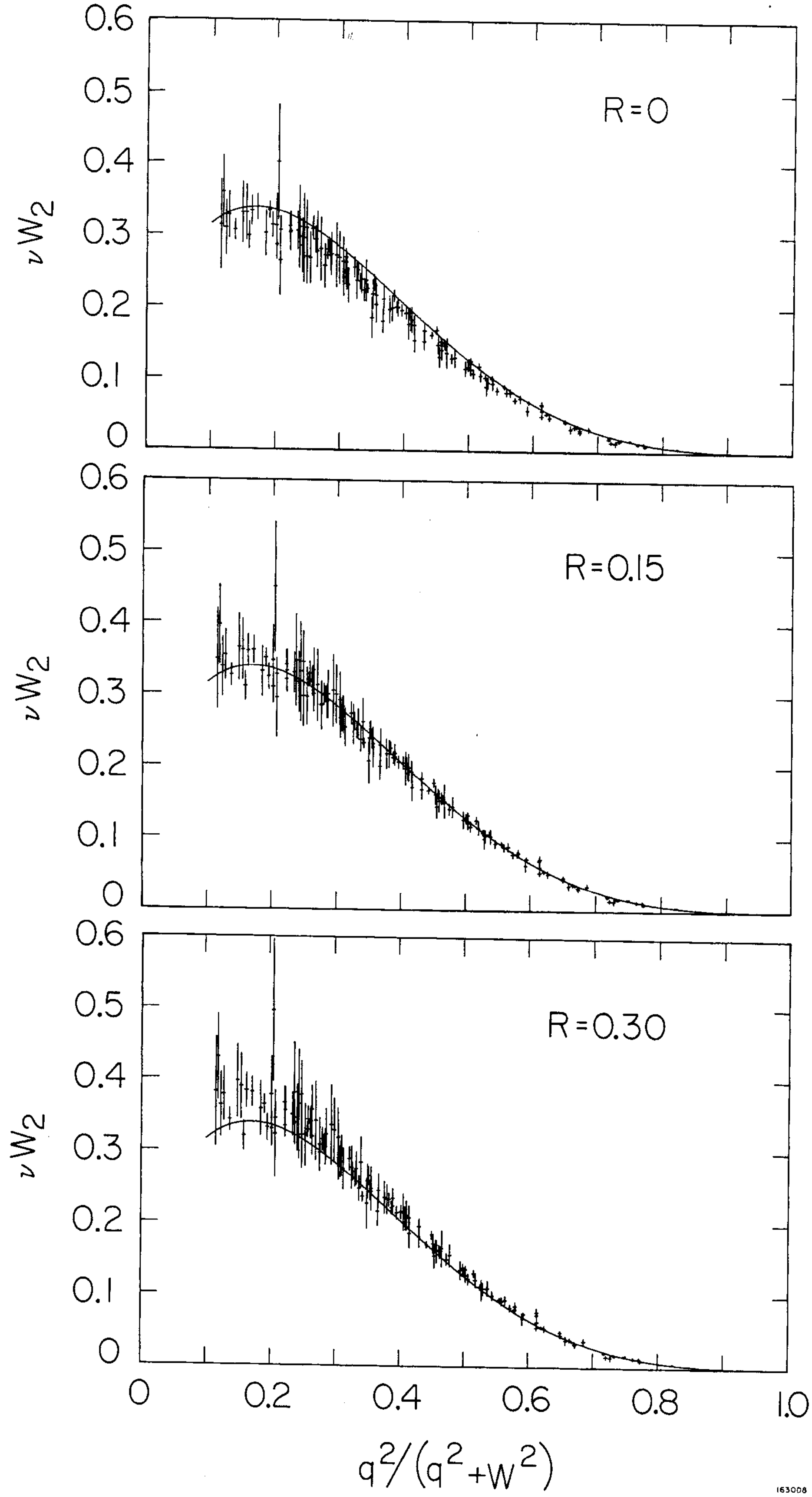

Fig. 12

cubic term, a fourth-order term, and a fifth-order term, as follows:

$$\nu W_2 = P(1-x') = C_3(1-x')^3 + C_4(1-x')^4 + C_5(1-x')^5$$

$$C_3 = .557$$

$$C_4 = 2.1978$$

$$C_5 = -2.5954 \qquad (2)$$

The cross section is given by

$$\frac{d\sigma}{d\Omega dE'} = \frac{\alpha^2}{4E^2}\,\frac{\cos^2\ \theta/2}{\sin^4\ \theta/2}\left(1 + \frac{2\tan^2\ \theta/2\,(1+\nu^2/q^2)}{1.15}\right)\frac{P(1-x')}{\nu} \qquad (3)$$

This fit obtained from the large-angle data also represents very well the 6° and 10° cross section data in the deep inelastic region $q^2 > 1$ GeV², $W > 1.8$ GeV over the range of the fit $0.8 > x' > 0.1$. For the 114 6° points in this kinematic region the total chi-squared was 114. For the 132 10° points the chi-squared was 91.

Figure 13 shows the dependence of νW_2 on W for constant $\omega = (2M\nu)/q^2$. The solid curve is the fit to the universal curve $P(1-x')$. The point $q^2 = 1$ GeV² is indicated on each graph. The main difference between the contours x = constant and x' = constant comes in the region of low W, where there are resonances. Along an x' contour the resonances appear to average out, while along an x contour the resonances are consistently high. For high W the difference between x and x' disappears. Scaling in the

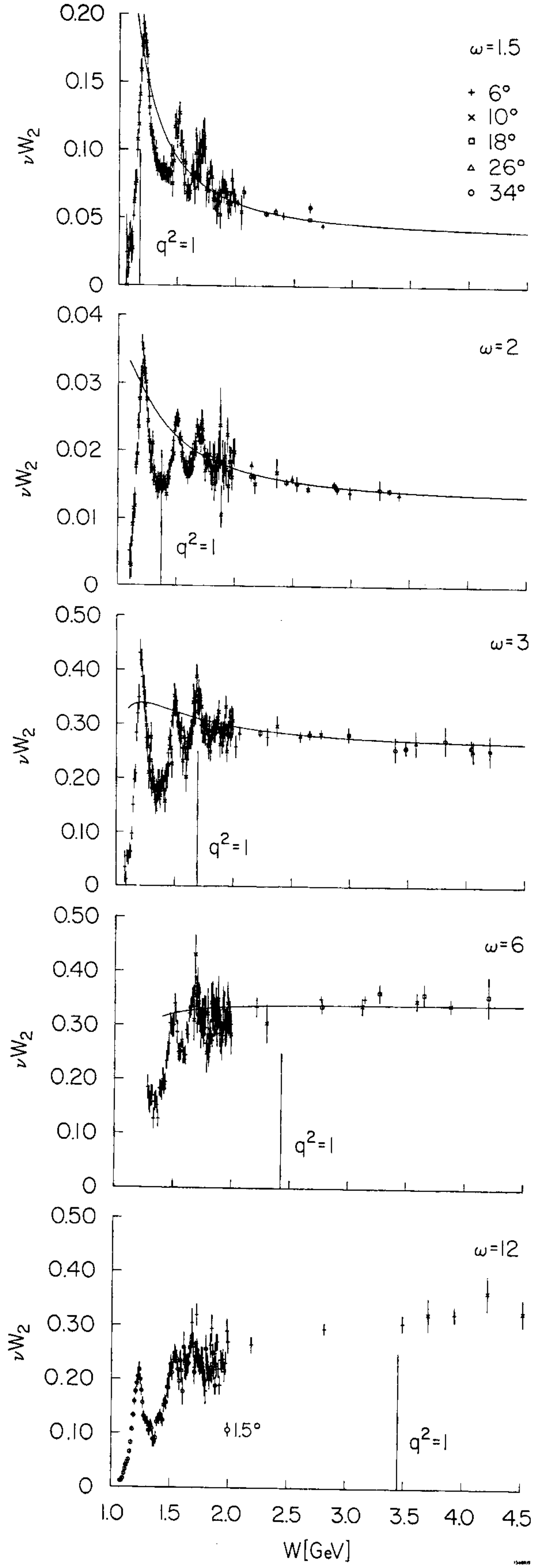

Fig. 13

variable x holds only for $W > 3$ GeV; for lower W the tails from the resonance region seem to make the data high relative to the $W \rightarrow \infty$ limit. For $q^2 < 1$ GeV^2, νW_2 seems to fall below the asymptotic limit. To the accuracy of the present data, the asymptotic scaling limit seemes to be reached for $W > 3$ GeV and $q^2 > 1$ Gev^2.

If we evaluate the universal curve fit given by $P(1-x')$ in the resonance region we obtain the interesting result shown in Fig. 14. The universal curve seems to go through the average value of the resonances and the elastic peak, although the elastic peak is not shown on these graphs. Comparison with the 6 and 10 degree data shows the same striking behavior, that the universal curve as a function of x' seems to pass in an average sense through the resonances and the elastic peak. Bloom and Gilman[14] discuss the significance of this.

From an empirical standpoint the x' contour is significant in that it allows a better determination of the $q^2 \rightarrow \infty$ νW_2 scaling function from the data at finite q^2. νW_2 can be fit as a universal function of x only for $W > 3$ GeV. The universal curve is then obtained only in the range of x from 0.1 to 0.6. This curve is shown in Fig. 15 along with the universal curve obtained by fitting νW_2 to a function of x' for $W > 1.8$ GeV. The universal curve obtained from the x' fit extends over the range of x' from 0.1 to 0.8.

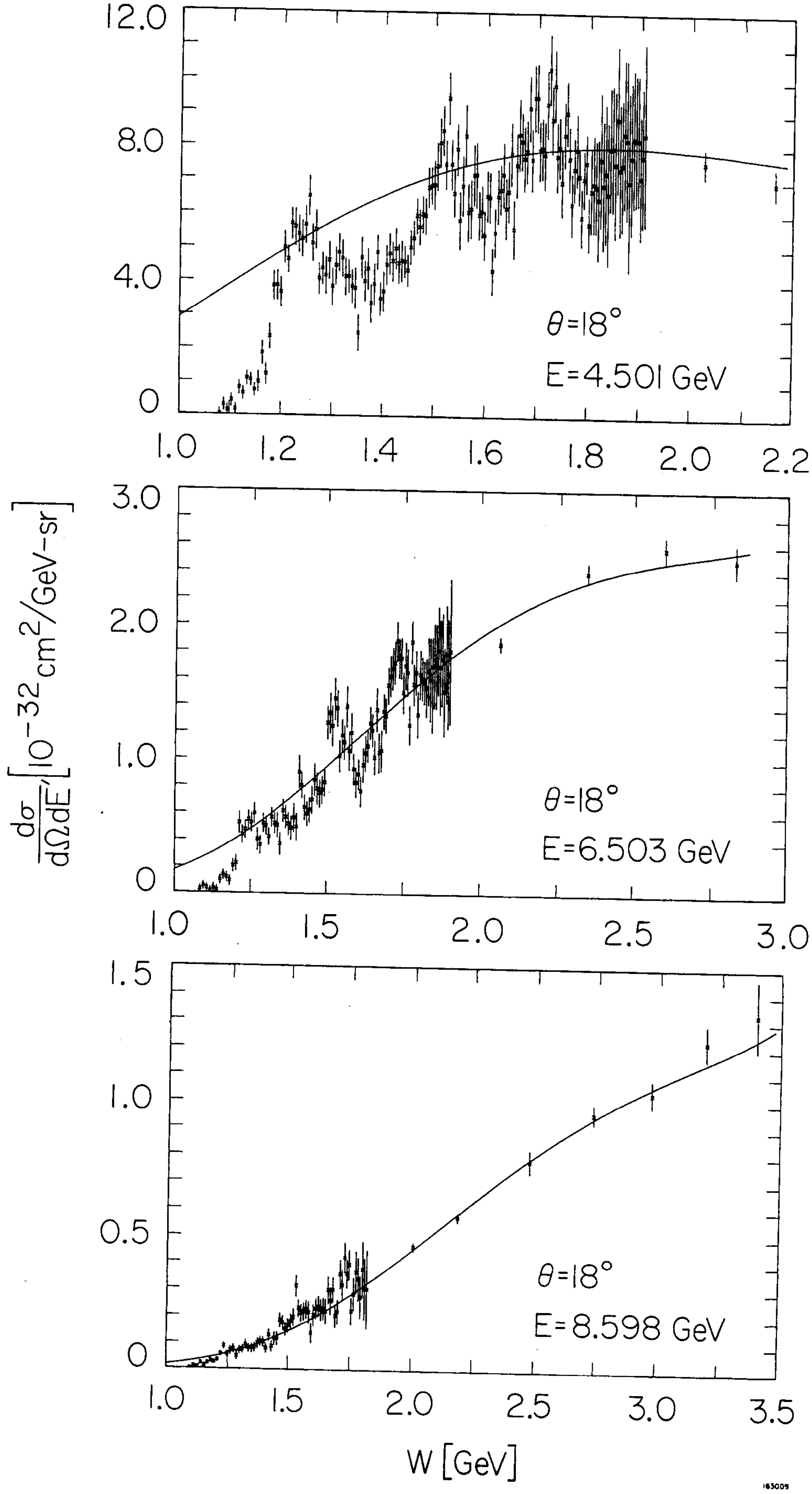

12.0
8.0
4.0
0
1.0 1.2 1.4 1.6 1.8 2.0 2.2
θ=18°
E=4.501 GeV
3.0
2.0
1.0
0
1.0 1.5 2.0 2.5 3.0
θ=18°
E=6.503 GeV
1.5
1.0
0.5
0
1.0 1.5 2.0 2.5 3.0 3.5
θ=18°
E=8.598 GeV
dσ/dΩdE′ [10⁻³² cm²/GeV-sr]
W [GeV]
163009

Fig. 14

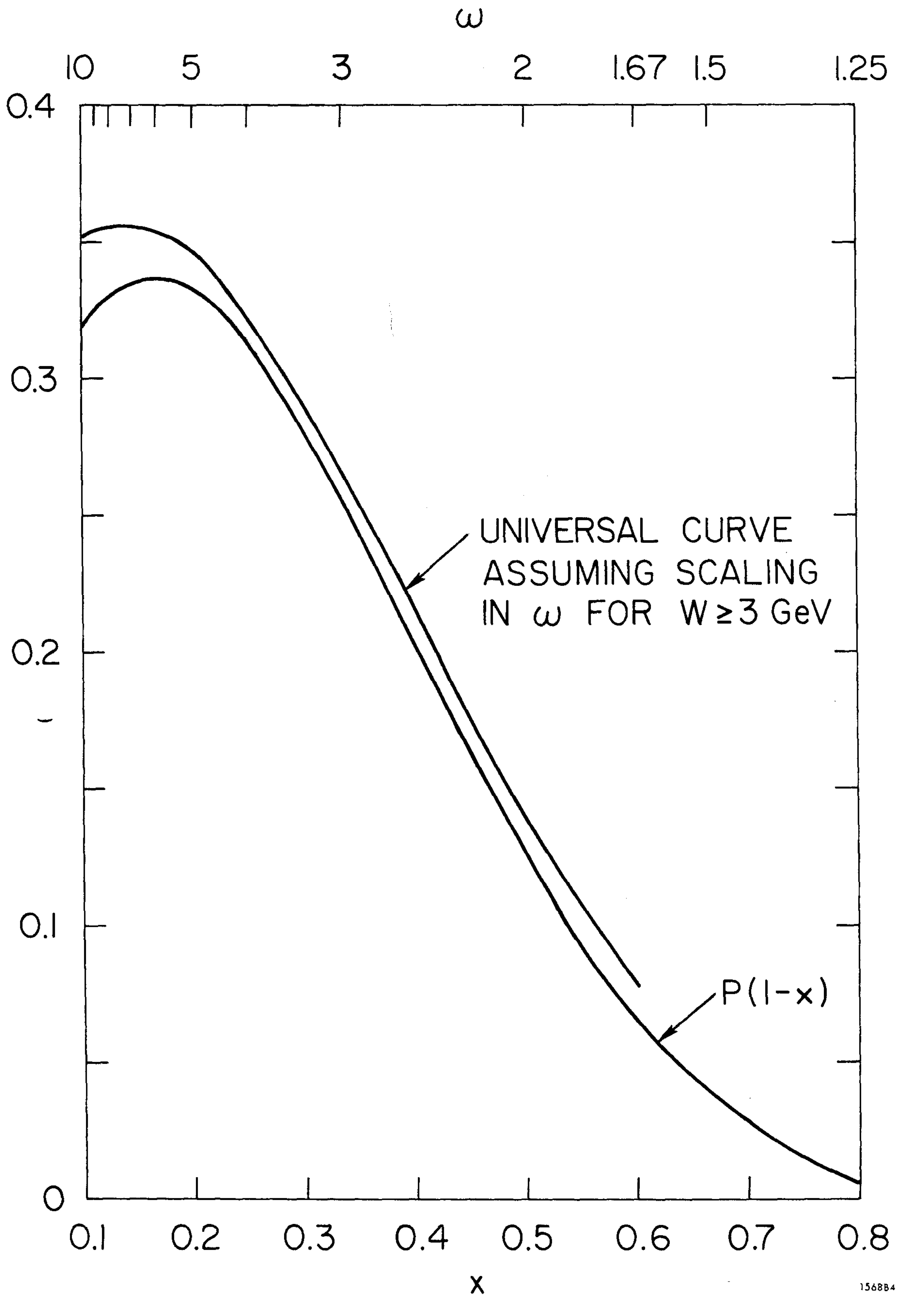
ω
10
5
3
2
1.67
1.5
1.25
0.4
0.3
0.2
0.1
0
UNIVERSAL CURVE
ASSUMING SCALING
IN ω FOR W ≥ 3 GeV
P(1-x)
0.1
0.2
0.3
0.4
0.5
0.6
0.7
0.8
x
1568B4

Fig. 15

CHAPTER 5 --- RESULTS

A method was used to interpolate the cross sections from each angle within the q^2 - W^2 triangle that depends on the universal (x') behavior of νW_2 in the deep inelastic refion and substantially reduced the error bars, refining the determination of R. Essentially νW_2 was averaged for constant x'. To obtain the cross section at a particular point q^2,x' first interpolated cross sections were obtained for that same value of x' along each line. A line corresponds to one of the initial energies for a particular angle. Then, assuming a small value of R, νW_2 was calculated from the interpolated cross sections from each line, and these values were averaged. Finally, using the assumed value of R, the average νW_2 was used to calculate the interpolated cross section. Only data in the deep inelastic region W > 1.8 GeV and q^2 > 1 GeV^2 were used in this procedure. Statistically νW_2 appeared to be fluctuating as expected about its mean value in the averaging process.

Typical plots using interpolated data are shown in Fig. 16. Again, the solid curve represents the global universal curve fit given by Eq. (3). The error bars are greatly reduced but the chi-squared distribution for the straight-line fits was quite good, which indicates that the error bars of the interpolated cross sections are not too small. Twenty separations of σ_T and σ_S were made using interpolated data. For these twenty fits the quantity

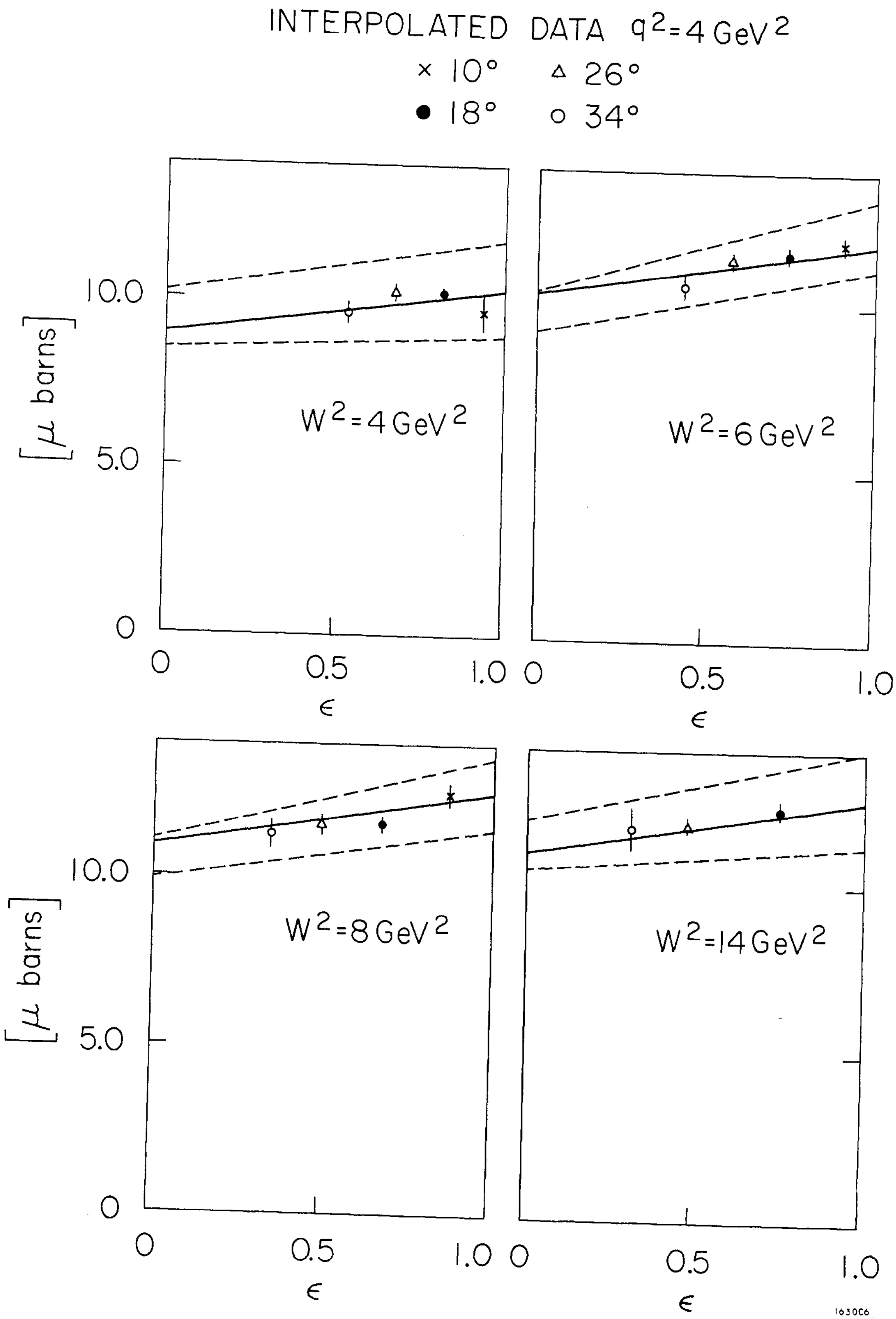
INTERPOLATED DATA q2=4 GeV2
× 10°
△ 26°
● 18°
○ 34°
10.0
5.0
0
[μ barns]
W2=4 GeV2
W2=6 GeV2
W2=8 GeV2
W2=14 GeV2
0
0.5
1.0
ϵ
1630C6

Fig. 16

$(\chi^2-n_D)/\sqrt{2n_D}$ was always less than 0.7. n_D is the number of degrees of freedom of the fit and a standard chi-squared distribution has mean n_D and variance $2n_D$.

This interpolation procedure depends on an assumed R value, but investigation showed this to have a small effect on the outcome for an assumed R in the range 0 to 0.5.

The ratio of σ_S to σ_T is always small. Taking into account systematic errors it is felt that $R = \sigma_S/\sigma_T$ is in the range .05 to 0.3 in the deep inelastic region. The data are not accurate enough to indicate any kinematic dependence and an adequate fit is to a constant value of R near 0.15.

The separated values of σ_T and σ_S are summarized in Figs. 17 and 18. Figure 17 shows σ_T and σ_S for constant q^2 = 1.5, 4, and 8 GeV² as a function of W^2 or ν. At $q^2 = 0$, i.e., photoproduction, σ_S is zero and σ_T falls from about 140 μb at W = 2 GeV to about 120 μb at W = 4 GeV. The solid curve is from universal curve fit given by formula 2 of this chapter, which assumes R = 0.15.

These measurements show σ_T and σ_S do not conform to the usual behavior of strong interaction total cross sections as functions of energy. At q^2 = 8 GeV² σ_T is increasing with energy quite far outside of the resonance region. These conclusions are not affected by other definitions of the virtual photon total absorption cross sections, for example, by using the definitions given in formula B.12.

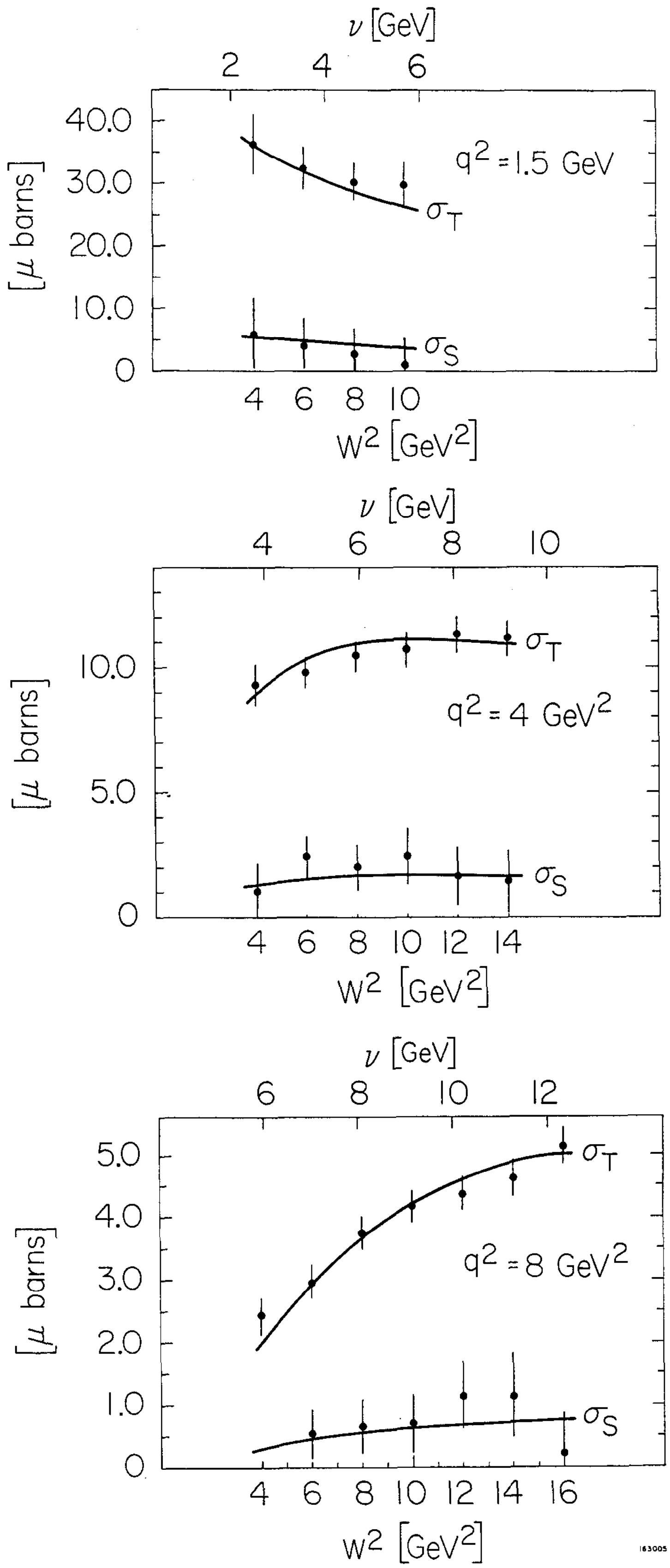

ν [GeV]
2
4
6
40.0
30.0
20.0
10.0
0
[μ barns]
q2 = 1.5 GeV
σT
σS
4
6
8
10
W2 [GeV2]
ν [GeV]
4
6
8
10
10.0
5.0
0
[μ barns]
σT
q2 = 4 GeV2
σS
4
6
8
10
12
14
W2 [GeV2]
ν [GeV]
6
8
10
12
5.0
4.0
3.0
2.0
1.0
0
[μ barns]
σT
q2 = 8 GeV2
σS
4
6
8
10
12
14
16
W2 [GeV2]

Fig. 17

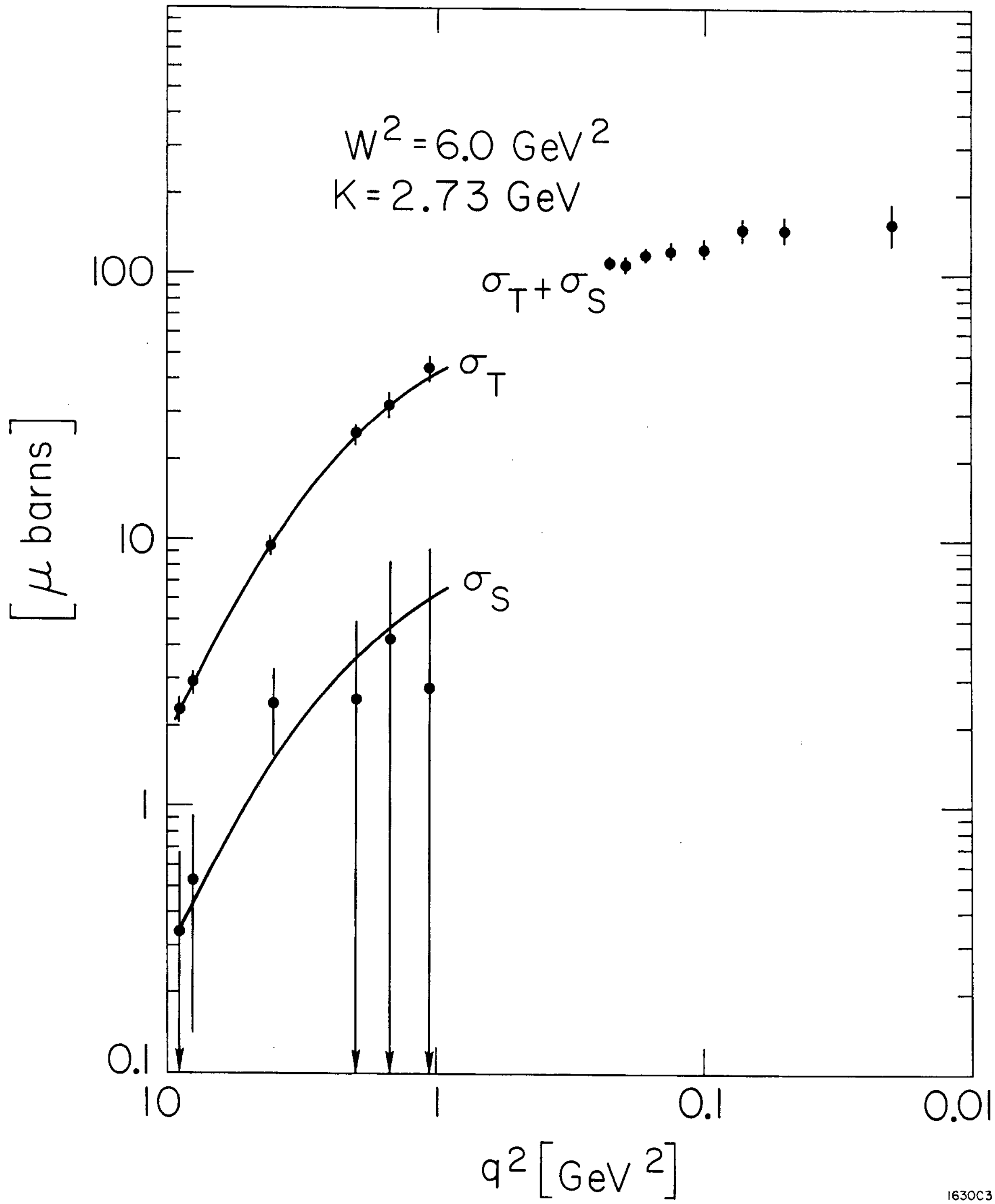
W^2 = 6.0 GeV^2
K = 2.73 GeV
$\sigma_T + \sigma_S$
σ_T
σ_S
[μ barns]
100
10
1
0.1
10
1
0.1
0.01
q^2 [GeV^2]
1630C3

Fig. 18

CHAPTER 5 --- RESULTS

Figure 18 shows the dependence of σ_T and σ_S on q^2 for constant W. The low q^2 points represent measurements at 1.5° done earlier by the SLAC-MIT collaboration.[15] No separation was possible, but at this small angle ϵ is near 1, so the cross section is proportional to $\sigma_T + \sigma_S$. Again, the solid curve is from the global universal curve fit which assumes R = 0.15. On such a log-log plot the slope of the σ_T curve indicates that it is falling like $1/q^4$ at the highest q^2, q^2 = 10 GeV^2.

The most interesting result of the large angle measurements is the determination of the universal curve over the region $0.1 < x < 0.8$. Figure 19 shows $\log(\nu W_2)$ plotted against $\log(1-x')$ under assumption of different values of R. νW_2 is consistent with a simple $(1-x')^3$ threshold dependence near $x' = 1$. On the basis of a field theoretic parton model, Yan and Drell[16] predicted that the universal curve would have a threshold dependence given by $(1-x)^p$, where p + 1 is the inverse power of q characterizing the $q^2 \longrightarrow \infty$ behavior of the elastic form factor, i.e., $G_M \longrightarrow (1/q)^{p+1}$.

This type of behavior of the deep inelastic continuum has very interesting consequences. If we assume that the elastic scattering is given by the usual dipole form, then as $q^2 \longrightarrow \infty$,

$$\nu W_2\Big|_{\mathrm{ELASTIC}} \longrightarrow (2.793)^2\, q^2 \left(\frac{.71}{q^2}\right)^4 \delta(W^2 - M^2)$$

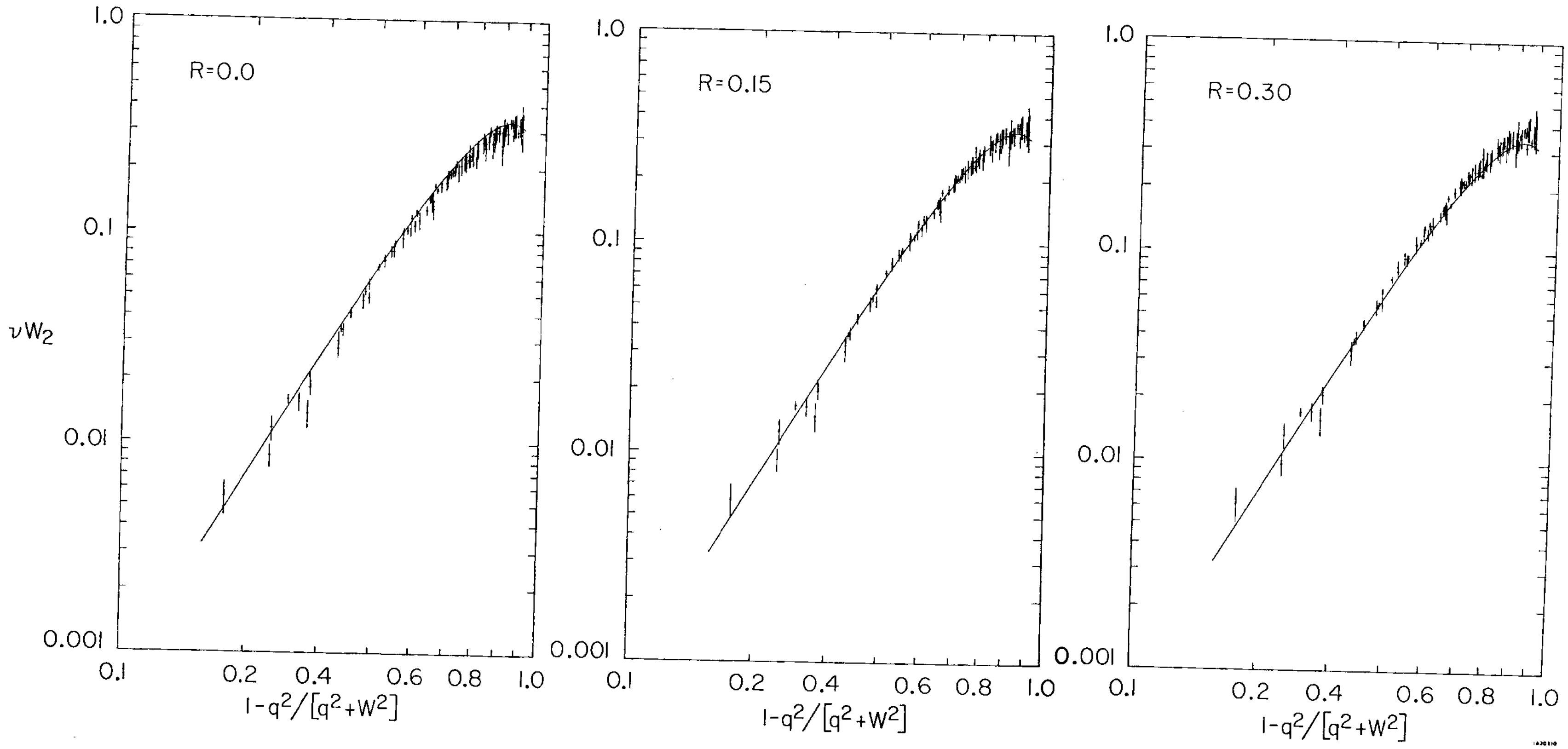

Fig. 19

It appears that the resonances show a similar q^2 dependence to that of the elastic peak, so that

$$\nu W_2\Big|_{\text{RESONANCE}} \sim \frac{1}{q^6}\,\delta\left(W^2 - M_j^2\right)$$

If we assume a $(1-x)^3$ threshold dependence of the universal curve, we have in addition

$$\nu W_2\Big|_{\text{CONTINUUM}} \longrightarrow C_3\left(\frac{W^2}{q^2}\right)^3$$

Thus, the elastic peak, resonances, and the inelastic continuum may all be asymptotically falling with the same power of q^2 and the continuum background seems not to have a much slower falloff with q^2 than either the resonances or the elastic peak.

From a theoretical standpoint, certain moments of the universal curve are particularly interesting. In the parton theories[17] the following integrals appear:

$$\int_0^1 F(x)\,dx = \overline{\sum_i} \lambda_i^2 \overline{x_i}$$

$$\int_0^1 F(x)\,\frac{dx}{x} = \overline{\sum_i} \overline{\lambda_i^2} \qquad (3)$$

where $F(x)$ is the asymptotic νW_2 curve, λ_i is the charge of the i-th parton, and x_i is its fractional longitudinal momentum in the infinite momentum frame. If only integral charges are allowed, the second integral represents the average number of charged partons and hence must be greater than 1.

Figure 20 shows the behavior of νW_2 at constant q^2 for $q^2 = 1.5$, 4, and 8 GeV^2. The solid curve is $F(1-x')$ given by formula 2. The data for $q^2 = 1.5$ GeV^2 was used to evaluate numerically the integrals (3) over the partial range x = 0.1 to 1. The results were

$$\int_{.1}^{1} \nu W_2 \, dx \Big|_{q^2=1.5} = .156 \pm 2\%$$

$$\int_{.1}^{1} \nu W_2 \frac{dx}{x} \Big|_{q^2=1.5} = .563 \pm 2\%$$

The errors reflect only the variation in νW_2 caused by varying R from 0 to 0.3. The statistical error is quite small and the overall systematic error of ± 5% is not included. Extending the range of the data by means of the fit to the cross section given by formula (3), these integrals were evaluated at $q^2 = 4$ GeV^2 and $q^2 = 8$ GeV^2. The results are summarized in the following table. Again the errors show only the variation in νW_2 caused by varying R from 0 to 0.3.

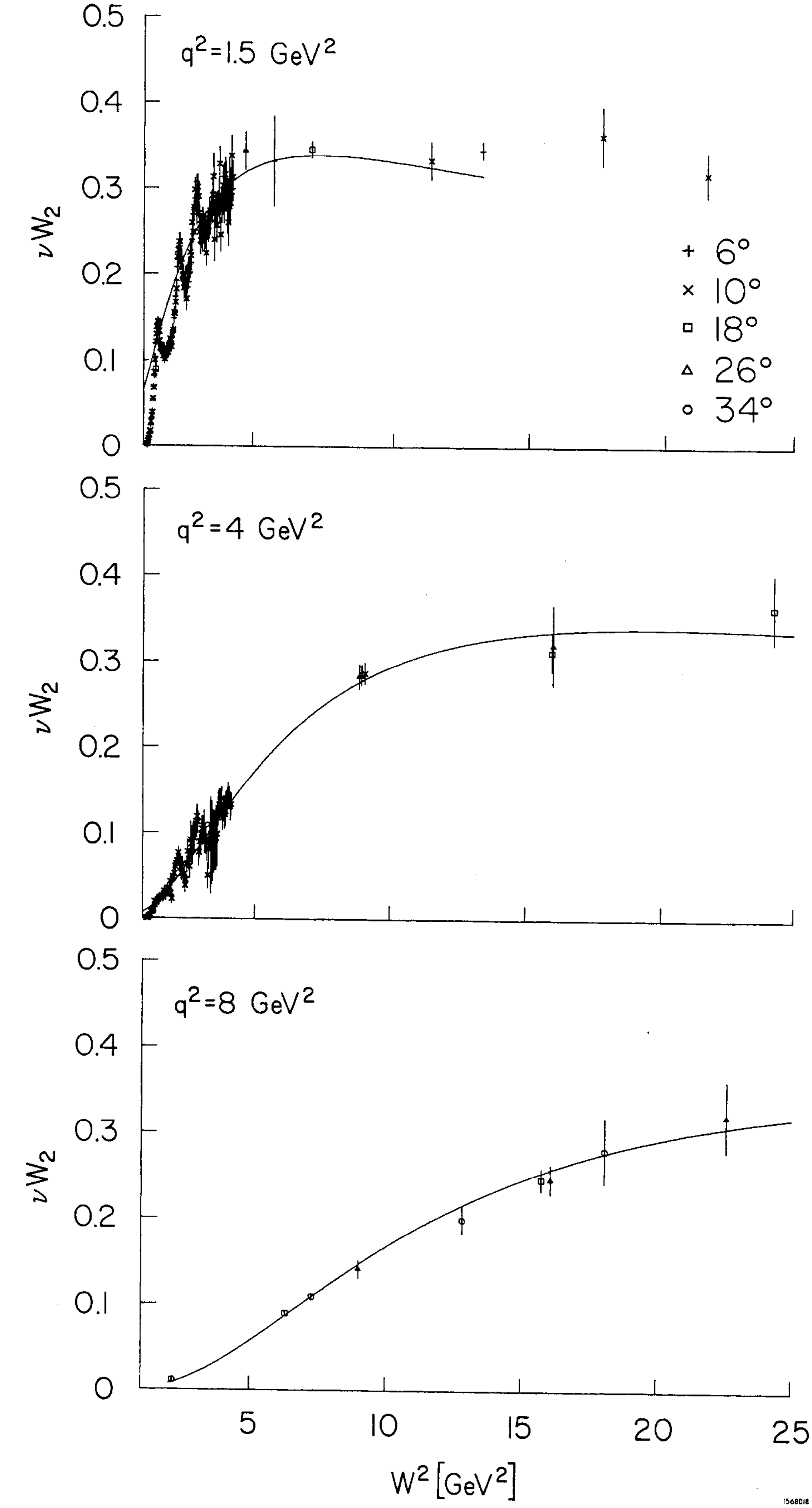

q²=1.5 GeV²
q²=4 GeV²
q²=8 GeV²
νW₂
W² [GeV²]
+ 6°
× 10°
□ 18°
△ 26°
○ 34°
0
0.1
0.2
0.3
0.4
0.5
5
10
15
20
25

Fig. 20

	$q^2 = 1.5$	$q^2 = 4$	$q^2 = 8$
$\int \nu W_2 dx$	.156 ± 2%	.141 ± 6%	.130 ± 10%
$\int \nu W_2 \frac{dx}{x}$	.563 ± 2%	.530 ± 7%	.509 ± 10%

The small value of the quantity $\overline{\sum_i \lambda_i^2}$ coming from x in the range 0.1 to 1 does not necessarily imply existence of fractional charges since it is not at all clear that the contribution coming from x = 0 to 0.1 is even finite. This will be finite if, and only if, $\nu W_2 \sim x^\alpha$, as $x \longrightarrow 0$, with $\alpha > 0$. The whole matter is obscured by the possibility of a substantial contribution from diffractive processes in the small x region, which should not be included in the parton sum rule. There is certainly a diffractive component at small q^2, and how much of this remains at higher q^2 to mask a possible quasi-elastic peak is perhaps the most interesting question at this time.

In Table 3 are listed all the large angle cross sections with W > 1.8 GeV. The data are listed line by line, starting with 18°, then 26° and 34°. The disposition of the data points in the kinematic q^2-W^2 plane is clarified by referring to Fig. 2.

TABLE 3

θ (deg)	E (GeV)	E' (GeV)	$d^2\sigma/d\Omega dE'$ (10^{-35} cm^2/sr-GeV)
18	4.501	2.250	7600. ± 430.
		2.000	7000. ± 450.
	6.503	3.500	1879. ± 54.
		3.000	2413. ± 75.
		2.500	2593. ± 93.
		2.000	2510. ± 120.
	8.598	4.780	460. ± 15.
		4.500	572. ± 17.
		4.000	779. ± 44.
		3.500	957. ± 36.
		3.000	1036. ± 50.
		2.500	1229. ± 65.
		2.000	1330. ± 130.
	10.404	5.500	180.6 ± 6.3
		5.000	284. ± 10.
		4.500	409. ± 16.
		3.940	512. ± 23.
		3.500	604. ± 32.
		3.000	630. ± 40.
		2.500	751. ± 47.
		2.000	801. ± 99.
	13.299	7.000	19.88 ± .90
		6.500	49.2 ± 1.9
		6.000	93.0 ± 3.6
		5.500	135.8 ± 5.6
		5.000	178.2 ± 7.7
		4.500	208. ± 15.
		4.000	263. ± 21.
		3.500	306. ± 28.
		3.090	315. ± 23.
		2.500	417. ± 49.
		2.000	533. ± 74.
	17.000	8.000	7.08 ± .35
		7.500	15.17 ± .56
		7.000	29.9 ± 1.1
		6.500	44.8 ± 1.7
		6.000	64.3 ± 2.6
		5.500	86.9 ± 3.4
		5.000	101.1 ± 7.4
		4.500	122.8 ± 9.4
		4.000	145. ± 12.
		3.500	173. ± 16.
		3.000	191. ± 20.
		2.500	239. ± 31.
		2.000	271. ± 54.
26	4.494	2.000	1410. ± 67.
		1.800	1518. ± 81.

θ (deg)	E (GeV)	E' (GeV)	$d^2\sigma/d\Omega dE'$ (10^{-35} cm^2/sr-GeV)
26	6.700	2.940	212.6 ± 7.8
		2.750	283.1 ± 10.
		2.500	340. ± 14.
		2.250	407. ± 19.
		2.000	504. ± 25.
		1.750	585. ± 51.
	8.696	3.750	32.2 ± 2.0
		3.500	57.2 ± 3.0
		3.250	91.7 ± 3.7
		3.000	119.9 ± 5.0
		2.750	154.9 ± 6.8
		2.500	195.5 ± 9.7
		2.270	229. ± 12.
		2.000	275. ± 17.
		1.750	317. ± 20.
	11.905	4.500	4.70 ± .48
		4.250	9.34 ± .99
		4.000	17.7 ± 1.0
		3.750	25.9 ± 1.6
		3.500	35.1 ± 2.2
		3.250	47.0 ± 4.5
		3.000	63.4 ± 6.2
		2.750	76.9 ± 7.7
		2.500	91.2 ± 9.9
		2.250	113. ± 12.
		2.000	121. ± 17.
		1.670	161. ± 23.
	15.006	5.000	1.34 ± .17
		4.750	2.87 ± .26
		4.500	5.55 ± .39
		4.250	8.07 ± .50
		4.000	13.83 ± .91
		3.750	18.4 ± 1.5
		3.500	23.3 ± 1.3
		3.250	31.6 ± 1.8
		3.000	39.6 ± 2.3
		2.750	45.9 ± 4.3
		2.500	52.0 ± 5.4
		2.250	62.7 ± 7.6
		2.000	76. ± 10.
		1.750	79. ± 15.
	18.030	5.500	.500 ± .090
		5.250	1.09 ± .15
		5.000	1.31 ± .20
		4.750	2.76 ± .29
		4.500	4.78 ± .39
		4.250	7.66 ± .55
		4.000	10.14 ± .99

θ (deg)	E (GeV)	E' (GeV)	$d^2\sigma/d\Omega dE'$ (10^{-35} cm^2/sr-GeV)
26	18.030	3.750	12.9 ± 1.2
		3.500	15.3 ± 1.7
		3.250	21.5 ± 1.7
		3.000	25.7 ± 2.5
		2.750	32.9 ± 4.1
		2.500	39.4 ± 5.2
		2.250	45.7 ± 7.3
		2.000	56. ± 10.
		1.750	81. ± 16.
34	4.501	1.600	404. ± 22.
		1.400	533. ± 31.
		1.200	652. ± 41.
	5.795	2.020	108.0 ± 7.6
		1.750	175.3 ± 9.6
		1.500	252. ± 21.
		1.250	356. ± 33.
	7.899	2.500	24.8 ± 1.6
		2.250	38.2 ± 3.3
		2.000	62.4 ± 5.1
		1.750	90.4 ± 8.0
		1.480	125. ± 12.
		1.250	153. ± 21.
	9.999	3.000	3.02 ± .35
		2.750	8.60 ± .57
		2.500	15.03 ± .86
		2.250	26.1 ± 1.2
		2.000	36.4 ± 2.9
		1.750	47.2 ± 4.4
		1.500	70.3 ± 7.4
		1.250	104. ± 13.
	12.500	3.250	1.22 ± .19
		3.000	3.52 ± .40
		2.750	7.57 ± .55
		2.500	10.32 ± .64
		2.250	17.1 ± 1.7
		2.000	21.9 ± 2.4
		1.750	32.1 ± 4.0
		1.500	47.8 ± 6.6
		1.250	61. ± 13.
	14.996	3.250	0.85 ± .25
		3.000	2.29 ± .38
		2.750	4.30 ± .53
		2.500	7.21 ± .99
		2.250	11.8 ± 1.8
		2.000	16.7 ± 2.0
		1.750	19.6 ± 3.0
		1.500	32.6 ± 5.4

1687A44

APPENDIX A.I --- RADIATION OF SOFT PHOTONS

Since photons have zero mass, the total energy of a photon can be arbitrarly small. As the photon energy goes to zero the effect of the radiation process on the source currents also goes to zero. That is, the motion of the charged particles involved is independent of the process of photon radiation if the photons are sufficiently soft. In that case the probability to radiate a photon with momentum k_i and polarization ϵ_i, to first order in α, is given by,

$$\bar{n}_i = \left| \int j_\mu(x)\ \epsilon_{i\mu}\ e^{ik_i x}\ d^4x \right|^2 \tag{1}$$

Where $j_\mu(x)$ is the current represented by all the charged particles, and it is assumed to be a fixed function of x, not affected by the radiation process. For example consider an electron undergoing a collision which occurs in a very short time interval τ around t=0. Then for times large compared to τ,

$$j_\mu(x) = \begin{cases} e(\underset{\sim}{v}, i)\ \delta(\underset{\sim}{r} - \underset{\sim}{v}t), & t < 0 \\ e(\underset{\sim}{v}', i)\ \delta(\underset{\sim}{r} - \underset{\sim}{v}'t), & t > 0 \end{cases} \tag{2}$$

Neglecting the contribution to the integral from times on the order of τ, we get,

$$\int j_\mu(x)\ \epsilon_{i_\mu}\ e^{ik_i x}\ d^4x = -ie \left(\frac{p_\mu}{(pk_i)} - \frac{p'_\mu}{(p'k_i)} \right) \epsilon_{i\mu} \tag{3}$$

and

$$\bar{n}_i = e^2 \left| \left(\frac{p_\mu}{(pk)} - \frac{p'_\mu}{(p'k)} \right) \left(\frac{p_\nu}{(pk)} - \frac{p'_\nu}{(p'k)} \right) \epsilon_{i\mu} \epsilon_{i\nu} \right| \tag{4}$$

The sum over polarizations can be done using the following rule. We imagine taking the limit $k^2 \to 0$ later on.

$$\sum_\lambda \epsilon_{\lambda\mu} \epsilon_{\lambda\nu} = \delta_{\mu\nu} - \frac{k_\mu k_\nu}{k^2} \tag{5}$$

Thus we arrive at the following well known expression for the probability of radiating a soft photon with momentum k.

$$\bar{n}_i = e^2 \left| \frac{p_\mu}{(pk)} - \frac{p'_\mu}{(p'k)} \right|^2 \tag{6}$$

In fact always more than one photon is radiated. The problem of photon radiation from a fixed source can be solved exactly [18]. The result is the familiar Poisson distribution formula. The probability to emit n_1 photons into mode 1, n_2 photons into mode 2,... n_i photons into mode i is found to be,

$$P_{\{n_i\}} = \left(\exp - \sum_i \bar{n}_i \right) \prod_i \frac{(\bar{n}_i)^{n_i}}{n_i!} \tag{7}$$

Notice that $P_{\{n_i\}}$ is correctly normalized.

$$\sum_{n_1, n_2 \ldots = 0}^{\infty} P_{\{n_i\}} = \exp\left(-\sum_i \overline{n}_i\right) \sum_{n_1, n_2 \ldots = 0}^{\infty} \prod_i \frac{(\overline{n}_i)^{n_i}}{n_i\,!}$$

$$= \exp\left(-\sum_i \overline{n}_i\right) \prod_i \exp \overline{n}_i$$

$$= \exp\left(-\sum_i \overline{n}_i\right) \exp\left(\sum_i \overline{n}_i\right)$$

$$= 1 \qquad (8)$$

We are interested in the probability that the total energy of all photons emitted is in the interval ω to $\omega + d\omega$. First define a quantity $\overline{n}(\omega)$ by the equation

$$\int \overline{n}(\omega)d\omega = \sum_i \overline{n}_i \qquad (9)$$

That is, $\overline{n}(\omega)\,d\omega$ is just $\overline{n}_i$ summed over all modes having energy in the interval $d\omega$.

The sum of the probabilities $P_{\{n_i\}}$ for all $\{n_i\}$ gives 1 as has been shown.

$$1 = \exp\left(-\sum_i \overline{n}_i\right) \exp\left(\sum_i \overline{n}_i\right)$$

$$= \exp\left(-\sum_i \overline{n}_i\right)\left[1 + \sum_i \overline{n}_i + \frac{1}{2}\sum_{i,j} \overline{n}_i \overline{n}_j + \ldots\right] \qquad (10)$$

A general term of this series is of the form

$$\exp\left(-\sum_i \overline{n}_i\right) \frac{1}{n!} \sum_{i_1, i_2 \ldots i_n} \overline{n}_{i_1} \overline{n}_{i_2} \ldots \overline{n}_{i_n} \qquad (11)$$

This is the probability to radiate n photons. If we require that the total energy radiated be ω we must evaluate

$$\frac{1}{n!} \sum_{i_1, i_2 \ldots i_n} \overline{n}_{i_1} \overline{n}_{i_2} \ldots \overline{n}_{i_n} \tag{12}$$

such that $\omega_{i_1} + \omega_{i_2} + \ldots \omega_{i_n} = \omega$.
In terms of $\overline{n}(\omega)$ this is given by

$$\frac{1}{n!}\int_0^{\omega} d\omega_1 \overline{n}(\omega_1) \int_0^{\omega-\omega_1} d\omega_2 \overline{n}(\omega_2) \ldots \int_0^{\omega-\omega_1-\ldots-\omega_{n-2}} d\omega_{n-1} \overline{n}(\omega_{n-1}) \overline{n}(\omega-\omega_1-\ldots-\omega_{n-1}) \tag{13}$$

So the problem is solved once we determine the form of $\overline{n}(\omega)$ and do the integrals (13).

In the case of an electron scattering from momentum p to momentum p', we have by definition,

$$\int \overline{n}(\omega) d\omega = \sum_i \overline{n}_i = \int \frac{d^3k}{(2\pi)^3 2\omega} e^2 \left| \frac{p_\mu}{(pk)} - \frac{p'_\mu}{(p'k)} \right|^2 \tag{14}$$

Therefore

$$\overline{n}(\omega) = \frac{\alpha}{\pi} \int \frac{k d\Omega_k}{4\pi} \left| \frac{p_\mu}{(pk)} - \frac{p'_\mu}{(p'k)} \right|^2 \tag{15}$$

This integration can be done exactly giving,

$$\overline{n}(\omega) = t/\omega$$

APPENDIX A.I --- RADIATION OF SOFT PHOTONS

$$t = \frac{2\alpha}{\pi} \frac{-(pp')}{\sqrt{(pp')^2 - m^4}} \left[\log\left(\frac{-(pp') + \sqrt{(pp')^2 - m^4}}{m^2} \right) - 1 \right] \qquad (16)$$

t will be referred to from now on as the equivalent radiator associated with the scattering process.

In the more general case where several charged particles are involved in a collision process, with particle i having charge Z_i and direction θ_i (+ for incoming, - for outgoing), t is given by

$$t = \sum_{i,j} \frac{\alpha}{\pi} \int \frac{k d\Omega_k}{4\pi} Z_i Z_j \theta_i \theta_j \frac{(p_i p_j)}{(p_i k)(p_j k)} \qquad (17)$$

The assumption is implicitly made that the collision time τ is short compared with a characteristic time of the radiation process $1/\omega$. This is necessary so that the simple form of $j_\mu(x)$ used will be valid.

Using the general form of $\overline{n}(\omega)$ we can proceed to evaluate the integral (13). It is necessary to introduce a limiting soft photon energy ϵ to obtain convergence.

$$\frac{1}{n!} \int_{\omega > \omega_i > \epsilon} t \frac{d\omega_1}{\omega_1} \, t \frac{d\omega_2}{\omega_2} \cdots t \frac{d\omega_{n-1}}{\omega_{n-1}} \, \frac{t}{\omega_n}$$

$$= \frac{t}{\omega} \frac{t^{n-1}}{n!} \int_{1 > x_i > \epsilon/\omega} \frac{dx_1}{x_1} \frac{dx_2}{x_2} \cdots \frac{dx_{n-1}}{x_{n-1}} \frac{1}{x_n} \qquad (18)$$

Where

$$\omega = \omega_1 + \omega_2 + \ldots + \omega_n$$

$$1 = x_1 + x_2 + \ldots + x_n$$

APPENDIX A.I --- RADIATION OF SOFT PHOTONS

There are n main contributions to this integral, when one denominator x_i is almost 1 and all the other x's are small. Each of the n contributions is approximately equal to

$$\frac{t}{\omega}\,\frac{t^{n-1}}{n!}\left[\int_{\epsilon}^{1}\frac{dx}{x}\right]^{n-1} = \frac{1}{n}\,\frac{t}{\omega}\,\frac{(t\log\omega/\epsilon)^{n-1}}{(n-1)!} \tag{19}$$

Thus the probability for radiating a total energy ω is,

$$P(\omega) = \exp\left(-\sum_i \overline{n}_i\right)\left(1 + t\log\omega/\epsilon + \frac{1}{2!}(t\log\omega/\epsilon)^2 + \ldots\right)t/\omega$$

$$= \exp\left(-\sum_i \overline{n}_i\right)\exp(t\log\omega/\epsilon)\;t/\omega \tag{20}$$

This probability must be normalized i.e.

$$\int_0^{\omega_{max}} P(\omega)\,d\omega = 1 \tag{21}$$

Strictly speaking there is no reason why ω_{max} should be anything but ∞. However we will take it to be some finite quantity to obtain a finite result. The normalization condition determines $\exp(-\sum_i \overline{n}_i)$ in terms of the auxillary quantities ϵ, and ω_{max}.

$$\exp\left(-\sum_i \overline{n}_i\right) = \exp\left(-t\log\frac{\omega_{max}}{\epsilon}\right) \tag{22}$$

So that we have,

$$\int_0^{\omega_{max}} P(\omega)d\omega = \int_0^{\omega_{max}} \frac{t}{\omega}\left(\frac{\omega}{\omega_{max}}\right)^t d\omega = 1$$

The result for $P(\omega)$ is now independent of ϵ so we can imagine taking the limit $\epsilon \to 0$, at this point. P now depends only on what we choose ω_{max} to be.

$$P(\omega) = \frac{t}{\omega}\left(\frac{\omega}{\omega_{max}}\right)^t = \frac{t\,\omega^{t-1}}{\omega_{max}^t} \qquad (23)$$

Since ω_{max} is poorly defined in this theoretical framework where the currents are imagined to be independent fixed functions, certain doubts are cast on the solution, particularly since if $\omega_{max} \to$, $P(\omega) \to 0$. However the effect of ω_{max} is just a normalization factor and the shape of $P(\omega)$ is determined to be ω^{t-1} independently of the choice of ω_{max}. This is what is probably correctly calculated here, namely the shape of the function $P(\omega)$ for small ω.

To check the approximation involved in evaluating the integral

$$\frac{1}{n!}\int \frac{dx_1}{x_1}\,\frac{dx_2}{x_2}\cdots\frac{dx_{n-1}}{x_{n-1}}\,\frac{1}{x_n} \cong \frac{1}{(n-1)!}\,(\log \omega/\epsilon)^{n-1} \qquad (24)$$

we can do the integration exactly for small values of n.

APPENDIX A.I --- RADIATION OF SOFT PHOTONS

n=1	1
n=2	$\log \omega/\epsilon$
n=3	$\frac{1}{2}(\log \omega/\epsilon)^2 - .822$

APPENDIX A.II--- QUANTUM MECHANICAL RADIATIVE CORRECTIONS

The result of the previous section is that any scattering process involving charged particles causes the radiation of photons. For small radiation energy loses ω, the cross section is

$$d\sigma = \sigma'_0 \, \frac{t}{\omega} \left(\frac{\omega}{\omega_{max}} \right)^t d\omega \qquad (1)$$

where σ'_0 is the cross section for the process without radiation, t is given by formula I.17, and ω_{max} is the maximum photon energy, introduced as a cutoff in the probability normalization integral I.21. The justification for a finite ω_{max} is that because of the quantum nature of the scattering particles, the maximum photon energy is limited to be on the order of the energies of these particles, and clearly cannot be infinite because of conservation of energy.

The problem remaining is to calculate ω_{max} and to find the electrodynamic corrections to the cross section. That is, if the cross section σ_0 were calculable from a complete theory, certain corrections due to higher order quantum electrodynamics would have to be made, and it is customary to remove these "radiative" effects before presenting the data for the cross section σ_0. σ'_0 is the cross section calculated to higher order than first in α.

From (1), the cross section allowing radiation of photons with any total energy less than k_1, which is small compared with the energies of the particles, is

$$\sigma(k_1) = \int_0^{k_1} \frac{d\sigma}{d\omega} d\omega = \sigma'_0 \left(\frac{k_1}{\omega_{max}} \right)^t = \sigma'_0 \left(1 + t \log \frac{k_1}{\omega_{max}} + \ldots \right) \quad (2)$$

If we make a calculation of this quantity taking into account higher order electrodynamic processes, we can identify ω_{max} and find the radiative corrections by comparing lowest order terms in α.

Consider electron scattering. There are three types of radiative corrections. Corrections to the photon-electron (or target particle) vertex, corrections to the photon propagator, and corrections due to the exchange of more than one photon. We will discuss only the first two, beginning with the photon propagator.

For the photon propagator the result is[19,20],

$$\frac{1}{q^2 - i\epsilon} \longrightarrow D(q^2)$$

$$D(q^2) = \frac{1}{q^2 - i\epsilon} + \int_{4m^2}^{\infty} dM^2 \, \frac{a(M^2)}{q^2 + M^2 - i\epsilon} + \ldots \quad (3)$$

with

$$a(M^2) = \frac{\alpha}{3\pi} \frac{1}{M^2} \sqrt{1 - \left(\frac{2m}{M}\right)^2} \left(1 + \frac{2m^2}{M^2}\right)$$

When $q^2 >> m^2$, $D(q^2)$ takes the familiar form

APPENDIX A.II--- QUANTUM MECHANICAL RADIATIVE CORRECTIONS

$$D(q^2) \cong \frac{1}{q^2}\left(1 + \frac{\alpha}{\pi}\left(\frac{1}{3}\log\frac{q^2}{m^2} - \frac{5}{9}\right)\right) \tag{4}$$

So the photon propagator contributes the following correction to the cross section at high q^2,

$$1 + \frac{2\alpha}{\pi}\left(\frac{1}{3}\log\frac{q^2}{m^2} - \frac{5}{9}\right) \tag{5}$$

The electron-photon vertex for $p^2=-m^2$ and $p'^2=-m^2$, is summarized by an electric and magnetic form factor, F_1 and F_2 [19,20].

$$\gamma_\mu \longrightarrow F_1(q^2)\,\gamma_\mu + \frac{\mu'}{2m}\,F_2(q^2)\;\tau_{\mu\nu}\,q_\nu \tag{6}$$

Where

$$F_1(q^2) = 1 - q^2\int_{2m}^{\infty}\frac{dM\,\phi_1(M)}{q^2 + M^2 - i\epsilon} + \ldots$$

$$\phi_1(M) = \frac{\alpha}{\pi}\,\frac{1}{M}\,\frac{1}{\sqrt{1-\left(\frac{2m}{M}\right)^2}}\left[\left(1 - \frac{2m^2}{M^2}\right)\log\frac{M^2 - 4m^2}{\lambda^2} - \frac{3}{2} + \left(\frac{2m}{M}\right)^2\right]$$

$$F_2(q^2) = \int_{2m}^{\infty}\frac{dM\,\phi_2(M)}{q^2 + M^2 - i\epsilon} + \ldots$$

$$\phi_2(M) = \frac{(2m)^2}{M}\;\frac{1}{\sqrt{1-\left(\frac{2m}{M}\right)^2}}$$

$$\mu' = \frac{\alpha}{2\pi}$$

λ is a small "photon mass" which must be introduced to prevent an infared divergence.

For $q^2 >> m^2$ the magnetic form factor is negligible and the non-logarithmic correction terms in F_1 give

$$- \frac{\alpha}{\pi} q^2 \int_{2m}^{\infty} \frac{dM}{M} \frac{1}{\sqrt{1 - \left(\frac{2m}{M}\right)^2}} \frac{-\frac{3}{2} + \left(\frac{2m}{M}\right)^2}{q^2 + M^2} \cong \frac{\alpha}{\pi} \left(\frac{3}{4} \log \frac{q^2}{m^2} - 1 \right) \qquad (7)$$

In the log term it is convient to go over to a new integration varible x, defined by $(M/2m)^2 = 1/(1-x^2)$.

$$- \frac{\alpha}{\pi} q^2 \int_{2m}^{\infty} \frac{dM}{M} \frac{1}{\sqrt{1 - \left(\frac{2m}{M}\right)^2}} \frac{1 - \frac{2m^2}{M^2}}{q^2 + M^2} \log \frac{M^2 - 4m^2}{\lambda^2}$$

$$= - \frac{\alpha}{\pi} \int_0^1 \frac{dx}{1 - x^2 + \frac{4m^2}{q^2}} \frac{1 + x^2}{2} \log \frac{x^2}{\left(\frac{\lambda}{2m}\right)^2 (1 - x^2)} \qquad (8)$$

The λ dependent part can be separated giving,

$$- \frac{\alpha}{\pi} \int_0^1 \frac{dx}{1 - x^2 + \frac{4m^2}{q^2}} \frac{1 + x^2}{2} \log \frac{4m^2 x^2}{1 - x^2} + \frac{\alpha}{\pi} \log \lambda^2 \int_0^1 \frac{dx}{1 - x^2 + \frac{4m^2}{q^2}} \left(\frac{1 + x^2}{2} \right) \qquad (9)$$

The first term can be further reduced to,

$$- \frac{\alpha}{\pi} \left(1 + \frac{2m^2}{q^2} \right) \int_0^1 \frac{dx}{1 - x^2 + \frac{4m^2}{q^2}} \log \frac{4m^2 x^2}{1 - x^2} + \frac{\alpha}{2\pi} \log m^2 + \frac{\alpha}{2\pi} \int_0^1 dx \log \frac{4x^2}{1 - x^2} \qquad (10)$$

The last integral is zerc.

$$\int_0^1 dx \log \frac{4x^2}{1 - x^2} = 0 \qquad (11)$$

Thus we are left with the following expression for F_1,

$$F_1(q^2) = 1 - \frac{\alpha}{\pi} q^2 \int_{2m}^{\infty} \frac{dM}{M(q^2+M^2)} \frac{1}{\sqrt{1-\left(\frac{2m}{M}\right)^2}} \left(-\frac{3}{2} + \left(\frac{2m}{M}\right)^2\right)$$

$$- \frac{\alpha}{\pi}\left(1+\frac{2m^2}{q^2}\right)\int_0^1 \frac{dx}{1-x^2+\frac{4m^2}{q^2}} \log \frac{4m^2x^2}{1-x^2} + \frac{\alpha}{2\pi}\log m^2 + \frac{\alpha}{\pi}\log\lambda^2 \int_0^1 \frac{dx}{1-x^2+\frac{4m^2}{q^2}} \frac{1+x^2}{2} \qquad (12)$$

In calculating corrections to the electron-photon vertex we cannot ignore radiation of soft photons from the external electron lines. The probability of radiation of a soft photon of energy k is t/k dk with t given by I.17. If soft photons of any energy up to k_1 are allowed we must integrate this probability from 0 to k_1. An infared divergence occurs at k=0 unless the photon is given a small mass λ. Considering only radiation from the electron lines, and not from the target particle, or interference the one with the other, we have [21]

$$\frac{\alpha}{\pi}\int_0^{k_1} \frac{k d\Omega_k}{4\pi} \left| \frac{p_\mu}{(pk)} - \frac{p'_\mu}{(p'k)} \right|^2$$

$$= \frac{\alpha}{\pi}\left\{(pp')\int_0^1 \frac{dx}{P_x^2}\left[\log\frac{k_1^2}{E_x^2} - 2G(x)\right] - \log\frac{k_1^2}{EE'} + G(1) + G(-1)\right.$$

$$\left. + (pp')\int_0^1 \frac{dx}{P_x^2}\log(-P_x^2) - \log m^2 + \log\lambda^2 \frac{q^2}{4}\int_0^1 \frac{dx}{P_x^2}(1+x^2)\right\} \qquad (13)$$

with

$$P_x = \frac{1}{2}(1+x)p + \frac{1}{2}(1-x)p'$$

$$P_x^2 = -m^2 - q^2/4(1-x^2)$$

$$G(x) = \frac{E_x - |p_x|}{2\,|p_x|} \log \frac{E_x + |p_x|}{E_x - |p_x|} + \log \frac{E_x + |p_x|}{2E_x}$$

t is defined by equation I.16, but it can also be written as

$$t = -\frac{\alpha}{\pi} \sum_{i,j} Z_i Z_j \theta_i \theta_j (p_i p_j) \int_0^1 \frac{dx}{(P_x^2)_{i,j}} \qquad (14)$$

$$p_i = p, p'$$

Thus the probability to radiate a photon with energy less than k_1 is

$$t \log k_1 + \text{TERMS INDEPENDENT OF } k_1 \qquad (15)$$

At high energies, the terms involving G are negligible and

$$\frac{\alpha}{\pi}\left[(pp')\int_0^1 \frac{dx}{P_x^2} \log E_x^2 - \log EE'\right] \cong t \log \sqrt{EE'}$$

$$t \cong \frac{2\alpha}{\pi}\left(\log \frac{q^2}{m^2} - 1\right) \qquad (16)$$

Now we combine the probability of photon radiation with the form factor corrections. In the cross section the electric form factor corrections given in (12) are doubled since the amptitude is squared. The total correction to the cross section coming from the electron-photon vertex can be written as

APPENDIX A.II--- QUANTUM MECHANICAL RADIATIVE CORRECTIONS

$$\frac{2\alpha}{\pi} q^2 \int_{2m}^{\infty} \frac{dM}{M(q^2+M^2)} \frac{1}{\sqrt{1-\left(\frac{2m}{M}\right)^2}} \left(\frac{3}{2} - \left(\frac{2m}{M}\right)^2\right)$$

$$+ t \log k_1 - \frac{\alpha}{\pi}\left\{(pp')\int_0^1 \frac{dx}{P_x^2}\left[\log E_x^2 + 2\, G(x)\right] - G(1) - G(-1) - \log EE'\right\}$$

$$+ \frac{\alpha}{\pi}\left\{(pp')\int_0^1 \frac{dx}{P_x^2} \log(-P_x^2) - \log m^2 - \left(1+\frac{2m^2}{q^2}\right)\int_0^1 \frac{2\,dx}{1-x^2+\frac{4m^2}{q^2}} \log\frac{4m^2x^2}{1-x^2}\right.$$

$$\left. + \log m^2 + \log\lambda^2 \frac{q^2}{4}\int_0^1 \frac{dx}{P_x^2}(1+x^2) + \log\lambda^2 \int_0^1 \frac{dx}{1-x^2+\frac{4m^2}{q^2}}(1+x^2)\right\} \tag{17}$$

The log λ terms cancel exactly. The first integral in the last bracket can be written as

$$\frac{-q^2-2m^2}{2}\int_0^1 \frac{dx}{-\frac{q^2}{4}(1-x^2)-m^2} \log\left(\frac{q^2}{4}(1-x^2)+m^2\right)$$

$$= \left(1+\frac{2m^2}{q^2}\right)\int_0^1 \frac{2\,dx}{1-x^2+\frac{4m^2}{q^2}} \log\left[\frac{q^2}{4}(1-x^2)+m^2\right]$$

This when combined with the second integral in the last bracket gives

$$\left(1+\frac{2m^2}{q^2}\right)\int_0^1 \frac{2\,dx}{1-x^2+\frac{4m^2}{q^2}} \log\left[\frac{\frac{q^2}{4m^2}(1-x^2)+1}{\frac{4x^2}{1-x^2}}\right] = 2q^2\left(1+\frac{2m^2}{q^2}\right)\int_{2m}^{\infty} \frac{dM}{M\sqrt{1-\left(\frac{2m}{M}\right)^2}} \frac{\log\frac{m^2\left(\frac{q^2}{M^2}+1\right)}{M^2-4m^2}}{q^2+M^2} \tag{18}$$

As $q^2/(4m^2) \to \infty$ this integral $\to 0$, also when $q^2 \to 0$. At this point it is convient to call the corrections that depend only on q^2, corrections to the electron's form factor. They represent the increase in the electron's effective interaction at small distances. The remaining terms of (17) go into ω_{max} as defined by (2). The result is,

$$F_1^2(q^2) = 1 + \frac{2\alpha}{\pi} q^2 \int_{2m}^{\infty} \frac{dM}{M\sqrt{1-\left(\frac{2m}{M}\right)^2}} \left[\frac{\frac{3}{2} - \left(\frac{2m}{M}\right)^2 - \left(1 + \frac{2m^2}{q^2}\right) \log \frac{M^2 - 4m^2}{m^2\left(\frac{q^2}{M^2} + 1\right)}}{q^2 + M^2} \right]$$

$$t \log \frac{k_1}{\omega_{max}} = t \log k_1$$

$$- \frac{\alpha}{\pi} \frac{q^2 + 2m^2}{2} \int_0^1 \frac{dx}{\frac{q^2}{4}(1-x^2)+m^2} \left[\log E_x^2 + \frac{E_x - |p_x|}{|p_x|} \log \frac{E_x + |p_x|}{E_x - |p_x|} + 2 \log \frac{E_x + |p_x|}{2E_x} \right]$$

$$+ \frac{\alpha}{\pi} \left[\frac{E-P}{2P} \log \frac{E+P}{E-P} + \log \frac{E+P}{2E} + \frac{E'-P'}{2p'} \log \frac{E'+P'}{E'-P'} + \log \frac{E'+P'}{2E'} + \log EE' \right] \quad (19)$$

where t is given by equation I.16 and

$$E_x = \frac{1}{2}(1+x)E + \frac{1}{2}(1-x)E'$$

$$|p_x| = \sqrt{E_x^2 - m^2 - \frac{q^2}{4}(1-x^2)}$$

When $q^2/(4m^2) >> 1$ this greatly simplifies, giving

APPENDIX A.II--- QUANTUM MECHANICAL RADIATIVE CORRECTIONS

$$F_1^2(q^2) \cong 1 + \frac{2\alpha}{\pi}\left(\frac{3}{4}\log\frac{q^2}{m^2} - 1\right)$$

$$t \log \frac{k_1}{\omega_{max}} \cong \frac{2\alpha}{\pi}\left(\log\frac{q^2}{m^2} - 1\right)\log\frac{k_1}{\sqrt{EE'}} \qquad (20)$$

Formula (19) is an exact result, with no assumptions about the magnitude of the energies or neglect of the electron mass.

Using (5) and (20) for the radiative corrections coming from the photon propagator and the electron-photon vertex, we have the following result for high q^2 electron scattering allowing for radiation of soft photons with energy less than k_1, including only the corrections to lowest order in α,

$$\sigma(k_1) = \sigma_0\left(1 + \frac{2\alpha}{\pi}\left(\frac{1}{3}\log\frac{q^2}{m^2} - \frac{5}{9}\right) + \frac{2\alpha}{\pi}\left(\frac{3}{4}\log\frac{q^2}{m^2} - 1\right)\right)$$

$$\times\left(1 + \frac{2\alpha}{\pi}\left(\log\frac{q^2}{m^2} - 1\right)\log\frac{k_1}{\sqrt{EE'}}\right) \qquad (21)$$

The first correction factor, which depends only on q^2 and not on the frame in which energies are measured is lumped together with σ_0 to give σ_0'. The second factor when compared with equation (2) allows the identification of $\sqrt{EE'}$ with ω_{max}.

Now using the results of I with $\omega_{max} = \sqrt{EE'}$ we obtain the following expression for the cross section for high q^2 electron scattering (from a heavy target particle so that radiation involving the target particle is negligible, i.e. $q^2 \ll M_t^2$, with a total small amount of energy ω radiated,

$$d\sigma = \sigma'_0 \frac{t}{\omega} \left(\frac{\omega}{E}\right)^{t/2} \left(\frac{\omega}{E'}\right)^{t/2} d\omega \tag{22}$$

Integrating this from 0 to k_1 we obtain

$$\sigma(k_1) = \int_0^{k_1} d\sigma = \sigma'_0 \left(\frac{k_1}{E}\right)^{t/2} \left(\frac{k_1}{E'}\right)^{t/2} \tag{23}$$

APPENDIX A.III --- ENERGY STRAGGLING IN THE TARGET

As the incident and scattered electrons travel through the material of the target, they lose energy by the processes of bremsstralung and ionization. There is also the possibility of a change in the direction of the electrons momemtum, but at high energies this is small. The deflection is mainly caused by elastic scattering from the atoms of the material. The mean square angle of elastic scattering after a particle passes through 1 radiation length of material is approximately given by,

$$\bar{\theta}^2 = \frac{2\pi}{\alpha} \frac{m^2}{p^2 v^2} \qquad (1)$$

Neglecting this small change in angle, the electron's kinetic equation is the following,

$$\frac{\partial \pi(E,t)}{\partial t} = -\pi(E,t)\int_0^E w(E,E')dE' + \int_E^\infty \pi(E',t)\, w(E',E)dE' \qquad (2)$$

where $\pi(E,t)dE$ is the probability that the electron has energy in dE at thickness t and $w(E,E')dt$ is the probability that the electron loses energy $E-E'$ in thickness dt.

Bremsstralung is the main cause of large energy loses. Using the Thomas-Fermi model for the elastic form factor of the atom, under the conditions,

$$\frac{EE'}{m(E-E')} \gg 137\ Z^{-1/3}$$

$$E \gg 137\ mZ^{-1/3}$$

APPENDIX A.III --- ENERGY STRAGGLING IN THE TARGET

the cross section is [22],

$$d\sigma_{ELAS} = 4\alpha Z^2 r_0^2 \frac{dE'}{E-E'}\left\{\left(1+\left(\frac{E'}{E}\right)^2-\frac{2}{3}\frac{E'}{E}\right)\left(\log(191Z^{-1/3})-1.2(\alpha Z)^2\right)+\frac{1}{9}\frac{E'}{E}\right\} \quad (3)$$

In energy units, $r_0 = \alpha/m$ with m the electron mass. The cross section for bremsstralung along with inelastic excitation of the atom is,

$$d\sigma_{INELAS} = 4\alpha Z r_0^2 \frac{dE'}{E-E'}\left\{\left(1+\left(\frac{E'}{E}\right)^2-\frac{2}{3}\frac{E'}{E}\right)\log(1440\,Z^{-2/3})+\frac{1}{9}\frac{E'}{E}\right\} \quad (4)$$

Thus the total probability for energy loss E-E' due to bremsstralung in a thickness dt radiation lengths is given by

$$w(E,E')dt = \frac{dt}{E-E'}\left(1+\left(\frac{E'}{E}\right)^2-\frac{E'}{E}\left(\frac{2}{3}-a\right)\right) \quad (5)$$

with

$$a = \frac{1}{9}\,\frac{Z+1}{Z+\zeta}\;\frac{1}{\log(191\,Z^{-1/3})-1.2(\alpha Z)^2}$$

$$\zeta = \frac{\log(1440\,Z^{-2/3})}{\log(191\,Z^{-1/3})-1.2(\alpha z)^2} \quad (6)$$

The radiation length is defined by

APPENDIX A.III --- ENERGY STRAGGLING IN THE TARGET

$$\frac{1}{x_0} = 4N\alpha r_0^2 Z(Z+\zeta)\left[\log(191Z^{-1/3}) - 1.2(\alpha Z)^2\right] \qquad (7)$$

N is the number of atoms per cm³.

Energy loss can also occur because of ionization of the target atoms. For large energy loses, the process of ionization is the same as elastic scattering from the electrons of the atom, since the atomic binding energy of the electrons can be neglected. The cross section for electron-electron scattering with energy loss E-E' is given by [18],

$$d\sigma = \frac{2\pi\ r_0^2}{v^2(x-1)}\ \frac{d\Delta}{\Delta^2(1-\Delta)^2}\left\{1-\left(3-\left(\frac{x-1}{x}\right)^2\right)\Delta(1-\Delta)+\left(\frac{x-1}{x}\right)^2\Delta^2(1-\Delta)^2\right\} \qquad (8)$$

where

$$\Delta = \frac{E-E'}{E-m}$$

$$x = \frac{E}{m}$$

For high energy E and small energy loss,

$$d\sigma = \frac{2\pi\alpha^2}{m}\ \frac{d\epsilon}{\epsilon^2} \qquad (9)$$

with

$$\epsilon = E - E'$$

APPENDIX A.III --- ENERGY STRAGGLING IN THE TARGET

So for ϵ much greater than the binding energy of an electron in the atom, the probability of an energy loss E-E' in thickness dt radiation lengths due to ionization is,

$$w(E, E')dt = w(\epsilon)dt = \frac{\xi dt}{\epsilon^2} \tag{10}$$

with

$$\xi = \frac{2\pi N Z \alpha^2}{m} X_0 = m \frac{\pi}{2\alpha(Z + \zeta)\left[\log(191\, Z^{-1/3}) - 1.2(\alpha Z)^2\right]}$$

In order to solve equation (2) at high energies compared with the energies of atomic binding, it is not necessary to know the exact form of $w(\epsilon)$ for small ϵ. It turns out that it is sufficient to know the following integral relation [12].

$$\int_0^{\delta} w(\epsilon)\epsilon \, d\epsilon = \xi \, \ell n \, \delta/\epsilon' \tag{11}$$

with

$$\epsilon' = 2.718 \, m \frac{I^2}{2E^2}$$

and I a certain ionization potential of the atom, here taken to be

$$I = 13.5 \text{ eV} \times Z$$

APPENDIX A.III --- ENERGY STRAGGLING IN THE TARGET

The complete expression for the energy loss probability including bremsstralung and ionization is the following,

$$w(E,E')dt = \frac{dt}{E-E'}\left[1+\left(\frac{E'}{E}\right)^2 - \frac{E'}{E}\left(\frac{2}{3}-a\right)\right] + \frac{\xi\, dt}{(E-E')^2} \qquad (12)$$

and the knowledge of w for small values of the argument necessary to solve the equation (2) is summarized by,

$$\int_{E-\delta}^{E} (E-E')\, w(E,E')dE' = \xi \log\, \delta/\epsilon' + (4/3+a)\delta \qquad (13)$$

A solution of (2) for the initial condition that at t=0, $\pi(E) = \delta(E_0 - E)$, and w(E,E') given by (12) and (13) has been obtained by R. Early using numerical methods[23, 24]. For thicknesses up to .1 radiation length, energies in the range 1 to 20 Gev and Z up to 30, the numerical solution can be adequately represented by the following analytical form.

$$\pi(E_0, E, t) = w(E_{0c}, E)t\, \frac{\left(\log \frac{E_{0c}}{E}\right)^{bt}}{\Gamma(1+bt)} \left[1 + bt\, P\left(\frac{E_{0c}-E}{E_{0c}}\right)\right] \qquad (14)$$

Where,

$$E_{0c} = E_0 - \Delta_0$$

$$b = 4/3 + a$$

APPENDIX A.III --- ENERGY STRAGGLING IN THE TARGET

$$P(x) = x(.53875 + x(-2.1938 + .9634\, x))$$

The first factor is the correct single scattering probability. As $t \to 0$ the straggling probability must be just $w(E,E')t$. The other factors are corrections for multiple processes. The log and gamma functions are suggested by analogy with the case when $w(E,E') = b/(E \log(E/E'))$, which is exactly soluble. In this case the solution is

$$\pi(E_0, E, t) = \frac{bt}{E_0} \left(\log \frac{E_0}{E}\right)^{bt-1} \frac{1}{\Gamma(1+bt)} \tag{15}$$

So the effect of multiple processes is the factor $(\log(E_0/E))^{bt}/\Gamma(1+bt)$. The last factor of (14) is the additional multiple process correction necessary when (12) is used for the single scattering energy loss probability.

Part of the effect of ionization energy losses is just to shift down the energy an amount

$$\Delta_0 = \xi t\,(\log \xi/\epsilon' + .37) \tag{16}$$

This is a well known expression for the most probable ionization energy loss [12]. This energy shift is not particularly important experimentally since the absolute energy is usually not known that precisely. The important quantity, $E_{0c}-E$ is what is normally best known in an experimental situation. So henceforth the subscript c will be dropped.

Disregarding ionization, this solution is accurate to a fraction of a percent for t up to .1, Z up to 30 and E_0-E as small as .2 percent of E_0. For energies in the Gev range, the effect of ionization loss is mostly small except for E near E_0. The ionization loss correction is of order $\xi/b\epsilon$. When this quantity is less than 10 percent the analytic form given by (14) is accurate to 1 or 2 percent. For smaller thicknesses than .1 the accuracy is better. When the energy loss is small, but not too small, so that the ionization effects can be neglected, a useful approximate form of is the following,

$$\pi(E_0, E, t) = \frac{bt}{E_0 - E}\left(\frac{E_0 - E}{E_0}\right)^{bt} \frac{1}{\Gamma(1+bt)} \tag{17}$$

This is also the limit of (15) for $E \to E_0$.

Energy losses in the target material produce a "radiative tail" to a scattering process. Consider the process $eP \to eP_j$ where the final proton state P_j has mass M_j, with only the scattered electron detected in solid angle $d\Omega$ and energy interval dE'. Because of target energy loses, the cross section as a function of E' has a tail extending down from the "elastic peak" ,

APPENDIX A.III --- ENERGY STRAGGLING IN THE TARGET

$$E'_{ELAS} = \frac{E - \left(M_j^2 - M^2\right)/2M}{\eta} \tag{18}$$

where

$$\eta = 1 + \frac{2E}{M} \sin^2 \theta/2$$

The radiative tail is given by

$$\frac{d\sigma}{d\Omega dE'}(E, E', \theta) = \int_{E_{min}}^{E} \pi(E, E_1, t_b) \frac{d\sigma_0}{d\Omega}(E_1, \theta)\, \pi(E'_1, E', t_a) dE_1 \tag{19}$$

with $d\sigma_0/d\Omega$ the basic scattering cross section, and

$$E'_1 = \frac{E_1 - \left(M_j^2 - M^2\right)/2M}{\eta_1}$$

$$E' = \frac{E_{min} - \left(M_j^2 - M^2\right)/2M}{\eta_{min}} \tag{20}$$

Let us introduce the notation

$$\Delta E = E - E_{min}$$

$$\Delta E' = \frac{E - \left(M_j^2 - M^2\right)/2M}{\eta} - E' = \frac{\Delta E}{\eta \eta'} \tag{21}$$

with

$$\eta' = \frac{1}{1 - \frac{2E'}{M} \sin^2 \theta/2}$$

APPENDIX A.III --- ENERGY STRAGGLING IN THE TARGET

Substituting into the integral the approximate form of π for small bremsstralung energy loses given by (17), and assuming that the basic cross section doesn't vary appreciably over the range of the integration, we get the following expression for the radiative tail.

$$\frac{d\sigma}{d\Omega dE'} = \frac{d\sigma_0}{d\Omega} \int_{\frac{\omega}{\Delta E} + \frac{\omega'}{\Delta E'} = 1} \frac{bt_b}{\omega} \left(\frac{\omega}{E}\right)^{bt_b} \frac{1}{\Gamma(1+bt_b)} \frac{bt_a}{\omega'} \left(\frac{\omega'}{E'}\right)^{bt_a} \frac{1}{\Gamma(1+bt_a)} \, d\omega$$

$$= \frac{d\sigma_0}{d\Omega} \frac{b(t_b+t_a)}{\Delta E'} \left(\frac{\Delta E}{E}\right)^{bt_b} \left(\frac{\Delta E'}{E'}\right)^{bt_a} \frac{1}{\Gamma(1+b(t_b+t_a))} \qquad (22)$$

If we integrate this from the "elastic peak" E' down a small $\Delta E'$ we obtain,

$$\int_{\Delta E'} dE' \frac{d\sigma}{d\Omega dE'} = \frac{d\sigma_0}{d\Omega} \left(\frac{\Delta E}{E}\right)^{bt_b} \left(\frac{\Delta E'}{E'}\right)^{bt_a} \frac{1}{\Gamma(1+b(t_b+t_a))} \qquad (23)$$

APPENDIX A.IV --- MULTIPLE PHOTON RADIATION

Consider the process $eP \to eP_j$ where the final proton state j has mass M_j and may consist of several particles. Actually this process with no photons radiated never occurs. The cross section for the same process but with an arbitrary number of photons radiated and only the scattered electron detected is what is meant by the radiative tail. The measured cross section is the sum of radiative tails for all possible final proton states j.

Say the scattered electron is detected in solid angle d and energy dE'. The missing mass W is defined by

$$W^2 = -(P + p - p')^2 \tag{1}$$

where P is the four-momentum of the target proton, p the four momentum of the incoming electron, and p' the four momentum of the scattered electron. The missing mass is always greater than the mass of the proton final state M_j, the difference being made up by the energy of all the radiated photons. For a given inelastic process involving the proton, say $M \to M_j$, the missing mass W determines the total energy of all radiated photons.

The cross section for the process without radiation can be written as

$$d\sigma'_0 = \frac{|A'|^2}{J} \frac{d^3p'}{(2\pi)^3\, 2E'}\, 2\pi\delta\left((P + p - p')^2 + M_j^2\right) = \frac{|A'|^2}{J} \frac{E'}{8\pi^2} \frac{d\Omega}{2M\eta} \tag{2}$$

where $|A'|^2$ is the probability and J the flux. As usual the prime indicates that higher order q^2 dependent electrodynamic corrections to the probability are made.

With radiation of n soft photons the cross section is

$$d\sigma = \frac{|A'|^2}{J} \frac{d^3p'}{(2\pi)^3 2E'} \frac{d^3k_1}{(2\pi)^3 2\omega_1} \cdots \frac{d^3k_n}{(2\pi)^3 2\omega_n} \bar{n}_{k_1} \cdots \bar{n}_{k_n} 2\pi\delta\left((P+p-p'-k)^2 + M_j^2\right) \quad (3)$$

In the special Lorentz frame denoted by subscript s, where P-p+p' has zero space components, the delta function argument is

$$-W^2 + 2W\omega_s + M_j^2 + k^2 \quad (4)$$

where

$$\omega_s = \omega_{s_1} + \ldots \omega_{s_n}$$

$$k^2 = (k_1 + \ldots k_n)^2$$

Assuming most of the energy-momentum is concentrated in a single photon we can neglect k^2. Then, working in the special frame, the delta function restricts only the total energy of all the radiated photons, and this energy must be

$$\omega_s = \frac{W^2 - M_j^2}{2W} \quad (5)$$

APPENDIX A.IV --- MULTIPLE PHOTON RADIATION

Repeating the arguments of I, we sum the cross sections (3) integrated over the momenta of all undetected photons for n=0,1,2,... and arrive at the following result for the cross section with an arbitrary number of photons radiated

$$d\sigma = \frac{|A'|^2}{J}\,\frac{d^3p'}{(2\pi)^3\,2E'}\int \frac{t}{\omega_s}\left(\frac{\omega_s}{\sqrt{E_s E'_s}}\right)^t 2\pi\delta\left(-W^2+2W\omega_s+M_j^2\right)d\omega_s \quad (6)$$

To get this result, the ω_{max} of I is taken to be $\sqrt{E_s E'_s}$ by the arguments of II.

Doing the integration, and expressing the result in terms of the cross section for scattering without radiation, (2),

$$d\sigma = \frac{|A'|^2}{J}\,\frac{E'\,dE'\,d\Omega}{16\pi^2 W}\,\frac{t}{\omega_s}\left(\frac{\omega_s}{\sqrt{E_s E'_s}}\right)^t$$

$$d\sigma = d\,r'_0\,dE'\,\frac{tM\eta}{\omega_s W}\left(\frac{\omega_s}{\sqrt{E_s E'_s}}\right)^t \quad (7)$$

Expressing energies in the special frame in terms of lab frame quantities, we have,

$$\omega_s = \frac{M\eta\omega'}{W} = \frac{M\omega}{\eta' W}$$

$$E_s = \frac{ME}{W\eta'}$$

$$E'_s = \frac{M\eta E'}{W} \quad (8)$$

where

$$\eta = 1 + \frac{2E}{M} \sin^2 \theta/2$$

$$\eta' = \frac{1}{1 - \frac{2E'}{M} \sin^2 \theta/2}$$

$$\omega = E - \left(E' + \left(M_j^2 - M^2\right)/2M\right)\eta'$$

$$\omega' = \frac{E - \left(M_j^2 - M^2\right)/2M}{\eta} - E' \tag{9}$$

So in the lab frame, the cross section for electron scattering $eP \rightarrow eP_j$, allowing arbitrary radiation, but with $W^2 = M_j^2$ so the photons are soft is given by,

$$\frac{d\sigma}{d\Omega dE'} = \frac{d\sigma'_0}{d\Omega} \frac{t}{\omega'} \left(\frac{\omega}{E}\right)^{t/2} \left(\frac{\omega'}{E'}\right)^{t/2} \tag{10}$$

If the target has a finite thickness we must take into account energy loss processes occuring in the target before and after the scattering. Using the known straggling probability $\pi(E,E',t)$ we must evaluate the following convolution integral.

$$\int \pi(E, E_1, t_b) \frac{d\sigma}{d\Omega dE'} (E_1, E_1', \theta)\, \pi(E_1', E', t_a) dE_1 dE_1' \tag{11}$$

The cross section $d\sigma/d\Omega dE'$ is given by formula (10).

APPENDIX A.IV --- MULTIPLE PHOTON RADIATION

The region of integration is the shaded triangular area shown in the diagram. It is bounded above by the contour $W^2 = M_j^2$ which is the dotted line in the figure.

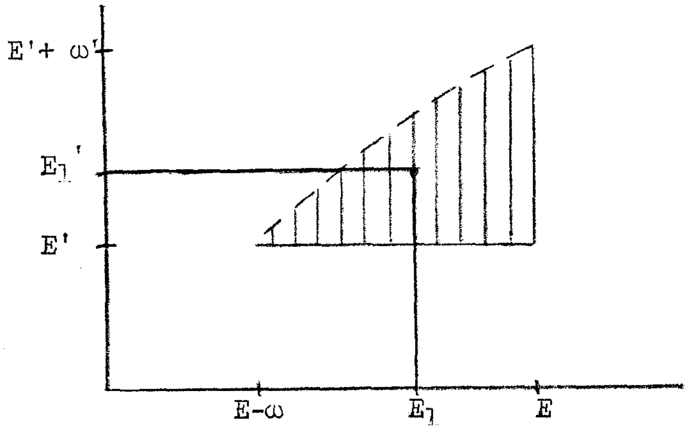

The integral (11) can be done exactly if we use the soft photon form of the straggling function , given by III. 15. The result for the soft photon radiative tail from the process $eP \to eP_j$ is then,

$$\frac{d\sigma}{d\Omega dE'} = \frac{d\sigma'_0}{d\Omega} \frac{t + bt_b + bt_a}{\omega'} \left(\frac{\omega}{E}\right)^{t/2 + bt_b} \left(\frac{\omega'}{E'}\right)^{t/2 + bt_a} \frac{\Gamma(1+t)}{\Gamma(1 + bt_b + bt_a + t)} \qquad (12)$$

It is interesting to compare this result with a calculation to lowest order in α, that is, allowing only a single radiated photon. The one photon radiative tail for small photon energy is

$$\frac{d\sigma}{d\Omega dE'} = \frac{d\sigma'_0}{d\Omega} \frac{t + bt_b + bt_a}{\omega'} \qquad (13)$$

So the effect of multiple photon radiation is to multiply the one photon result by a factor approximately equal to

$$\left(\frac{\omega}{E}\right)^{t/2+bt_b}\left(\frac{\omega'}{E'}\right)^{t/2+bt_a}\frac{1}{\Gamma(1+bt_b+bt_a)} \tag{14}$$

We can apply the foregoing arguments to the case where the basic process itself involves the radiation of a single photon, i.e. we imagine the final state P_j includes a single photon. The cross section for scattering with one hard photon radiated, allowing arbitrary soft radiation is the following, where k is the total energy of the soft photons and is small.

$$\frac{d\sigma}{d\Omega dE'} = \frac{d\sigma_1'}{d\Omega dE'}\int_0^k \frac{t}{\omega}\left(\frac{\omega}{\sqrt{EE'}}\right)^t d\omega = \frac{d\sigma_1'}{d\Omega dE'}\left(\frac{k}{E}\right)^{t/2}\left(\frac{k}{E'}\right)^{t/2} \tag{15}$$

$d\sigma_1'/d\Omega dE'$ is the cross section for the process $eP \to eP_j\gamma$ calculated to lowest order in α, but with higher order in α small distance corrections to the photon propagator and vertex functions.

As long as k is sufficiently small so that the secondary photons are actually soft, (15) is a correct calculation of a part of the measured radiative tail, namely the cross section for all the times when the total radiation consists of only 1 hard photon and the remainder soft, with total energy less than k. Including energy straggling in

APPENDIX A.IV --- MULTIPLE PHOTON RADIATION

the target, the result for this part of the radiative tail is,

$$\frac{d\sigma}{d\Omega dE'}(E,E',\theta) = \left\{\frac{d\sigma_1'}{d\Omega dE'}(E,E',\theta) + w(E,E-\omega)t_b\frac{d\sigma_0'}{d\Omega}(E-\omega,\theta)\eta'^2\right.$$

$$\left. + \frac{d\sigma_0'}{d\Omega}(E,\theta)\, w(E'+\omega',E')t_a\right\}\left(\frac{k}{E}\right)^{t/2+bt_b}\left(\frac{k}{E'}\right)^{t/2+bt_a}\frac{1}{\Gamma(1+bt_b+bt_a)} \qquad (16)$$

Where $w(E,E')t$ is the probability for energy straggling in the target calculated to lowest order in α, given by formula III.12, and $d\sigma_0'/d\Omega$ is the cross section for the process $eP \rightarrow eP_j$ without radiation.

In order to rigorously calculate the radiative tail including multiple photon effects is is necessary to go further and, using the well defined rules of quantum electrodynamics, attempt to calculate the processes where two or more hard photons are radiated. It doesn't seem likely that these probabilities can be estimated by simple arguments since the photons, being hard, have an important effect on the electron and the situation is complicated.

Hovever it does seem likely that multiple hard photon processes are not very probable, this for the simple reason that is small and the photon energy cannot become small since we are excluding soft photons which can be taken into account. We might expect the radiation of an additional hard photon to be of order $t+bt_b+bt_a$ less probable than the one photon process.

APPENDIX A.IV --- MULTIPLE PHOTON RADIATION

If we neglect entirely all multiple hard photon radiation we get the formula (16) for the radiative tail from the process $eP \rightarrow eP_j$. The quantity k is arbitrary, being the limiting soft photon energy. When all the photons are soft the result (12) can be put into the form of (16) if k is replaced by its maximum possible value for radiation in the initial direction in the first factor and its maximum possible value for radiation in the final direction in the second factor. All the photons are soft when W^2 is near M_j^2. Otherwise we expect k should be a small fraction of E, E' in order for the soft photon arguments to hold. As k goes to zero, the cross section given by (16) also goes to zero, which means physically that soft photon radiation always occurs.

The result (16) is unsatisfactory in that it depends on k which is not determined. However this dependence on k is quite small. We expect that the correct answer can be put in the form (16) with some k that a fairly small fraction of the energies E and E'. A reasonable guess for the actual radiative tail would be formula (16) with $\left(\frac{k}{E}\right)^{t/2+bt_b}\left(\frac{k}{E'}\right)^{t/2+bt_a} \rightarrow \left(\frac{k}{E}\right)^{t/2+bt_b}\left(\frac{k'}{E'}\right)^{t/2+bt_a}$

$$k = \min\left(\frac{1}{3}E, \omega\right)$$

$$k' = \min\left(\frac{1}{3}E', \omega'\right) \tag{17}$$

The fraction 1/3 is quite arbitrary and the variation of the result with this fraction is a measure of our ignorance of the actual size of multiple hard photon effects.

It is interesting to consider the case of target energy losses only, that is, $t \ll t_b, t_a$. The radiative tail is then known exactly using the known form of the straggling function $\pi(E,E',t)$ given by III.14.

$$\frac{d\sigma}{d\Omega dE'} = \int \pi(E, E_1, t_b) \frac{d\sigma_0'}{d\Omega}(E_1, \theta)\, \pi(E_1', E', t_a) dE_1 \tag{18}$$

We choose $t_b = t_a$. If we compare this with the radiative tail calculated by formula (16), we can find the effective soft photon limiting energy in this case. The effective soft photon energy k is defined so that the result of formula (16) agrees with the result of the integration (18) with $w(E,E')$ given by III.5.

$$\int \pi(E, E_1, t_b) \frac{d\sigma_0}{d\Omega}(E_1, \theta)\, \pi(E_1', E', t_a) dE_1 = \left(\frac{k}{\sqrt{EE'}}\right)^{bt_b + bt_a} \frac{1}{\Gamma(1 + bt_b + bt_a)}$$
$$\times \left\{ t_b w(E, E-\omega)\eta'^2 \frac{d\sigma_0}{d\Omega}(E-\omega, \theta) + t_a w(E'+\omega', E') \frac{d\sigma_0}{d\Omega}(E, \theta) \right\} \tag{19}$$

The effective k defined in this way is found to be quite independent of t_b and t_a as Figure A.1 shows. The Figure is a plot of $k/\sqrt{EE'}$ versus $\sqrt{\omega\omega'}/\sqrt{EE'}$ for various choices of $t_b = t_a$. The cross section is for elastic scattering, $eP \rightarrow eP$. However, as Figure A.1 shows, k depends on how rapidly the cross section is varying. The graphs compare the k obtained when the cross section is given by the Rosenbluth formula, with the usual dipole form factors , and with the form factors taken to be $G_E(q^2)=1$, and $G_M(q^2)=2.793$.

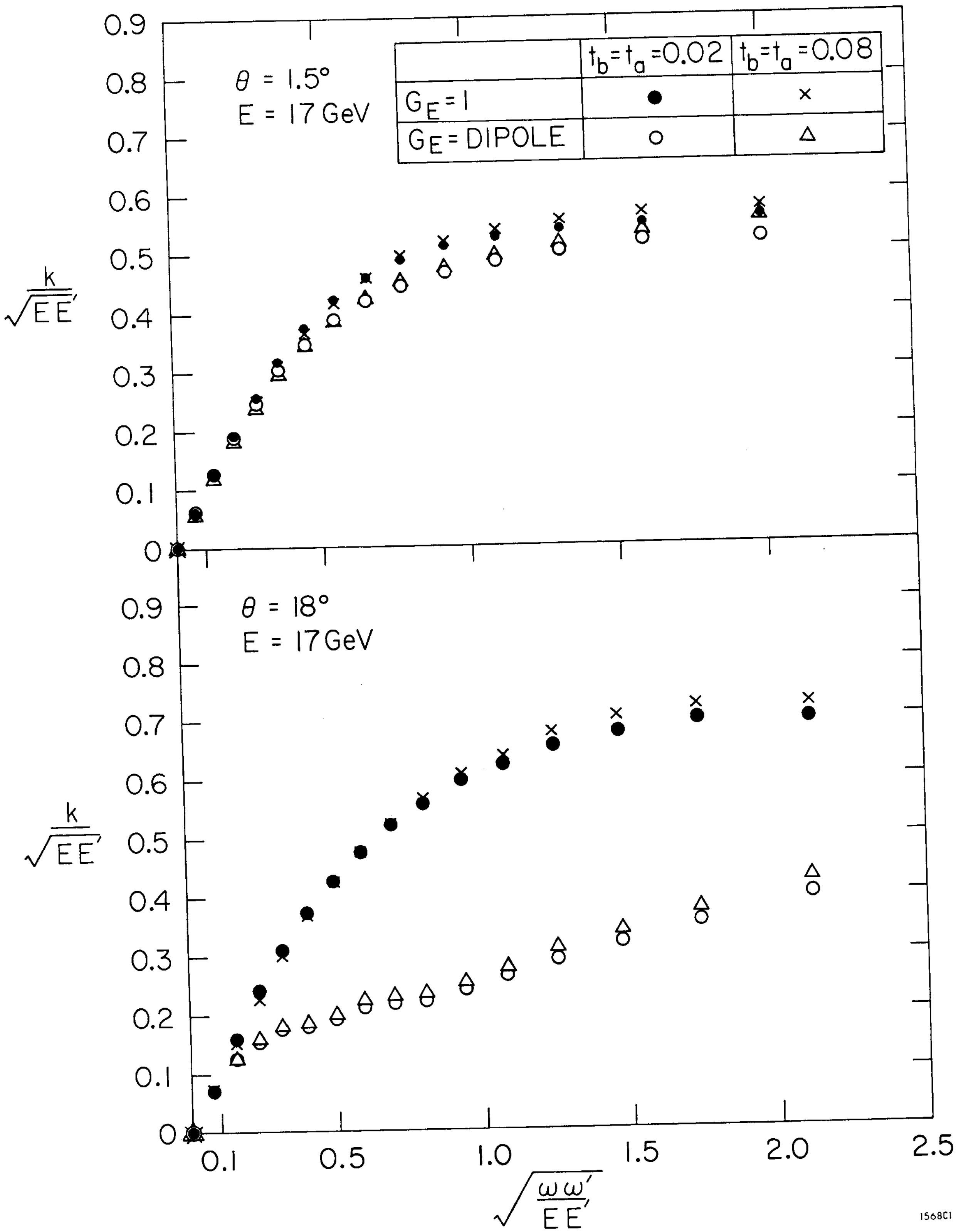

0.9
0.8
0.7
0.6
0.5
0.4
0.3
0.2
0.1
0
$t_b = t_a = 0.02$
$t_b = t_a = 0.08$
$G_E = 1$
$G_E =$ DIPOLE
θ = 1.5°
E = 17 GeV
$\frac{k}{\sqrt{EE'}}$
θ = 18°
E = 17 GeV
0.1
0.5
1.0
1.5
2.0
2.5
$\sqrt{\frac{\omega\omega'}{EE'}}$
1568C1

Fig. A.1

APPENDIX A.V --- RADIATIVE CORRECTION FORMULAS

The measured cross section for the scattering of electrons of energy E from target protons into solid angle $d\Omega$ and energy dE' will be denoted by $d\sigma_{RAD}/d\Omega dE'$. The corrected cross section is by definition the cross section for the hadronic process calculated to lowest order in α, that is, assuming the exchange of a single photon with the lowest order expressions for the photon propagator and electron-photon vertex used. The corrected cross section will be denoted by $d\sigma/d\Omega dE'$.

Part of the measured cross section consists of radiative tail from elastic eP scattering. The formula used for the elastic radiative tail was the following.

$$\frac{d\sigma_{ELAS\ RAD}}{d\Omega dE'}(E,E',\theta) = \left\{\frac{d\sigma'_1}{d\Omega dE'}(E,E',\theta)\,\frac{t}{t_{EL}} + t_b\, w(E,E-\omega)\eta'^2\,\frac{d\sigma'_0}{d\Omega}(E-\omega,\theta) + t_a\, w(E'+\omega',E')\,\frac{d\sigma'_0}{d\Omega}(E,\theta)\right\} \frac{\left(\frac{k}{\sqrt{EE'}}\right)^{t+bt_b+bt_a}}{\Gamma(1+bt_b+bt_a)} \qquad (1)$$

$d\sigma'_1/d\Omega dE'$ is the cross section for bremsstralung during elastic scattering, calculated to lowest order in α, but with higher order in α corrections to the photon propagator and electron-photon vertex. It is given by the formula B.5 of Mo and Tsai, reference 24, with the modified proton elastic form factors F and G, of B.5 as follows.

$$F(q^2) = \frac{4\left(G_E^2(q^2) + \frac{q^2}{4M^2}\,G_M^2(q^2)\right)}{1+\frac{q^2}{4M^2}}\left(1+\delta'(q^2)\right)$$

APPENDIX A.V --- RADIATIVE CORRECTION FORMULAS

$$G(q^2) = 4G_M^2(q^2)\left\{1 + \delta'(q^2)\right\} \qquad (2)$$

$\delta'(q^2)$ represents the q^2 dependent electrodynamic correction.

$$\delta'(q^2) = \frac{2\alpha}{\pi}\left(\frac{13}{12}\log\frac{q^2}{m^2} - \frac{14}{9}\right)$$

G_E and G_M were determined by a fit to all available SLAC elastic eP data, taken with both the 8 and 20 Gev spectrometers and analyzed assuming the scaling law, $G_M = 2.793 G_E$. Figure A.2 is a graph of G_E obtained from the six parameter fit, which summarizes the cross section data over the range of q from 0 to 5 GeV.

$d\sigma'_0/d\Omega$ is the corrected electron proton elastic cross section given by the usual Rosenbluth formula, but with electrodynamic corrections.

$$\frac{d\sigma'_0}{d\Omega}(E,\theta) = \frac{\alpha^2}{4E^2}\frac{\cos^2\frac{\theta}{2}}{\sin^4\frac{\theta}{2}}\left[\frac{2M\;G_E^2(q^2) + \frac{q^2}{4M^2}G_M^2(q^2)}{1 + q^2/4M^2} + 2\tan^2\frac{\theta}{2}\frac{q^2}{2M}G_M^2(q^2)\right]\frac{1}{2M\eta}\left\{1 + \delta'(q^2)\right\} \qquad (3)$$

t_{EL} is the equivalent radiator for radiation coming from the electron lines alone, as given by I.16. t is the total equivalent radiator defined by I.17 with the integration preformed as in II.14. Both t_{EL} and t are calculated at $E-\omega, E', \theta$ instead of E, E', θ since this gives the q^2 which is most important in the large angle

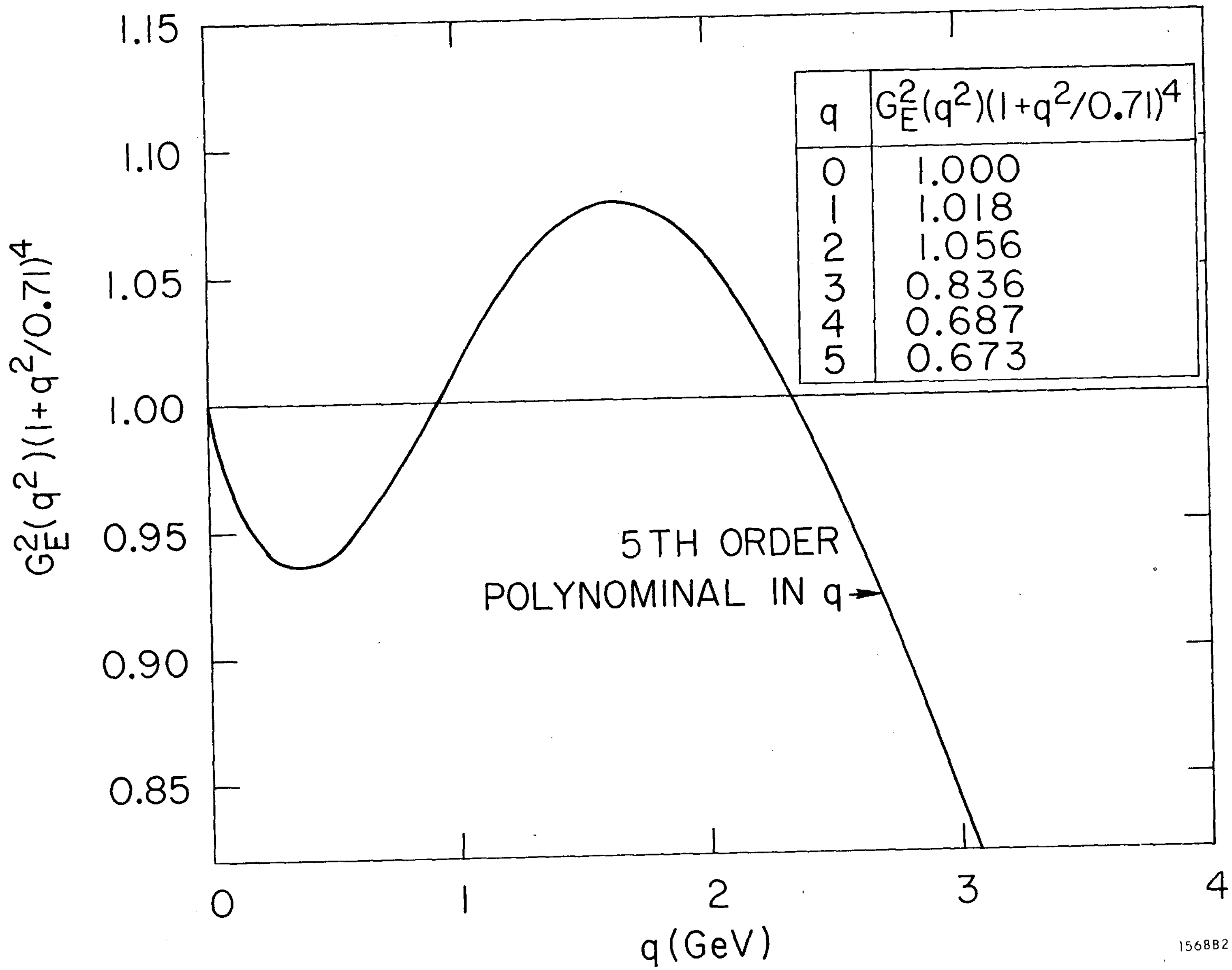
q | $G_E^2(q^2)(1+q^2/0.71)^4$
0 | 1.000
1 | 1.018
2 | 1.056
3 | 0.836
4 | 0.687
5 | 0.673
5TH ORDER
POLYNOMINAL IN q
$G_E^2(q^2)(1+q^2/0.71)^4$
1.15
1.10
1.05
1.00
0.95
0.90
0.85
0
1
2
3
4
q (GeV)
1568B2

Fig. A.2

bremsstralung process. That is, this is the most probable momentum transfer to the proton. This factor t/t_{EL} is an attempt to estimate the extra hard radiation coming from the proton. $w(E,E')t$ is the first order probability to lose energy $E-E'$ in target thickness t radiation lengths as given in III. As usual $b=4/3+a$ with a given by III.6. t_b and t_a are the thicknesses of material before and after the point of scattering, measured in radiation lengths. k is the soft photon limiting energy as defined by equation (19) of IV. Other kinematic quantities are defined as follows.

$$\eta = 1 + \frac{2E}{M} \sin^2 \cdot/2$$

$$\eta' = \frac{1}{1 - \frac{2E'}{M} \sin^2 \theta/2}$$

$$\omega = E - \eta' E'$$

$$\omega' = \frac{E}{\eta} - E' \qquad (4)$$

It is possible to check formula (1) experimentally to some extent. This is done in the most straightforward way in the region above pion threshold, that is for the missing mass W less than the proton mass plus one pion mass. In that kinematic region the entire measured cross section consists of elastic radiative tail. Also all the photons are soft so the theoretical uncertainties about the soft photon limiting energy k are not important. Cross sections of this kind with fairly small errors were measured at 6 and 10 degrees . Figure A.3 shows a comparison of the cross section predicted by formula (1), averaged over the spectrometer acceptance, with the observed cross section. The observed cross section for scattering from hydrogen is the full target minus the empty target background.

The Figure shows several different types of data points since points above and below the elastic peak are plotted together, that is, the absissca is actually $|\omega'|$. As can be seen there is a wing on the distribution extending a considerable distance above the elastic peak. In lieu of having a detailed model of the spectrometer and initial beam that would allow calculation of the complete shape of the elastic peak including this high energy wing it was decided that the most correct expediency would be to assume a symmetrical low energy wing and to subtract it from the measured cross section. The difference between the solid dots and the x's is the effect of this subtraction.

Two spectrometer settings with half overlapping energy acceptance where used to obtain the full target cross section. The empty target cross section amounts to approximately ten per cent of the full, and it is obtained from a single spectrometer setting. In addition a smooth polynomial fit is made to the empty target cross section.

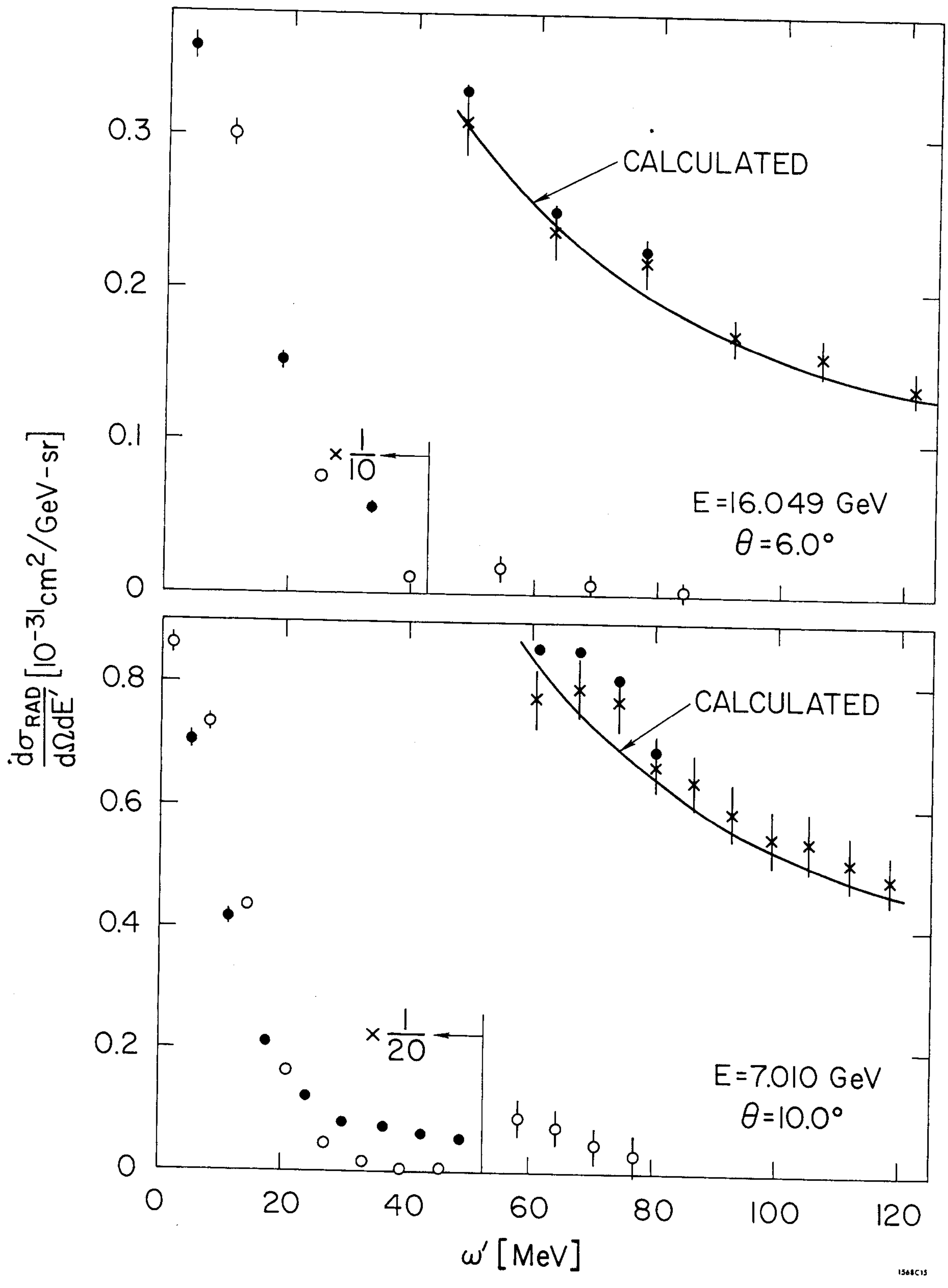
0.3
0.2
0.1
0
CALCULATED
$\times \frac{1}{10}$
E=16.049 GeV
θ=6.0°
$\frac{d\sigma_{RAD}}{d\Omega dE'}$ [10^{-31} cm^2/GeV-sr]
0.8
0.6
0.4
0.2
0
CALCULATED
$\times \frac{1}{20}$
E=7.010 GeV
θ=10.0°
0
20
40
60
80
100
120
ω′ [MeV]
1568C15

Fig. A.3

APPENDIX A.V --- RADIATIVE CORRECTION FORMULAS

An important source of error in this comparison is the uncertainty in the missing energy ω'. This is a small error as long as the elastic peak is centered around $\omega'=0$. Finally there is always the error caused by ignorance of the elastic cross section itself, which amounts to several per cent.

In the deep inelastic, which is the region of main interest, it was possible to place an upper limit on the elastic radiative tail by experimental measurement. For small E' (W large), the radiative tail from elastic scattering predominates, the remainder of the cross section being non-radiative (only soft radiation) and the sum of radiative tails from inelastic transistions $eP \rightarrow eP_j$ with M_j less than W. Figure A.4 shows the elastic tail from formula (1) (averaged over spectrometer acceptance) compared to the measured inelastic cross section spectrum for E=4.5 Gev and $\theta=6$ degrees. The x's are the elastic tail plus the inelastic cross section $d\sigma/d\Omega dE'(E,E',\theta)$ obtained from a fit given in reference 15. The circles are the measured cross sections which have negligible statistical error bars. However there may be quite large systematic errors at small E' as indicated. The difference between the circles and the x's is the sum of radiative tails from inelastic transistions.

Unfortunately with the limited accuracy of the availiable data, it is impossible to experimentally justify

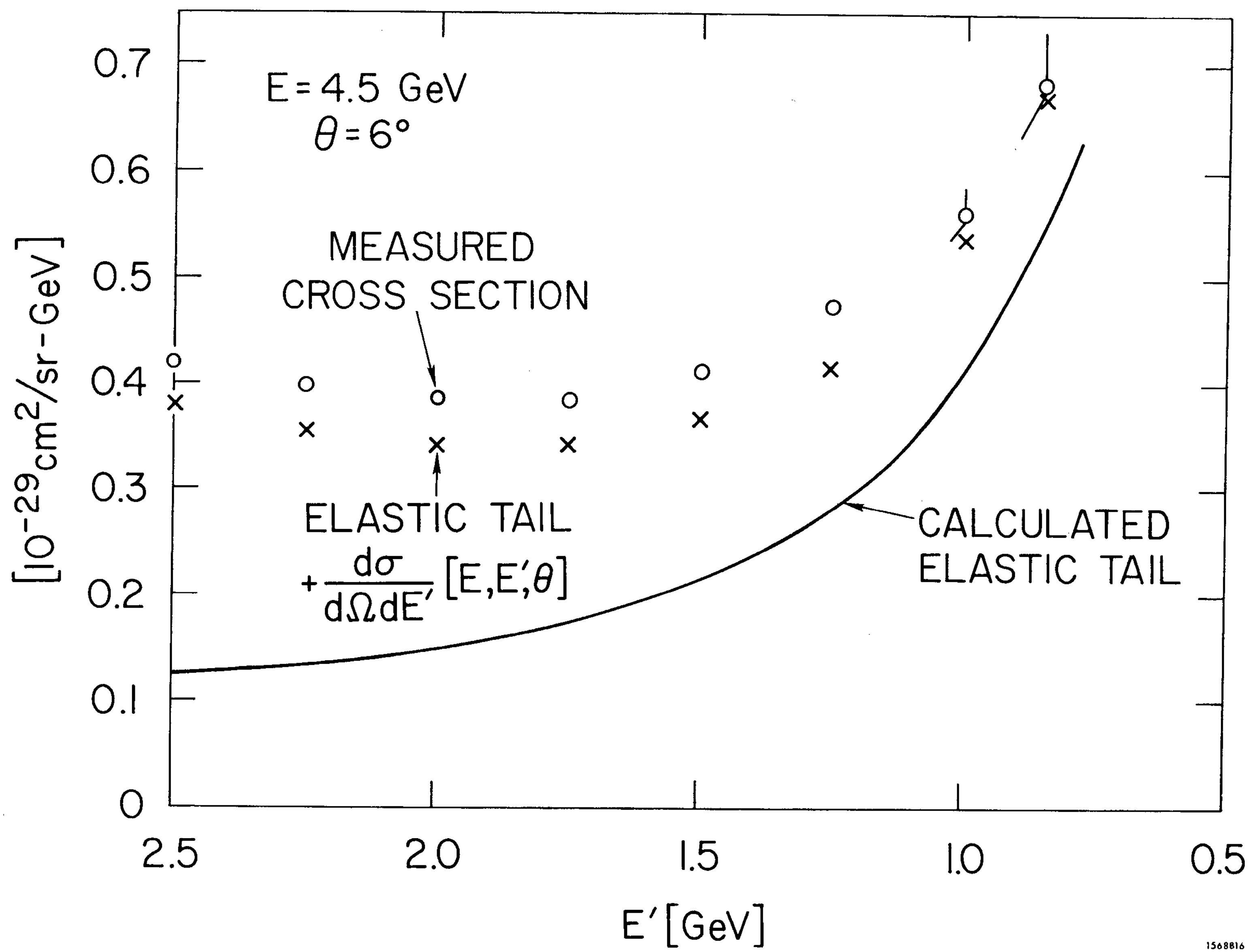

E = 4.5 GeV
θ = 6°
MEASURED CROSS SECTION
ELASTIC TAIL
$+\frac{d\sigma}{d\Omega dE'}[E,E';\theta]$
CALCULATED ELASTIC TAIL
$[10^{-29}\mathrm{cm}^2/\mathrm{sr\text{-}GeV}]$
0
0.1
0.2
0.3
0.4
0.5
0.6
0.7
2.5
2.0
1.5
1.0
0.5
E′[GeV]
1568816

Fig. A.4

formula (1) or more generally the treatment of higher order effects given here. These comparisons are meant as rough checks that the results are reasonable.

The formula used to radiatively correct the measured inelastic cross section was the following.

$$\frac{d\sigma}{d\Omega dE'}(E, E', \theta) = \frac{1}{\left(\frac{\Delta E}{E}\right)^{t/2+bt_b}\left(\frac{\Delta E'}{E'}\right)^{t/2+bt_a}\frac{1+\delta'(q^2)}{\Gamma(1+bt_b+bt_a)}}$$

$$\times\left\{\frac{d\sigma_{RAD}}{d\Omega dE'}(E, E', \theta) - \frac{d\sigma_{ELAS\ RAD}}{d\Omega dE'}(E, E', \theta)\right.$$

$$-\int_{E_{min}}^{E-\Delta E} dE_1\left(\frac{v_b}{E-E_1}+t_b w(E, E_1)\right)\frac{d\sigma}{d\Omega dE'}(E_1, E', \ )\left(\frac{k_1}{E}\right)^{t/2+bt_b}\left(\frac{k_1'}{E'}\right)^{t/2+bt_a}\frac{1+\delta'(q_1^2)}{\Gamma(1+bt_b+bt_a)}$$

$$\left.-\int_{E'+\Delta E'}^{E'_{max}} dE_1'\left(\frac{v_a}{E_1'-E'}+t_a w(E_1', E')\right)\frac{d\sigma}{d\Omega dE'}(E, E_1', \theta)\left(\frac{k_1}{E}\right)^{t/2+bt_b}\left(\frac{k_1'}{E'}\right)^{t/2+bt_a}\frac{1+\delta'(q_1^{2\prime})}{\Gamma(1+bt_b+bt_a)}\right\} \quad (5)$$

The two integrals involve the already corrected cross section and represent the radiative tails from inelastic production of higher mass states of the proton. E'_{max} and E_{min} are the energies at pion threshold along the path of integration.

$$E_{min} = \left(E' + m_\pi + m_\pi^2/2M\right)\eta'$$

$$E'_{max} = \left(E - m_\pi - m_\pi^2/2M\right)/\eta$$

$$\Delta E = \eta\eta' \Delta E' \qquad (6)$$

It is only an approximation that the radiative tail can be expressed only in terms of the corrected cross section at two points $E-\omega, E', \theta$ and $E, E'+\omega', \theta$ instead of as an integral involving the two inelastic form factors individually. However this so called "peaking-factorization" approximation causes an error of order ten per cent in the calculated radiative tail, which is tolerable in this case. v_b and v_a play the role of equivalent radiators for the hard photon bremsstralung process. They are not well defined theoretically and the peaking-factorization approximation is valid by virtue of being tested numerically by comparing it to formula B.5 of Mo-Tsai. Of course to do this one must know the inelastic form factors beforehand - so at best one can find equivalent radiators v_b and v_a that work well for "reasonable" behavior of the form factors, but mathematically the peaking-factorization approximation is by usual standards, quite bad.

The following peaking-factorization approximation equivalent radiators were used.

APPENDIX A.V --- RADIATIVE CORRECTION FORMULAS

$$v_b = \frac{t}{2}\left[\frac{E_1}{E} - .2\left(1 - \frac{E_1}{E}\right) + .7\left(1 - \frac{E_1}{E}\right)^2\right]$$

$$v_a = \frac{t}{2}\left[\frac{E'}{E'_1} - .2\left(1 - \frac{E'}{E'_1}\right) + .7\left(1 - \frac{E'}{E'_1}\right)^2\right] \qquad (7)$$

The equivalent radiator t in the exponent of the soft photon factor and above in Equ. 7 is taken to be,

$$t = \frac{2\alpha}{\pi}\left(\log \frac{q^2}{m^2} - 1\right) \qquad (8)$$

The soft photon limiting energies are defined as follows

$$k_1 = \min\left(\frac{1}{3}E, \omega_1\right)$$

$$k'_1 = \min\left(\frac{1}{3}E', \omega'_1\right) \qquad (9)$$

For the E integral $\omega_1 = E - E_1$, $\omega'_1 = \omega'/\eta\eta'$. For the E' integral $\omega'_1 = E'_1 - E'$, $\omega_1 = \eta\eta'\omega'$. The resulting corrected cross section must not be sensitive to the choice 1/3 above since this fraction is uncertain in the range say .2 to .8.

The q^2's in formula (5) are defined as follows.

$$q^2 = 4EE' \sin^2 \theta/2$$

$$q_1^2 = 4E_1E' \sin^2 \theta/2$$

$$q_1'^2 = 4EE'_1 \sin^2 \theta/2 \qquad (10)$$

$\Delta E'$ is arbitrary as long as it is sufficiently small so that the cross section $d\sigma/d\Omega dE'$ does not vary appreciably over this range of energies. More precisely $d\sigma/d\Omega dE'$ is defined as the limit of the above expression (5) for $\Delta E' \rightarrow 0$.

Assuming the cross section is measured only for a certain number of lines or spectra (E, θ constant, E' varying), the corrected cross section must be interpolated and extrapolated from the measured lines in order to do the first integration in formula (5). The precise relationship of the corrected cross section to the measured cross section is that the corrected cross section when interpolated-extrapolated according to the scheme chosen, satisfies equation (5) along the measured lines. The final answer can be quite sensitive to the method of interpolation-extrapolation used.

APPENDIX A.VI --- ELASTIC PEAK RADIATIVE CORRECTIONS

The technique of radiatively correcting the measured elastic electron-proton cross section is rather different than in the inelastic case although the physics of the higher order electromagnetic processes is entirely the same. The measured cross section $d\sigma_{RAD}/d\Omega dE'$ is obtained in the region of the elastic peak, that is, $W \cong M$. From the measured cross section it is desired to obtain the radiatively corrected cross section $d\sigma_0/d\Omega$, that is, the cross section for the process $eP \to eP$ calculated to lowest order in α. In this kinematic region no radiated photon can have a large energy so the theoretical uncertainties about multiple hard photon radiation are absent. If W is less than the proton mass plus one pion mass, no inelastic processes are possible except photon radiation.

The situation is complicated because the resolution of the spectrometer measuring E' and θ, and the initial beam definition in energy and spacial and angular extent have an important effect on the measured cross section. The radiated elastic electron-proton cross section is given by

$$\frac{d\sigma_{RAD}}{d\Omega dE'}(E,E',\theta) = \int_{\eta' E'}^{E} \frac{\frac{t}{2}+bt_b}{E-E_1} \frac{\left((E-E_1)/E_1\right)^{t/2+bt_b}}{\Gamma(1+bt_b)} \times \frac{d\sigma_0}{d\Omega}(E_1,\theta)(1+\delta') \frac{\frac{t}{2}+bt_a}{(E_1/\eta_1)-E'} \frac{\left[\left((E_1/\eta_1)-E'\right)/E'\right]^{t/2+bt_a}}{\Gamma(1+bt_a)} dE_1 \qquad (1)$$

where t is the total equivalent radiator, t_b and t_a are the radiation lengths of material before and after the point of scattering, b is 4/3 + a, with a defined by Eq. A.III.6 and δ' is the correction due to quantum mechanical effects not involving radiation. As usual, the kinematic quantities η, η' are defined as follows:

$$\eta = 1 + \frac{2E}{M} \sin^2 \theta/2$$

$$\eta_1 = 1 + \frac{2E_1}{M} \sin^2 \theta/2$$

$$\eta' = \frac{1}{1 - \frac{2E'}{M} \sin^2 \theta/2}$$

When E' is sufficiently near the elastic peak E/η so that the cross section $d\sigma_0/d\Omega$ does not vary appreciably over the range of integration, Eq. 1 reduces to

$$\frac{d\sigma_{RAD}}{d\Omega dE'}(E, E', \theta) = \frac{d\sigma_0}{d\Omega}(E,\theta) \frac{1 + \delta'}{\Gamma(1 + bt_b + bt_a)} \frac{t + bt_b + bt_a}{\omega'} \left(\frac{\omega}{E}\right)^{t/2 + bt_b} \left(\frac{\omega'}{E'}\right)^{t/2 + bt_a} \quad (2)$$

where $\omega = E - \eta' E'$, $\omega' = E/\eta - E'$.

Tsai has calculated the radiative corrections to elastic electron scattering to lowest order in α including corrections to the proton (or charge Z)-photon vertex, two photon exchange and radiation involving the proton (or charge Z). This correction is defined by the following equation:

APPENDIX A.VI --- ELASTIC PEAK RADIATIVE CORRECTIONS

$$\int_{E/\eta-\omega'}^{E/\eta} \frac{d\sigma_{RAD}}{d\Omega dE'}(E, E', \theta) dE' = \frac{d\sigma_0}{d\Omega}(E, \theta)(1 + \delta(\omega')) \qquad (3)$$

Tsai's expression for δ is given by Eq. II.6 of Ref. 24.

Substituting expression (2) for $d\sigma_{RAD}/d\Omega dE'$, in the case when $t_b = t_a = 0$ and dropping higher order terms in α, we find that

$$\delta = \delta' + t \log \sqrt{\eta}\ \frac{\omega'}{E'} \qquad (4)$$

We use Eq. 4 to define δ'. In the case when radiation from the target particle is not significant, that is, when Z and Z^2 terms in Mo-Tsai, II.6 can be dropped, we have the approximate result that

$$\delta' = \frac{2\alpha}{\pi}\left(\frac{13}{12} \log \frac{q^2}{m^2} - \frac{14}{9}\right)$$

Also, it is seen that the dependence of δ on the energy interval ω' is determined by the total equivalent radiator t

$$\frac{d\delta}{d\omega'} = \frac{t}{\omega'}$$

In practice this allows t to be obtained from Mo-Tsai formula II.6.

Given the physics of the ideal process summarized by formula 1, there remains the problem of extracting the corrected cross section from the data. There are many schemes for doing this, the most straightforward forward being to calculate the expected yields on a counter-by-counter (or counter bin) basis from a detailed model of the initial beam and the spectrometer using formula 1, and compare with the measurement. This method has the advantage that it does not confuse the real apparatus-related problems involved in the measurement. The disadvantage is that the Monte Carlo computer calculations are rather time consuming.

Figure A.5 shows a comparison of the calculated with the observed elastic cross section spectrum in missing energy. Events within the spectrometer acceptance are binned according to their missing energy ω'. The data points (with error bars) represent the cross section for each bin, that is, $N/(\Delta\Omega N_{in}\, n)$, where N is the number of electrons scattered from hydrogen into the bin for N_{in} incident electrons, $\Delta\Omega$ is the solid angle of the bin and n is the number of target protons per cm². The solid curve is that same quantity, calculated using formula 1 for the cross section.

Formula 1 involves folding the elastic cross section with a probability distribution for radiation before and after. This was accomplished in the Monte Carlo program by generating soft photon radiation energy losses with the proper distribution, and ionization losses as well.

If R is uniformly distributed in (0,1), then the quantity $\epsilon = ER^{1/(t/2+bt_b)}$ will be distributed like $(t/2+bt_b)/\epsilon\ \ (\epsilon/E)^{t/2+bt_b}$, which is the distribution of soft photon energy losses before scattering for an equivalent radiator t and a real radiator t_b.

The distribution of energy losses due to ionization has the approximate form $\xi t_b/\epsilon$ for $\epsilon > \Delta_0$, where Δ_0 is given by III.16 and ξ by III.10. This is simulated by $\Delta_0 + E/((E-\xi t_b)/\xi t_b R+1)$ for R a random number uniformly distributed in (0,1).

For the example shown in Figure A.5, E = 9.999 GeV, $\theta = 12.5^{\circ}$ (q^2 = 3.784 GeV^2). The generated spectrum assumed the elastic form factors were given a fit to SLAC data shown in Figure A.2. The ratio of the sum of all bins from experiment to that of theory is 1.037 ± 0.032.

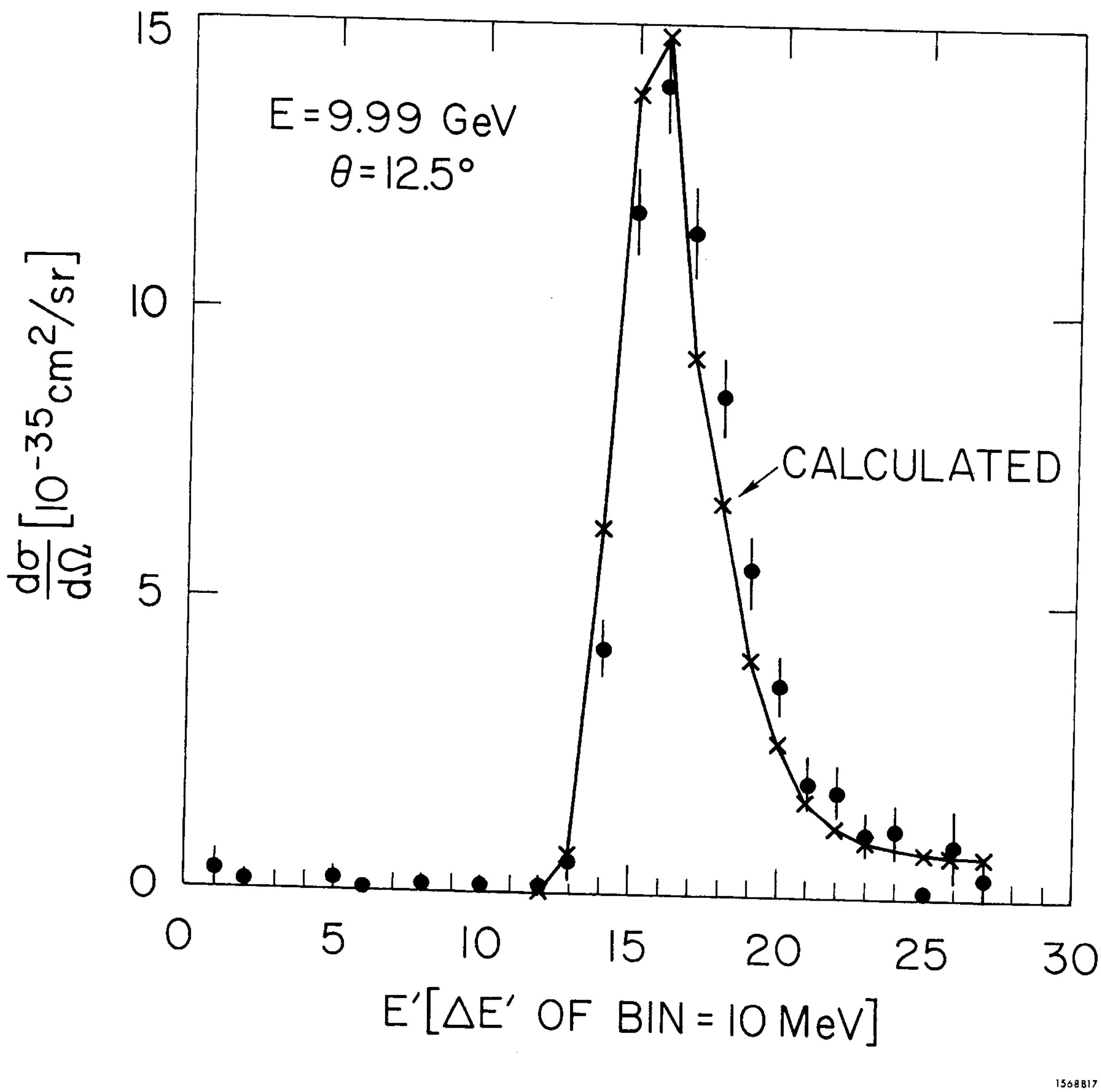
E = 9.99 GeV
θ = 12.5°
CALCULATED
dσ/dΩ [10^-35 cm^2/sr]
E′ [ΔE′ OF BIN = 10 MeV]
0
5
10
15
20
25
30
1568B17

Fig. A.5

APPENDIX B--- ELECTRON SCATTERING CROSS SECTION FORMULAS

The radiatively corrected cross section for a proton at rest to scatter a high-energy electron from initial momentum p_μ to final momentum p'_μ in the range d^3p' can be written as follows:

$$d\sigma = \frac{j_{\mu\nu}\, 4\pi^2\alpha\, W_{\mu\nu}}{q^4} \frac{d^3p'}{(2\pi)^3} \qquad (1)$$

where $q_\mu = p_\mu - p'_\mu$ and $j_{\mu\nu}$ and $4\pi^2\alpha W_{\mu\nu}$ are the averaged electromagnetic currents represented by the electron and hadronic system, for example,

$$4\pi^2\alpha W_{\mu\nu} = \frac{E_p}{M}\frac{1}{2}\sum_{\text{spin}}\int \langle P|J_\mu(x)\, J_\nu(0)|P\rangle e^{iqx} d^4x$$

In the laboratory system $j_{\mu\nu}$ takes the following form:

$$j_{\mu\nu} = \frac{e^2 q^2}{2EE'(1-\epsilon)} \begin{bmatrix} 2\epsilon\frac{\nu^2}{q^2} & 0 & 0 & \frac{2i\epsilon\nu}{q^2}\sqrt{q^2+\nu^2} \\ 0 & 1+\epsilon & 0 & i\sqrt{2\epsilon(1+\epsilon)} \\ 0 & 0 & 1-\epsilon & 0 \\ \frac{2i\epsilon\nu}{q^2}\sqrt{q^2+\nu^2} & i\sqrt{2\epsilon(1+\epsilon)} & 0 & -2\epsilon\left(1+\frac{\nu^2}{q^2}\right) \end{bmatrix} \qquad (2)$$

where the momentum transfer is along the 1-axis and the scattering takes place in the 1-2 plane.

$$q^2 = q_\mu q_\mu = 4EE' \sin^2 \frac{\theta}{2}$$

$$\nu = q_0 = E - E'$$

$$\epsilon = \frac{1}{1 + 2\tan^2 \frac{\theta}{2}\left(1 + \frac{\nu^2}{q^2}\right)} \qquad (3)$$

The quantity ϵ lies in the range 0 to 1 and is the longitudinal-transverse polarization ratio of the source of virtual photons provided by the scattering electron.

$4\pi^2\alpha W_{\mu\nu}$ is the electromagnetic current tensor of the proton system. $W_{\mu\nu}$ is a function of the proton momentum P_μ and q_μ and satisfies the gauge conditions $W_{\mu\nu} q_\nu = q_\nu W_{\nu\mu} = 0$. $W_{\mu\nu}$ can be written in the general form.[25]

$$W_{\mu\nu} = W_1\left(\delta_{\mu\nu} - \frac{q_\mu q_\nu}{q^2}\right) + \frac{W_2}{M^2}\left(P_\mu - \frac{Pq}{q^2} q_\mu\right)\left(P_\nu - \frac{Pq}{q^2} q_\nu\right) \qquad (4)$$

where W_1 and W_2 are functions of the invariants q^2 and ν.

In the laboratory system the proton electromagnetic current $W_{\mu\nu}$ looks as follows:

$$W_{\mu\nu} = \begin{bmatrix} \frac{\nu^2}{q^2} W_L & 0 & 0 & \frac{i\nu\sqrt{q^2+\nu^2}}{q^2} W_L \\ 0 & W_T & 0 & 0 \\ 0 & 0 & W_T & 0 \\ \frac{i\nu\sqrt{q^2+\nu^2}}{q^2} W_L & 0 & 0 & -\left(1+\frac{\nu^2}{q^2}\right) W_L \end{bmatrix} \qquad (5)$$

where,

$$W_L = W_2\left(1+\frac{\nu^2}{q^2}\right) - W_1, \quad W_T = W_1$$

The differential cross section for detecting the scattered electron in solid angle $d\Omega$ and energy range dE' is the following:

$$\frac{d\sigma}{d\Omega dE'} = \frac{\alpha^2 E'}{Eq^2} \frac{2}{1-\epsilon} \left(W_T + \epsilon W_L\right) \qquad (6)$$

This is commonly written as

$$\frac{d\sigma}{d\Omega dE'} = \frac{\alpha^2}{4E^2} \frac{\cos^2\frac{\theta}{2}}{\sin^4\frac{\theta}{2}} \left(W_2 + 2\tan^2\frac{\theta}{2} W_1\right) \qquad (7)$$

APPENDIX B--- ELECTRON SCATTERING CROSS SECTION FORMULAS

The quantity R is defined as the ratio of the probability for longitudinal photon absorption to that for transverse photons,

$$R = \frac{W_L}{W_T} = \frac{q^2}{\nu^2}\,\frac{W_{11}}{W_{22}} \tag{8}$$

where the second equality refers to the tensor $W_{\mu\nu}$, given above. As $q^2 \rightarrow 0$, W_{11}/W_{22} has a finite limit, since it is the ratio of current components for a static proton; thus R 0 as q^2— 0.

In the limit of $q^2 \rightarrow 0$, $4\pi^2 \alpha W_{\mu\nu} \epsilon_\mu \epsilon_\nu / (2\nu)$ is the cross section for absorbing a real photon with polarization ϵ_μ and energy ν. The total photo-absorption cross section is

$$\sigma_{\gamma p} = \frac{4\pi^2 \alpha\, W_T}{\nu} \tag{9}$$

Hand[26] expresses the cross section in terms of total absorption cross sections for transverse and scalar virtual photons,

$$\frac{d\sigma}{d\Omega dE'} = \Gamma(\sigma_T + \epsilon\sigma_S) \tag{10}$$

where

$$\sigma_T = \frac{4\pi^2 \alpha}{K}\, W_T$$

APPENDIX B--- ELECTRON SCATTERING CROSS SECTION FORMULAS

$$\sigma_S = \frac{4\pi^2 \alpha}{K} W_L \tag{11}$$

Γ is the flux of virtual photons and K their effective momentum

$$\Gamma = \frac{\alpha}{4\pi^2} \frac{2E'K}{Eq^2(1-\epsilon)}$$

$$K = \frac{W^2 - M^2}{2M} \tag{12}$$

Another natural definition of these cross sections is the following:

$$\sigma'_T = \frac{4\pi^2 \alpha W_T}{\sqrt{q^2 + \nu^2}}$$

$$\sigma'_S = \frac{4\pi^2 \alpha W_L}{\sqrt{q^2 + \nu^2}} \tag{13}$$

with the virtual photon flux given by,

$$\Gamma' = \frac{\alpha}{4\pi^2} \frac{2E'\sqrt{q^2+\nu^2}}{E q^2 (1-\epsilon)} \tag{14}$$

For convenience in the description of resonance production, Bjorken and Walecka have introduced the form factors f_+, f_-, and f_c for the electroproduction of a final state with definite mass M_j.[27] The electron scattering cross section is given by

$$\frac{d\sigma}{d\Omega dE'} = \frac{\alpha^2}{4E^2}\,\frac{\cos^2\theta/2}{\sin^4\theta/2}\left(\frac{q^4}{q*^4}|f_c|^2 + \left(\frac{q^2}{2q*^2} + \frac{M_j^2}{M^2}\tan^2\theta/2\right)\right.$$

$$\left.\times\left(|f_+|^2 + |f_-|^2\right)\right) 2M\,\delta\left(W^2 - M_j^2\right) \qquad (15)$$

where W is the mass of the final state $W^2 = M^2 + 2M\nu - q^2$ and $q*$ is the momentum of the photon in the isobar rest frame.

$$q*^2 = q^2 + \frac{\left(M_j^2 - M^2 - q^2\right)^2}{4M_j^2} \qquad (16)$$

The transformation between these different structure functions is given by the following:

$$W_1 = \frac{K}{4\pi^2\alpha}\,\sigma_T = \frac{W^2}{M}\left(|f_+|^2 + |f_-|^2\right)\delta\left(W^2 - M_j^2\right)$$

$$W_2 = \frac{K}{4\pi^2\alpha}\,\frac{\sigma_T + \sigma_S}{1+\nu^2/q^2} = \frac{1}{1+\nu^2/q^2}\,\frac{W^2}{M}\left(|f_+|^2 + |f_-|^2 + \frac{2W^2}{M^2}\,\frac{1}{1+\nu^2/q^2}|f_c|^2\right)\delta\left(W^2 - M_j^2\right) \qquad (17)$$

$$\sigma_T = \frac{4\pi^2\alpha}{K}W_1 = \frac{4\pi^2\alpha W^2}{MK}\left(|f_+|^2 + |f_-|^2\right)\delta\left(W^2 - M_j^2\right)$$

$$\sigma_S = \frac{4\pi^2\alpha}{K}\left(\left(1 + \frac{\nu^2}{q^2}\right)W_2 - W_1\right) = \frac{4\pi^2\alpha W^2}{MK}\,\frac{2W^2}{M^2}\,\frac{1}{1+\frac{\nu^2}{q^2}}|f_c|^2\,\delta\left(W^2 - M_j^2\right) \qquad (18)$$

APPENDIX B--- ELECTRON SCATTERING CROSS SECTION FORMULAS

In the special case of elastic scattering ($\tau \equiv \nu^2/q^2 = q^2/(4M^2)$),

$$W_1 = 2M\tau \; G_M^2 \; \delta(W^2 - M^2)$$

$$W_2 = 2M \, \frac{G_E^2 + \tau \, G_M^2}{1 + \tau} \; \delta(W^2 - M^2) \tag{19}$$

$$\sigma_T = \frac{4\pi^2 \alpha}{K} \; 2M\tau \; G_M^2 \; \delta(W^2 - M^2)$$

$$\sigma_S = \frac{4\pi^2 \alpha}{K} \, 2M \, G_E^2 \, \delta(W^2 - M^2) \tag{20}$$

$$|f_+|^2 + |f_-|^2 = 2\tau \; G_M^2$$

$$|f_c|^2 = (1 + \tau) \, G_E^2 \tag{21}$$

REFERENCES

1. see for example <u>Electron Scattering and Nuclear and Nucleon Structure</u>, edited by Robert Hofstadter, W. A. Benjamin, 1963

2. J. L. Yarnell, G. E. Arnold, P. J. Bendt, and E. C. Kerr, Phys. Rev. <u>113</u>, 1379 (1959)

3. E. D. Bloom, D. H. Coward, H. DeStaebler, J. Drees, G. Miller, L. W. Mo, R. E. Taylor, M. Breidenbach, J. I. Friedman, G. C. Hartmann, and H. W. Kendall, Phys. Rev. Letters <u>23</u>, 930 (1969)

4. M. Breidenbach, J.I. Friedman, H. W. Kendall, E. D. Bloom, D. H. Coward, H. DeStaebler, J. Drees, L. W. Mo and R. E. Taylor, Phys. Rev. Letters <u>23</u>, 935 (1969)

5. <u>The Stanford Two-Mile Accelarator</u>, edited by R. B. Neal, W. A. Benjamin, 1968

6. ibid, page 217

7. R. S. Larsen and D. Horelick, <u>A Precision Toroidal Charge Monitor for SLAC</u>, Proceeding of the Symposium on Beam Intensity Measurement, Daresbury Nuclear Physics Laboratory, 1968

8. Luke Mo and C. Peck, Report No. SLAC TN-65-29, Stanford Linear Accelerator Center (1965)

9. K. L. Brown, "A First- and Second-order Matrix Theory for the Design of Beam Transport Systems and Charged Particle Spectrometers", Report No. SLAC-75, Stanford Linear Accelerator Center (1967)

10. D. Coward and G. C. Hartmann, SLAC Group A internal publication, August 1968

11. P. N. Kirk et al, "Elastic Electron-Proton Scattering at Large Four Momentum Transfer", (to be published)

12. L. D. Landau, "On the Energy Loss of Fast Particles by Ionization", <u>Collected Papers</u>, edited by D. Ter Haar, Pergamon Press, 1965

13. M. I. Breidenbach, PhD Thesis, Report No. MIT-2098-635, Massachusetts Institute of Technology (1970)

14. E. D. Bloom and F. J. Gilman, Report No. SLAC-PUB-779, Stanford Linear Accelerator Center (1970)

15. E. D. Bloom, R. L. Cottrell, D. H. Coward, H. DeStaebler, Jr., J. Drees, G. Miller, L. W. Mo, R. E. Taylor, J. I. Friedman, G. C. Hartmann, and H. W. Kendall, Report No. SLAC-PUB-653, Stanford Linear Accelerator Center (1969)

16. S. D. Drell and Tung-Mow Yan, Phys. Rev. Letters 24, 181 (1970)

17. R. P. Feynman (unpublished)
S. D. Drell, D. J. Levy and T. M. Yan, Phys. Rev. Letters 22, 744 (1969)
J. D. Bjorken and E. A. Paschos, Phys. Rev. 185, 1975 (1969)

18. A. I. Akhiezer and V. B. Berestetskii, Quantum Electrodynamics, second edition, Interscience Publishers, 1965, Section 30 - Emission of Photons of Long Wavelength and Section 36.1 - Electron-Electron Scattering

19. J. S. Schwinger, Particles and Sources, Gordon and Breach, 1969, Chapter 2 - Electrodynamics

20. V. B. Berestetskii, Soviet Physics Uspekhi, 5, 7, (1962), Section 4 - Electromagnetic Structure of Particles

21. D. R. Yennie, S. C. Frautschi and H. Suura, Annals of Physics, 13, 379 (1961), Appendix C

22. O. I. Dovzhenko and A. A. Pomanskii, Cosmic Rays, Volume 26, edited by D. V. Skobel'tsyn, Consultants Bureau, New York, 1965

23. R. A. Early, SLAC Group A internal publication, December 1969

24. L. W. Mo and Y. S. Tsai, Reviews of Modern Physics, 41, 205 (1969)

25. S. D. Drell and J. D. Walecka, Ann. of Phys. 28, 18 (1964)

26. L. N. Hand, PhD Thesis, Stanford University Physics Department (1961)

27. J. D. Bjorken and J. D. Walecka, Ann. of Phys. 38, 35 (1966)